INL/RPT-24-81276-Revision-0

Investigations into the Ternary NaF-KF-UF4 Salt System Phase A

January 2025

Toni Y Karlsson, Morgan Tess Kropp, Nick H Erfurth, Brynn McGrail, Kevin R Tolman, Michael Ellis Woods, Scott C Middlemas, Mikael Karlsson, Tyler J Rigoulot, Chase T Wren, Stephen A Warmann, Laura Voigt, James Amphlett, Lukasz Ruszczynski

INL/RPT-24-81276-Revision-0

Investigations into the Ternary NaF-KF-UF4 Salt System Phase A

Toni Y Karlsson, Morgan Tess Kropp, Nick H Erfurth, Brynn McGrail, Kevin R Tolman, Michael Ellis Woods, Scott C Middlemas, Mikael Karlsson, Tyler J Rigoulot, Chase T Wren, Stephen A Warmann, Laura Voigt, James Amphlett, Lukasz Ruszczynski

January 2025

Idaho National Laboratory
Idaho Falls, Idaho 83415

http://www.inl.gov

Prepared for the
U.S. Department of Energy
Under DOE Idaho Operations Office
Contract DE-AC07-05ID14517

INL/RPT-24-81276
Revision 1

Investigations into the Ternary NaF-KF-UF_4 Salt System – Phase A

22SP92 – Seaborg Technologies

Phase Diagram and Property Determination

OCTOBER 2024

Toni Karlsson,
Morgan Kropp,
Brynn McGrail,
Nick Erfurth,
Kevin Tolman,
Michael Woods,
Scott Middlemas,
Mikael Karlsson,
Tyler Rigoulot,
Chase Wren,
and Steve Warmann

Idaho National Laboratory

Laura Voigt,
Lukasz Ruszczynski,
and James Amphlett

Seaborg Technologies

Idaho National Laboratory

INL/RPT-24-81276
Revision

Investigations into the Ternary NaF-KF-UF4 Salt System – Phase A

Phase Diagram and Property Determination

Toni Karlsson,
Morgan Kropp,
Brynn McGrail,
Nick Erfurth,
Kevin Tolman,
Michael Woods,
Scott Middlemas,
Mikael Karlsson,
Tyler Rigoulot,
Chase Wren,
and Steve Warmann
Idaho National Laboratory

Laura Voigt,
Lukasz Ruszczynski,
and James Amphlett
Seaborg Technologies

OCTOBER 2024

Idaho National Laboratory
Pyrochemical Sciences, C420
Idaho Falls, Idaho 83415

http://www.inl.gov

Prepared for the
U.S. Department of Energy
Office of Nuclear Energy
Under DOE Idaho Operations Office
Contract DE-AC07-05ID14517

Page intentionally left blank

SUMMARY

A knowledge gap exists in the data and understanding of fresh fuel salt and irradiated multicomponent fuel salt systems thermophysical properties. Quantifying these properties is necessary for the design and construction of test reactors, as well as the licensing of future commercial molten-salt reactors. To facilitate thermal property determination on a proposed fuel salt composition for Seaborg Technologies, several samples containing depleted uranium tetrafluoride (UF_4), sodium fluoride (NaF), and potassium fluoride (KF) were blended, and a melt temperature analysis was performed. From the melting temperature analysis, it was determined that sample Seaborg-7, a ternary salt composition of 26.4UF4-24.7KF-48.9NaF (mol%), was very near a ternary eutectic point. Therefore, thermal properties such as melting temperature, salt stability, density, heat capacity, thermal diffusivity, and viscosity were experimentally determined on the Seaborg-7 salt. These measurements document the baseline properties of fresh fuel salt as a function of temperature, where future experiments on irradiated fuel salt will provide a holistic perspective on the change of thermophysical properties during reactor operations. Several precision instruments were used to collect property data, and instrument calibrations and data collection were performed and documented in a standardized and reproducible manner with meticulous detail. This process ensured that the measurement procedures and resulting data can readily be duplicated elsewhere. The Seaborg-7 salt was shown to be stable at temperatures up to 900°C, as no mass change was observed upon repeated heating and cooling. The peak melting temperature was determined to be 547°C (557°C endset). The enthalpy of fusion (was determined to be 167.5 ± 2.7 J/g while the enthalpy of crystallization (was determined to be -147.8 ± 13.3 J/g. In addition to the eutectic melting peak, upon heating, several pre-eutectic peaks were observed, occurring at 470°C (onset) and 499°C (peak). Specific heat capacity measurements showed a slightly increasing trend with respect to temperature in the solid phase, while the liquid-specific heat capacity showed a somewhat flat trend with an average value of 106.1 ± 1.24 J/mol·K between 600 to 800°C. Three independent trials using the Seaborg-7 salt determined the density to be $\rho(T) = 4.908 - 0.000363 \cdot T(^\circ C)$, validated between 32 to 200°C, and $\rho(T) = 4.808 - 0.00113 \cdot T(^\circ C)$, validated between ~575 to 850°C. Thermal diffusivity was determined for the liquid state and is represented by the linear equation $y = 0.1581 + 0.000207 \cdot T(^\circ C)$ between 550 to 850°C. The viscosity was determined from 600 to 800°C and is represented by the exponential fit equation, η (mPa·s) = 736.58. This report documents the conclusion of fuel salt thermophysical property measurements for the Seaborg SPP, Phase A project.

Page intentionally left blank

CONTENTS

FIGURES

TABLES

Page intentionally left blank

ACRONYMS

amu	Atomic Mass Unit
ARL	Analytical Research Lab
ASTM	American Society for Testing and Materials
Cp	Specific Heat Capacity
DSC	Differential Scanning Calorimeter
dUF_4	Depleted Uranium Tetrafluoride
EUCS	Enriched Uranium Check Standard
FASB	Fuels and Applied Science Building
FCF	Fuel Conditioning Facility
FCG	Fuel Cycle Glovebox
FFGB	Fresh Fuels Glovebox
FMF	Fuel Manufacturing Facility
FY	Fiscal Year
GPEC	Gas-Pressurized Extraction Chromatography
HFEF	Hot Fuel Examination Facility
ICP-OES	Inductively Coupled Plasma Optical Emission Spectrometer
IDL	Instrumental Detection Limit
IMCL	Irradiated Materials Characterization Laboratory
INL	Idaho National Laboratory
ISO	International Standards Organization
LFA	Laser Flash Analyzer
LWP	Laboratory-Wide Procedure
MC	Multi-collector
MFC	Materials and Fuels Complex
MQL	Method Quantification Limit
NIST	National Institute of Standards and Technology
NOP	Normal Operating Procedure
PCG	Pyrochemistry Glovebox
ppb	Parts Per Billion
ppm	Parts Per Million
Q-ICP-MS	Quadrupole – Inductively Coupled Plasma – Mass Spectrometer
rpm	Rotations Per Minute
RSD	Relative Standard Deviation
S&CL	Standards and Calibration Laboratory

SPP	Strategic Partnership Project
STA	Simultaneous Thermal Analyzer
RT	Room Temperature
S&CL	Standards and Calibration Laboratory
STA	Simultaneous Thermal Analyzer
UTEVA	Uranium and Tetra Valent Actinides
XRD	X-ray Diffraction

Page intentionally left blank

Investigations into the Ternary NaF-KF-UF4 Salt System – Phase A

Phase Diagram and Property Determination

1. INTRODUCTION

Thermophysical property (TPP) measurements serve to document the thermal behavior of pre-irradiated, near eutectic sodium fluoride (NaF)-potassium fluoride (KF)-uranium tetrafluoride (UF_4), also known as FUNaK, a candidate fuel salt for Seaborg Technologies. The FUNaK salt system was originally studied as part of the Aircraft Nuclear Propulsion Program at Oak Ridge National Laboratory. Since this time, several computational and experimental studies have been performed [1-3]. It was determined by Ocádiz Flores et al. (unpublished work) that there are two eutectic compositions:

- NaF-KF-UF_4 (55.6-18.7-25.7 mol%), at melting points of 809K ± 5 K (536°C)
- NaF-KF-UF_4 (50.4-23.2-26.4 mol%), at melting points of 810 ± 5 K (537°C).

When this work started in 2022, the ternary system, including the eutectic point, needed verification. Therefore, depleted UF_4 was used to make several ternary compositions and perform a melting point analysis. Once the ternary or near ternary eutectic point was known, a bulk salt sample was prepared for thermal and chemical property determination. The overall goal of this document is to summarize the experiments performed in Phase A as part of the Seaborg Technologies – Strategic Partnership Project (SPP). This document outlines the important experimental conditions and the calibration process, describes how experiments were performed, and examines the data generated for each property.

This work was carried out in accordance with Idaho National Laboratory (INL) procedures, processes, and controls. The overarching INL procedure governing the conduct of research is the laboratory-wide procedure (LWP)-20000. The thermal properties obtained as outlined in this report may be used for one or more of the following activities:

- Document key materials properties needed for establishing reactor safety basis
- Demonstrate, through testing and analyses, that certain fuel qualification requirements are met
- Establish targets and tolerances for implementing fuel product specifications
- Provide key inputs needed for fuel performance modeling
- Serve as documentation of an agreed-upon plan for performing molten salt property measurements.

The properties that were measured at INL as outlined in the SPP (22SP90), along with analysis information is provided in Table 1.

Table 1. Tasks/TPPs that can be performed at INL for Seaborg Technologies.

Task Name	Method	Location
Salt Blending	Glovebox and Furnace	Fuels and Applied Science Building (FASB)
Elemental Analysis	Inductively Coupled Plasma Optical Emission Spectrometer (ICP-OES), Quadrupole Inductively Coupled Plasma Mass Spectrometer (Q-ICP-MS)	Analytical Research Laboratory (ARL)
Density (Solid)	Gas Displacement Pycnometer	Fuel Conditioning Facility (FCF)
Density (Liquid)	Archimedean Hydrostatic Method	Fuel Manufacturing Facility (FMF)
Viscosity	Viscometer	FCF
Specific Heat Capacity	Differential Scanning Calorimeter (DSC)	ARL
Melting Point	Simultaneous Thermal Analyzer (STA)	ARL
Enthalpy of Fusion	STA & DSC	ARL
Thermal Diffusivity	Laser Flash Analyzer (LFA)	ARL, FASB

The molten fuel salt is a central design element for the Seaborg Technologies reactor. As with all fuel salt, the fuel salt investigated in this report may, eventually over time (reactor operations), deviate in composition, due to irradiation, fission, and corrosion product formation. Because of the expected change in the fuel-salt composition, it is important to understand the baseline fuel performance, mainly thermal properties, to facilitate engineering design, predict the behavior of the salt, track fissile isotopes, calculate the chemical and thermodynamic properties, predict the evolving composition, and provide a safety basis. A variety of characterization equipment is needed to perform the work scope outlined in 22SP90. The instruments that will be used to determine the properties of the FUNaK fuel salt(s) are briefly described in Table 2.

Table 2. Thermal property characterization instrumentation.

Viscometer	A Brookfield DV2T viscometer with a custom concentric cylinder Searle geometry, stand, and furnace. Viscosity of molten salts is one of the most critical properties because it provides an understanding of how the materials flow without significant constraints. An accurate characterization of viscosity is critical for describing the flow through the system.
Pycnometer	A device for measuring the density of a solid by determining the mass using and analytical balance followed by volume measurements using argon (Ar) pycnometry. The technique is applicable on sample volumes of 1 cm^3 or less and up to 200°C. This approach is nondestructive and simpler than the immersion density techniques.
Archimedes Densitometer	The Archimedes densitometer is an in-house design derived from the Archimedes principle, one of the simplest and most reliable methods for measuring the density of molten salt systems.
Simultaneous Thermal Analyzer (STA)	A multifunctional instrument for measuring weight change and heat flux as a function of temperature. It is also used for determining critical properties needed for experimental phase diagram development, such as invariant temperatures, phase transition temperatures, and enthalpies of fusion.
Laser Flash Analyzer (LFA)	A laser-based instrument for measuring thermal diffusivities, which can be used to calculate thermal conductivities as a function of temperature. Thermal conductivity is material specific and used to describe heat transport through a material in a stable temperature gradient.
Differential Scanning Calorimeter (DSC)	One of the most accurate instruments for measuring specific heat capacity. The DSC can also measure invariant temperatures and reaction enthalpies. The stable configuration of the samples and sample carriers of the DSC allow for more precise heat capacity measurements.
Furnace(s)	Provide temperatures up to 1000°C for salt synthesis, density, electrochemistry, corrosion, and other general long-term experiments using irradiated molten fuel salt. Ancillary work that may be performed within the furnace includes crucible bake-out, salt mixing and melting, and salt distillation. The furnace well is featureless to enable different process operations with a variety of internals that may be inserted.
Quadrupole Inductively Coupled Plasma Mass Spectrometer (Q-ICP-MS)	Forms positively charged ions from a liquid sample using an Ar plasma source. A quadrupole separates the ions according to their mass-to-charge ratios, which are then detected. Used for isotopic and elemental analyses. With detection limits as low as parts per billion (ppb), it is the most suitable technique for fission products and impurities measurements.
Inductively Coupled Plasma Optical Emission Spectrometer (ICP-OES)	Atomizes and ionizes a liquid sample using an Ar plasma source. The light spectra emitted by the atoms and ions is decomposed using a series of mirrors, lenses, and an Echelle grating, and the individual wavelengths intensities are detected. Due to the wide concentration range and detection limits as low as parts per million (ppm), it is the most suitable technique for major matrix components determination, as well as elemental analysis of impurities and fission products.

The selection of the characterization equipment above was made using multiple criteria including, but not limited to, ease of use, applicability for use with molten salts, ability to meet or exceed measurements at 1000°C, ability to use samples less than 1 cm^3 in volume, remote operability with manipulators, or the ability to be modified for use in an inert glovebox or hot cell. There is currently no facility at INL that contains all the equipment listed in Table 2. Therefore, subsamples of the fresh fuel salt will need to be prepared and transferred to facilities at the Materials and Fuels Complex (MFC).

2. STARTING MATERIAL

2.1. Analysis of NaF and KF

NaF (99.99%, trace metals basis, Sigma Aldrich) and KF (≥99.9%, trace metals basis, Sigma Aldrich) were heated under a 175 mbar absolute vacuum to 350°C in an Ar glovebox to ensure they were fully dry. Both the NaF and KF were individually ground using an agate mortar and pestle to ensure a more uniform particle size before being weighed out and transferred to the Pyrochemistry Glovebox (PCG) in the Fuels and Applied Science Building (FASB). X-ray diffraction (XRD) was performed on the KF and NaF to confirm no major impurities, see Figure 1. Additionally, samples of the NaF and KF were run on the DSC to determine the melting temperature and gain insights into purity as seen in Figure 2. The DSC curves (Figure 2, right) for NaF did not change significantly with vacuum drying, and it was determined the NaF had a melting temperature of 993.9°C. The DSC curve for KF showed two peaks prior to vacuum drying, a small peak occurring at 823.8°C and the larger melting peak occurring at 852.4°C. After vacuum drying, the first peak was nearly obsolete, and the melting temperature was determined to be 853.3°C.

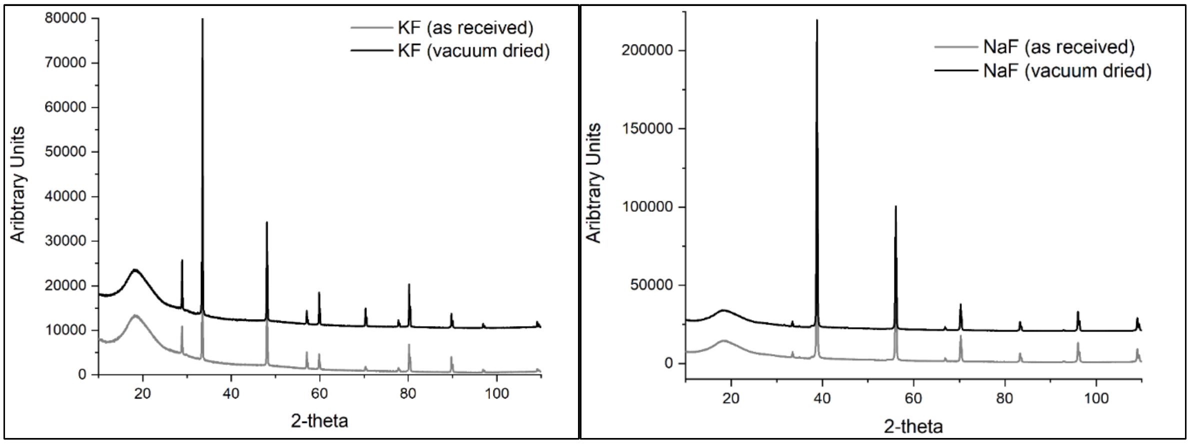

Figure 1. XRD patterns for the KF (left) and NaF (right), used to make all FUNaK (Seaborg) salt compositions.

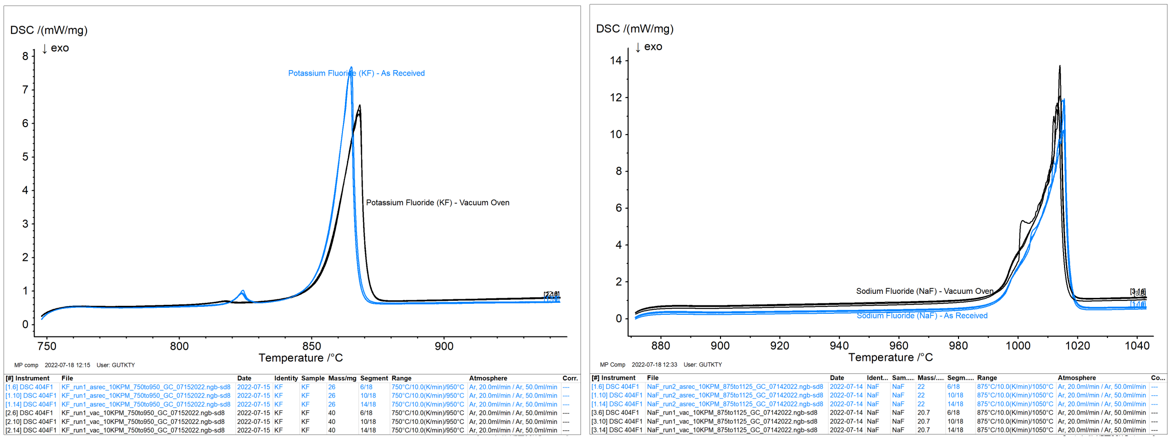

[#] Instrument	File	Date	Identity	Sample	Mass/mg	Segment	Range	Atmosphere	Corr.
[1.6] DSC 404F1	KF_run1_asrec_10KPM_750to950_GC_07152022.ngb-sd8	2022-07-15	KF	KF	26	6/18	750°C/10.0(K/min)/950°C	Ar, 20.0ml/min / Ar, 50.0ml/min	---
[1.10] DSC 404F1	KF_run1_asrec_10KPM_750to950_GC_07152022.ngb-sd8	2022-07-15	KF	KF	26	10/18	750°C/10.0(K/min)/950°C	Ar, 20.0ml/min / Ar, 50.0ml/min	---
[1.14] DSC 404F1	KF_run1_asrec_10KPM_750to950_GC_07152022.ngb-sd8	2022-07-15	KF	KF	26	14/18	750°C/10.0(K/min)/950°C	Ar, 20.0ml/min / Ar, 50.0ml/min	---
[2.6] DSC 404F1	KF_run1_vac_10KPM_750to950_GC_07152022.ngb-sd8	2022-07-15	KF	KF	40	6/18	750°C/10.0(K/min)/950°C	Ar, 20.0ml/min / Ar, 50.0ml/min	---
[2.10] DSC 404F1	KF_run1_vac_10KPM_750to950_GC_07152022.ngb-sd8	2022-07-15	KF	KF	40	10/18	750°C/10.0(K/min)/950°C	Ar, 20.0ml/min / Ar, 50.0ml/min	---
[2.14] DSC 404F1	KF_run1_vac_10KPM_750to950_GC_07152022.ngb-sd8	2022-07-15	KF	KF	40	14/18	750°C/10.0(K/min)/950°C	Ar, 20.0ml/min / Ar, 50.0ml/min	---

[#] Instrument	File	Date	Ident...	Sam....	Mass/....	Segm....	Range	Atmosphere	Co...
[1.6] DSC 404F1	NaF_run2_asrec_10KPM_875to1125_GC_07142022.ngb-sd8	2022-07-14	NaF	NaF	22	6/18	875°C/10.0(K/min)/1050°C	Ar, 20.0ml/min / Ar, 50.0ml/min	---
[1.10] DSC 404F1	NaF_run2_asrec_10KPM_875to1125_GC_07142022.ngb-sd8	2022-07-14	NaF	NaF	22	10/18	875°C/10.0(K/min)/1050°C	Ar, 20.0ml/min / Ar, 50.0ml/min	---
[1.14] DSC 404F1	NaF_run2_asrec_10KPM_875to1125_GC_07142022.ngb-sd8	2022-07-14	NaF	NaF	22	14/18	875°C/10.0(K/min)/1050°C	Ar, 20.0ml/min / Ar, 50.0ml/min	---
[3.6] DSC 404F1	NaF_run1_vac_10KPM_875to1125_GC_07142022.ngb-sd8	2022-07-14	NaF	NaF	20.7	6/18	875°C/10.0(K/min)/1050°C	Ar, 20.0ml/min / Ar, 50.0ml/min	---
[3.10] DSC 404F1	NaF_run1_vac_10KPM_875to1125_GC_07142022.ngb-sd8	2022-07-14	NaF	NaF	20.7	10/18	875°C/10.0(K/min)/1050°C	Ar, 20.0ml/min / Ar, 50.0ml/min	---
[3.14] DSC 404F1	NaF_run1_vac_10KPM_875to1125_GC_07142022.ngb-sd8	2022-07-14	NaF	NaF	20.7	14/18	875°C/10.0(K/min)/1050°C	Ar, 20.0ml/min / Ar, 50.0ml/min	---

Figure 2. DSC heat flow graphs for KF (left) and NaF (right), before (blue) and after (black) vacuum drying.

2.2. Analysis of UF_4 Salt

UF_4 (Aerojet Ordnance) was not purified in a vacuum oven prior to use. However, it was initially analyzed using XRD and the STA as shown in Figure 3A and Figure 3B, respectively. The melting temperature was determined to be 1034–1036°C from the first and second heating curves shown in Figure 3B. Volatilizing or mobilizing the UF_4 sample of the glassy carbon crucible resulted in a 32% mass loss through the STA heating program as seen by the mass change plot (as a function of temperature) in Figure 3C. The glassy carbon STA crucible, with the sample, after heating is shown in Figure 3D; at this point, the sample carrier in the STA was destroyed by the deposition and reaction of the UF_4 and the material of construction. The UF_4 from AeroJet arrived at INL with the specification sheet shown in Figure 4.

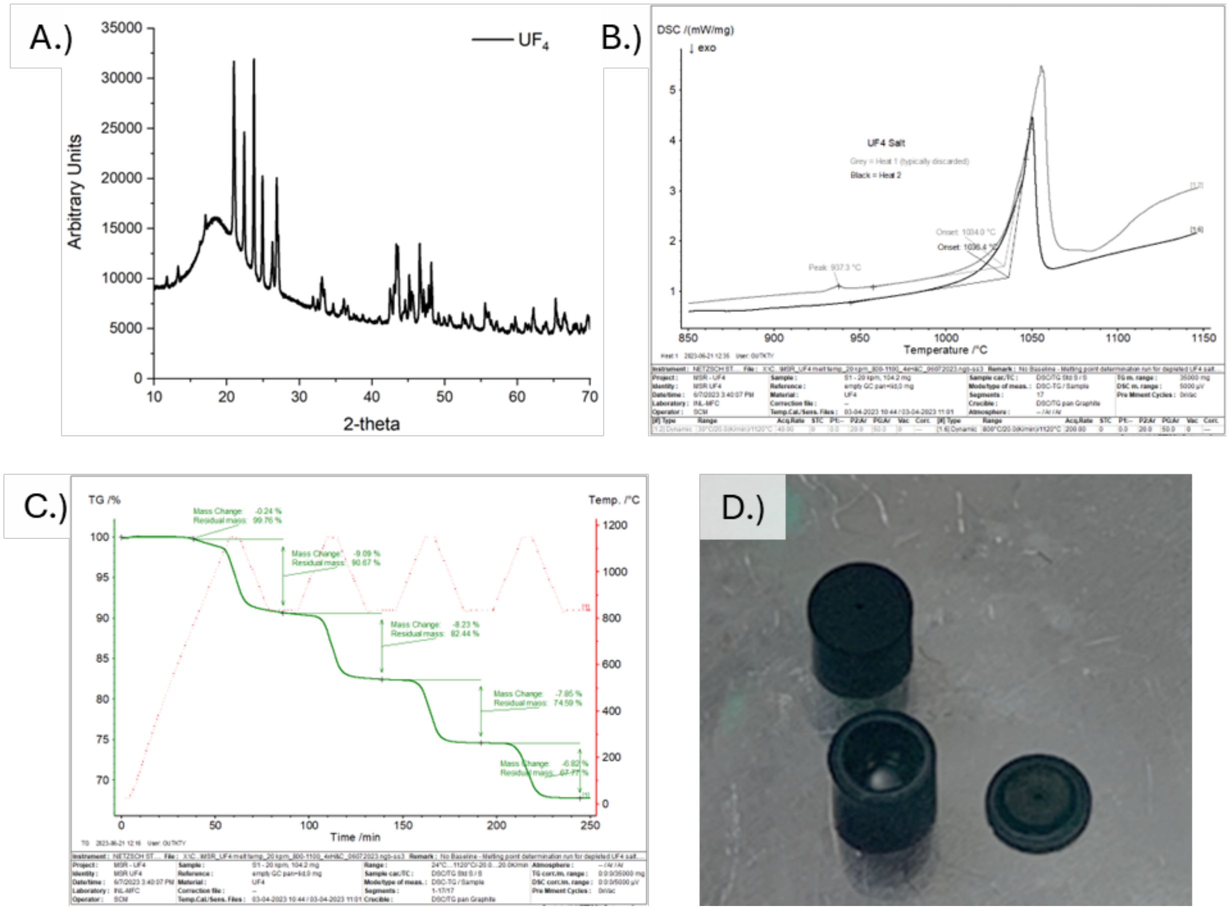

Figure 3. Properties of pure UF$_4$ used in these studies. (A) XRD pattern, (B) heat flow curves used to determine the melting temperature, (C) mass change curve for UF$_4$, and (D) glassy carbon STA crucible containing (initially) UF$_4$ after heating program was complete.

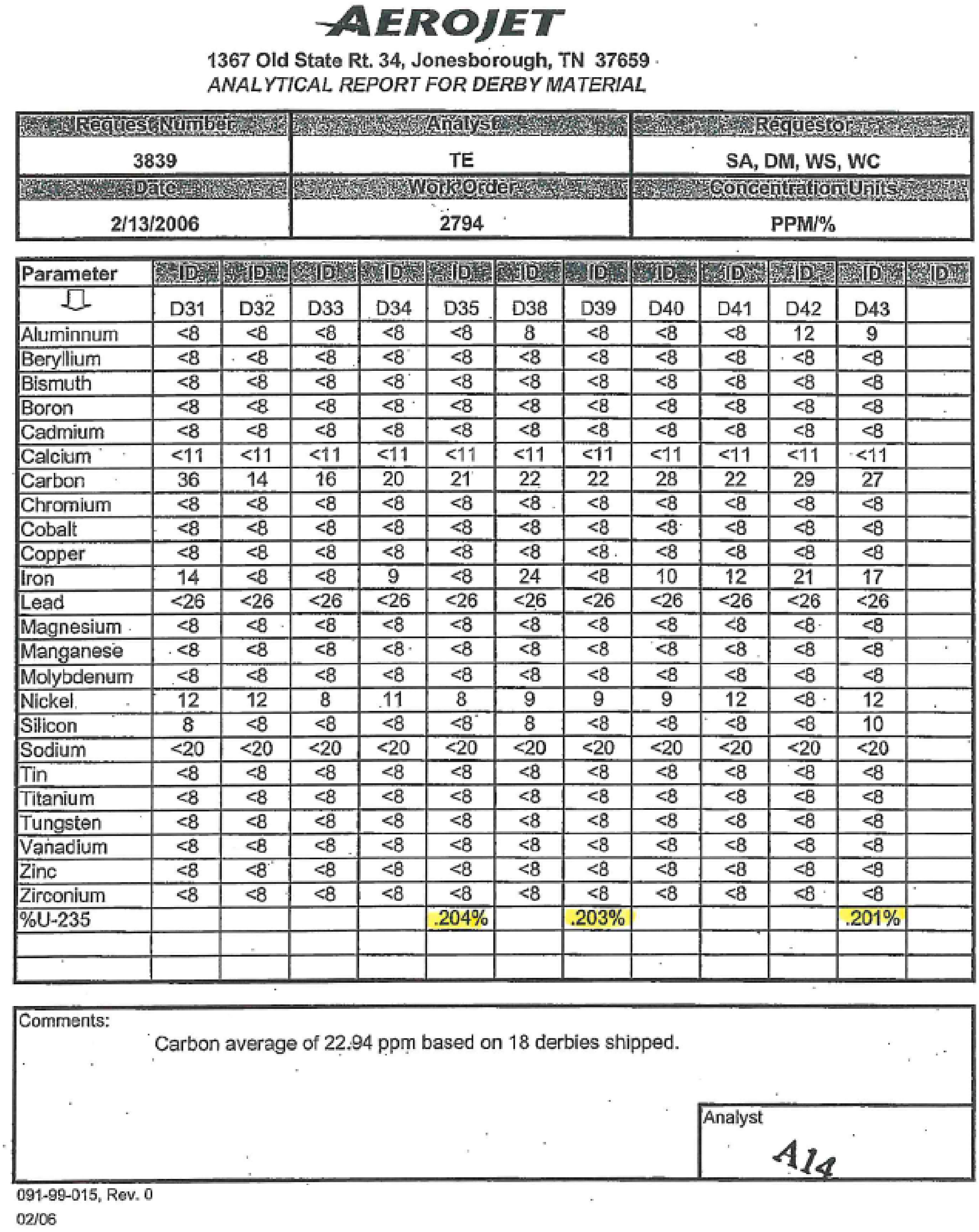

AEROJET

1367 Old State Rt. 34, Jonesborough, TN 37659

ANALYTICAL REPORT FOR DERBY MATERIAL

Request Number	Analyst	Requestor
3839	TE	SA, DM, WS, WC
Date	**Work Order**	**Concentration Units**
2/13/2006	2794	PPM/%

Parameter	ID	ID	ID	ID	ID	ID	ID	ID	ID	ID	ID	ID
⇩	D31	D32	D33	D34	D35	D38	D39	D40	D41	D42	D43	
Aluminnum	<8	<8	<8	<8	<8	8	<8	<8	<8	12	9	
Beryllium	<8	<8	<8	<8	<8	<8	<8	<8	<8	<8	<8	
Bismuth	<8	<8	<8	<8	<8	<8	<8	<8	<8	<8	<8	
Boron	<8	<8	<8	<8	<8	<8	<8	<8	<8	<8	<8	
Cadmium	<8	<8	<8	<8	<8	<8	<8	<8	<8	<8	<8	
Calcium	<11	<11	<11	<11	<11	<11	<11	<11	<11	<11	<11	
Carbon	36	14	16	20	21	22	22	28	22	29	27	
Chromium	<8	<8	<8	<8	<8	<8	<8	<8	<8	<8	<8	
Cobalt	<8	<8	<8	<8	<8	<8	<8	<8	<8	<8	<8	
Copper	<8	<8	<8	<8	<8	<8	<8	<8	<8	<8	<8	
Iron	14	<8	<8	9	<8	24	<8	10	12	21	17	
Lead	<26	<26	<26	<26	<26	<26	<26	<26	<26	<26	<26	
Magnesium	<8	<8	<8	<8	<8	<8	<8	<8	<8	<8	<8	
Manganese	<8	<8	<8	<8	<8	<8	<8	<8	<8	<8	<8	
Molybdenum	<8	<8	<8	<8	<8	<8	<8	<8	<8	<8	<8	
Nickel	12	12	8	11	8	9	9	9	12	<8	12	
Silicon	8	<8	<8	<8	<8	8	<8	<8	<8	<8	10	
Sodium	<20	<20	<20	<20	<20	<20	<20	<20	<20	<20	<20	
Tin	<8	<8	<8	<8	<8	<8	<8	<8	<8	<8	<8	
Titanium	<8	<8	<8	<8	<8	<8	<8	<8	<8	<8	<8	
Tungsten	<8	<8	<8	<8	<8	<8	<8	<8	<8	<8	<8	
Vanadium	<8	<8	<8	<8	<8	<8	<8	<8	<8	<8	<8	
Zinc	<8	<8	<8	<8	<8	<8	<8	<8	<8	<8	<8	
Zirconium	<8	<8	<8	<8	<8	<8	<8	<8	<8	<8	<8	
%U-235					.204%		.203%				.201%	

Comments:

Carbon average of 22.94 ppm based on 18 derbies shipped.

Analyst

A14

091-99-015, Rev. 0

02/06

Figure 4. UF_4 specifications provided to INL by AeroJet.

2.2.1. Elemental Analysis and Calibration

A set of three, approximately 1g, UF_4 salt samples was elementally and isotopically characterized in the ARL using QICPMS and ICP-OES. The goals of the characterization were to confirm that the salt was free from metal impurities and to get a mass balance to confirm the purity of the salt.

Since QICPMS and ICP-OES require a solution for analysis, the salt samples were dissolved in a mixture containing several strong inorganic acids. This ensured that the bulk of the sample and any metal impurities would be dissolved. Before trace analysis of impurities could be carried out by ICP-OES, a portion of the parent solution was chemically separated to remove U from the matrix. The removal of U is required before the ICP-OES analysis because emission from U can interfere with the determination of other elements of interest, specifically iron (Fe), potassium (K), and lithium (Li). ICP-OES analysis was also carried out on an unseparated sample to determine the concentration of U. The QICPMS analysis of these samples did not require separation prior to analysis, so a portion of the parent solution was simply diluted to prepare it for that analysis.

2.2.1.1. Physical Measurements and Dissolutions

Physical measurements of all sample masses were acquired using a calibrated, four decimal place analytical balance. Balances in the ARL are calibrated annually by the Standards and Calibration Laboratory (S&CL) at INL, and they are assigned an uncertainty for their measurement range (on the order of 0.6 to 0.7 mg). Daily checks are performed on these balances using National Institute of Standards and Technology (NIST) traceable external calibration weights, also calibrated by the S&CL, to confirm the balance's functionality and accuracy before use. Results from the external calibration weight checks are recorded on a control chart for each balance so that long-term bias can be evaluated. In addition, all dilutions prepared for Q-ICP-MS and ICP-OES analysis were prepared on a weight-to-weight basis.

The samples were transferred in airtight vials to ensure that the salts did not absorb moisture, and upon arrival, the samples weighed between 0.96 to 1.29 g. Because the dissolution took place in a fume hood, the mass of each sample was taken quickly after opening each vial to minimize any absorption of moisture from the air. As an additional check, the mass of each sample was taken just after it was placed in the vial before shipping to ARL. The masses obtained in ARL, after opening the vial, compared very well with the initial mass of the samples (the differences were on the order of ± 2 mg), indicating that the samples did not absorb significant amounts of moisture during the transfer between facilities. When the samples arrived at ARL, they were assigned individual ARL log numbers, as shown in Table 3.

Table 3. ARL analytical log numbers, sample identification, and description.

ARL Log #	Sample ID	Description
109876	Seaborg-1, UF4	UF4 salt, 0.9639g
109877	Seaborg-2, UF4	UF4 salt, 1.2936g
109878	Seaborg-3, UF4	UF4 salt, 1.2123g

After obtaining masses, the dissolution was performed by dissolving the solids into mixtures of 8 M nitric acid (HNO_3) and 6 M hydrochloric acid (HCl). The chlorides were removed through reaction with nitric acid and applying heat. The free fluorides were complexed by the addition of 4 % boric acid (H_3BO_4). Once the solutions were a clear yellow color with no precipitates, more 8 M nitric acid was added to bring the dissolved samples to a volume of 50 mL. A reagent and process blank were prepared alongside the samples to monitor for contamination.

2.2.1.2. Q-ICP-MS Analysis

The QICPMS analysis was performed in a NexIon 2000 (Perkin Elmer) per procedure ARL0530NOP002. The samples and reagent blank were analyzed for U (masses 233, 234, 235, 236, 237, and 238 amu). The reagent blank was found to be free from the above analytes within the method quantification limit (MQL) of the analysis. Duplicate analysis was carried out on each sample; in each case, the duplicate analyses were found to agree with each other well within the expected uncertainty, and the results were averaged to obtain the final reported value. Before analysis begins, the instrument must pass a daily performance check. This includes measuring the response of several analytes (beryllium [Be]-9, indium [In]-115, and U-238) in a standard provided by the instrument manufacturer and checking the double charge and oxide ratios of select analytes.

QICPMS is a sensitive technique. Dilutions of the dissolved sample were required to avoid saturating the detector or overloading the plasma and ensure that calibration standards were matrix matched to the sample. All dilutions were made in 5% HNO_3 (Optima-grade Fisher Scientific Nitric Acid and UltraTrace water, Fisher Scientific) on a weight-to-weight basis using calibrated analytical balances. U233, U234, and U236 were analyzed using a 1:1,000 dilution, U235 was analyzed using a 1:100,000 dilution, and U238 was analyzed using a 1:10,000,000 dilution.

The QICPMS instrument was calibrated using an external calibration curve. Calibration of the instrument is performed daily, and calibration standards are run prior to analyzing the samples. Non-radiological standards for the QICPMS analysis were prepared from stock solutions (High Purity Standards, 10 ug/g) and diluted to prepare working calibration standards with concentrations between 0–10 ng/g. The enriched uranium check standard (EUCS) was used to calibrate the instrument for U; the concentrations of the U isotopes were obtained from a multi-collector MCICPMS analysis and were measured against the Certified Reference Material (CRM) 125A traceable standard (New Brunswick Laboratory). The EUCS consisted of 0.69 U234, 69.36 U235, 0.37 U236, and 29.58 U238 wt%. For U, a four-point calibration curve was used with concentrations of the U isotopes varying between 0–20 ng/g. The calibration curve for U233 was assumed to be the same from U234, as this isotope is not present in the calibration standard.

After the measurements for a group of analytes were completed, a check standard with known concentrations of the analytes was measured to confirm that the calibrations were constant over the course of a run. For U, a depleted U standard was used from High Purity Standards because no independent standard is readily available for other isotopes of U. The concentration of the check standard was measured to be identical to the expected concentration within the uncertainty of the measurement (± 5%).

An internal standard was used in the analysis. Internal standards are used to account for plasma fluctuations and sample introduction deviations throughout the analysis. This is accomplished by adding an identical concentration of the internal standard to the calibration standards, samples, and blanks. The intensity of the internal standard is then normalized to the intensity of the element of interest. The internal standard Bi-209 was used for U. After the measurements for a given group of analytes were completed, a check standard with a known concentration of the analytes was measured to confirm that the calibrations were constant over the course of a run. The check standards are prepared in the same way as the calibration standards and were independent from the standards used to calibrate the instrument.

The uncertainty in the Q-ICP-MS measurements has been estimated using GUM Workbench Pro version 2.4.1.406 software. All reported uncertainties are 2-sigma values. The uncertainty has been estimated for two cases: one where the uncertainty in the signal intensity is small (less than 5% of the measured value) and one where it is large (greater than 5% of the measured value). The signal for each isotope was measured three times, from which the average values and relative standard deviations were calculated. For measurements which had low relative instrumental uncertainty, the uncertainty from the calibration and uncertainties in the sample weights and dilutions tended to dominate. This error has been estimated to be less than 5% at 2-sigma. The minimum reported uncertainty is ± 5%. For measurements in which the uncertainty in the signal intensity is greater than 5%, this source of uncertainty tends to dominate, and the uncertainty is rounded up to the nearest 5%. For example, an uncertainty of 7% would be rounded to 10%. If the signal intensity uncertainty was above 35% of the measured value, it was changed to a "less than" the MQL, and the uncertainty was reported as not applicable (N/A).

The MQL is the smallest concentration that can be accurately determined by the analytical method. For the QICPMS analysis, the measured intensity (in counts per second [cps]) of a sample is considered different from the intensity of the background when it was larger than the intensity of the background plus the standard deviation in the intensity of the background multiplied by 15, constituting the instrumental quantification limit (IQL). Assuming a Gaussian distribution, the chance of this occurring randomly is vanishingly small. For example, if the background intensity was measured to be 100 cps with a standard deviation of 10 cps, then the intensity of a sample must be at least 250 cps to be considered quantifiable from the background. The background intensity and standard deviation for a given mass in the QICPMS spectrum were determined by measuring the intensity of at least three instrumental blanks. The instrumental blanks consisted of the 5% nitric acid solution used to dilute the samples with internal standard added. To convert this to a concentration in the sample, the background intensity was taken to be zero (the background intensity was subtracted from the intensity of any samples). The IQL was then multiplied by the calibration constant and dilution factors, and the MQL was obtained. The MQL was influenced by not only the calibration constant but also by the factor in which the samples were diluted.

2.2.1.3. Chemical Separations

After dissolution, an aliquot of each parent solution was submitted to chemical separations. The goal of the separations was to remove the U from the matrix prior to analysis by ICP-OES. U has a rich emission spectrum which can interfere with the determination of other analytes of interest, particularly if they are present in only trace quantities and the U concentration is expected to be large. The separations were carried out using a technique called automated gas-pressurized extraction chromatography (auto-GPEC) per procedure AL4270OI001. The GPEC is a series of switchable valves connected by lengths of tubing. Inside one of these tubes is a resin to which elements of interest may or may not adhere, depending on the chemical matrix of the sample and type of resin used in the column. The sample is loaded into a length of tubing using a peristaltic pump (typically 0.5 mL), and a valve switches/rotates, opening a pressurized-gas line. The sample is pushed through the chromatographic column by the pressurized gas, and the eluate is collected on the other side. To remove the U, a 100–150 µm resin (Uranium and Tetra Valent Actinides [UTEVA], Eichrom) was employed as the stationary phase. In this separation process, the U was selectively retained to the stationary phase, and the other elements of interest in this study were eluted and collected for analysis.

Prior to separation, a threefold quantitative dilution was performed on a 0.5 mL aliquot of the parent solution using 6N HNO_3. This was done to keep the U concentration lower than 6000 µg/g to keep from overloading the column. Approximately 0.5 mL of the diluted sample was eluted through the GPEC UTEVA column where the U was retained. Two rinses (6M HNO_3) of 0.5 mL each were eluted through the column and collected in the same tube as the eluate from the sample loading step prior. The total final volume of the collected sample for ICP-OES analysis was approximately 1.5 mL. The rinses were done to quantitatively ensure that all the analytes had been removed from the column and to ensure that there was enough sample volume for the ICP-OES analysis. After the rinses, the U was removed from the column using 1% H_2SO_4 / 0.05 N HNO_3 to prepare it for use on the next sample.

To evaluate the separation efficiency and/or analyte loss due to interaction with the column, an aliquot of the samples was spiked with the requested analytes prior to the separation. Some analytes could not be added to the same samples due to their spectral overlap in the areas of interest. For this set of samples, there was a spike containing Fe, K, Li, magnesium (Mg), and Na, and a separate spike containing calcium (Ca), bismuth (Bi), cobalt (Co), lead (Pb), tin (Sn), and Zn, a third spike containing copper (Cu), Thorium (Th), vanadium (V), and tungsten (W), and a final spike that contained only titanium (Ti). ICP-OES analysis of the spiked samples showed quantitative recovery for the spiked elements, indicating that these elements were not retained during separation.

2.2.1.4. ICP-OES Analysis

The ICP-OES analysis was carried out on a Teledyne Leeman Prodigy ICP-OES per procedure AL-3300-OI-001. The instrument passed a daily performance check before analysis began. Before the ICP-OES was turned on, the Ar pressure was verified to be between 80 to 90 psi, the water level for the camera chiller was between the specified notches, and the temperature around the camera/optics was within the desired range. After instrument warm-up, a 10 µg/g manganese (Mn) standard was used to optimize the plasma viewing position. The spectrograph was checked for proper alignment using a mercury (Hg) lamp.

The samples and reagent blank were analyzed for several impurities, which included Ca, Fe, and Mg. In addition to the impurities, the concentration of U was measured. The concentration of the impurities was measured using a sample that had the U removed from the matrix by GPEC separation. Samples which had not undergone separations were used to measure Na a second time and U. For the unseparated samples, duplicate analyses were performed; for the separated samples, only one analysis was performed due to the lengthy sample preparation process involved. The reagent blank was found to be free from the above analytes within the MQL of the analysis. The concentrations of the impurities were found to be less than the MQL of the analysis for each sample.

For the separated samples, no further dilutions were performed. The dilution factor for these samples was about 9 from the parent solution. The samples that had not undergone separations were diluted by a factor of 100 from the parent solution. All dilutions were made in 6 M HNO_3 (Optima-grade Fisher Scientific Nitric Acid and UltraTrace water, Fisher Scientific) on a weight-to-weight basis using calibrated analytical balances.

The ICP-OES calibration was done externally. Calibration of the instrument was performed daily, and calibration standards were run prior to analysis of the samples. For the non-radiological elements, working calibration standards were prepared from a multielement stock standard (Inorganic Ventures) with concentration of the elements in the stock standard ranging from 40 to 150 µg/g. The working calibration standards were made in 6 M HNO_3. For the impurities, a five-point calibration curve was used. For U, a 1000 µg/g stock standard from Inorganic Ventures was diluted to make working standards in 6 M HNO_3. A three-point calibration curve was used with concentrations between 0 and 21 µg/g of U. Quality control check standards were run just after the calibration was completed and after the samples were analyzed. For the impurities, check standards were prepared from a multielement stock standard (High Purity Standards). For U, a check standard with a concentration similar to that measured in the samples was prepared. For all elements analyzed here, the concentration of the check standards were measured to be within the expected concentration and the associated uncertainty of the measurement (± 5–8%).

The uncertainty in the ICP-OES measurements was estimated using GUM Workbench Pro version 2.4.1.406 software. All reported uncertainties are 2-sigma values. The uncertainty was estimated for two cases: one where the uncertainty in the signal intensity was small (less than 5% of the measured value) and one where it was large (greater than 5% of the measured value). The signal for each element was measured three times, from which the average values and relative standard deviations were calculated. For measurements which had low relative instrumental uncertainty, the uncertainty from the calibration and uncertainties in the sample weights and dilutions tend to dominate. This error has been estimated to be less than 5% at 2-sigma. The minimum reported uncertainty is ±5%. For measurements in which the uncertainty in the signal intensity is greater than 5%, this source of uncertainty tends to dominate, and the uncertainty is rounded to up to the nearest 5%. For example, an uncertainty of 7% would be rounded to 10%. If the uncertainty in the signal intensity was above 35% of the measured value, it was changed to a "less than" the MQL, and the uncertainty was reported as N/A.

The MQL is the smallest concentration that can be accurately determined by the analytical method and has been defined in two ways for the ICP-OES measurements. The first method is identical to that outlined above for Q-ICP-MS. The second is to account for bias or non-linearity in the calibration curve for concentrations near the MQL. The larger of these two values was reported. For the ICP-OES method, there is likely bias in the calibration curves near the detection limit for the elements measured. This became apparent when comparing the concentrations of analytes between several different types of blanks (reagent, instrumental, and blanks run through the GPEC), since the calculated concentrations of these elements were nearly the same between them. According to the calibration curve, these elements were above the MQL as defined above (see Q-ICP-MS section 2.2.1.2).

To account for biases in the calibration curve near the MQL, the concentration of several blanks (of different types) was compared to the value measured in the sample. If the value measured in the sample was smaller than the blanks' values plus 50%, the value for the sample was reported as <MQL. In most cases, the MQLs calculated by either method were close to each other. Check standards with concentrations bracketed by the calibration curve did not show bias, within the uncertainty of the measurement.

2.2.2. Results of Elemental Analysis

Triplicate elemental and isotopic results from the QICPMS and ICP-OES for the UF_4 samples are provided in Table 4 and Table 5, respectively. The ICP-OES only detected copper as an impurity, and U was not detected as it was separated from the samples. Based on the elemental and isotopic analysis of the salt, there are no major impurities, and the salt only contains detectible amounts of U. Mass balance suggests there was a 97.1% recovery of the sample.

Table 4. Isotopic analysis of UF_4 performed using ICP-MS.

AL #	U-235 ug/g	U-238 ug/g	U-235 g/g	U-238 g/g	U235-F_4 g/g	U238-F_4 g/g	**UF_4 - total g/g**

109876	1540	737000	0.00154	0.737	0.0020	0.9723	**0.9744**
109877	1510	734000	0.00151	0.734	0.0020	0.9684	**0.9704**
109878	1520	733000	0.00152	0.733	0.0020	0.9670	**0.9691**
Average	1523.33	734666.7	0.00	0.73	0.00	0.97	**0.9713**
Std	15.28	2081.67	0.00	0.00	0.00	0.00	**0.00**
RSD, %	1.00	0.28	1.00	0.28	1.00	0.28	**0.28**

Table 5. Elemental analysis of UF_4 performed using ICP-OES—after UTEVA separation (ug/g).

	109876		109877		109878	
Analyte	Results	Error	Results	Error	Results	Error
Be	<10	N/A	<10	N/A	<10	N/A
Bi	<65	N/A	<50	N/A	<55	N/A
Ca	<55	N/A	<55	N/A	<60	N/A
Cd	<20	N/A	<20	N/A	<20	N/A
Ce	<45	N/A	<45	N/A	<45	N/A
Co	<15	N/A	<15	N/A	<20	N/A
Cr	<10	N/A	<10	N/A	<10	N/A
Cu	8.47	± 25 %	<10	N/A	9.7	± 25 %
Fe	<15	N/A	<15	N/A	<20	N/A
Mg	<25	N/A	<20	N/A	<25	N/A
Mn	<5	N/A	<5	N/A	<5	N/A
Mo	<35	N/A	<35	N/A	<35	N/A
Na	<25	N/A	<35	N/A	<50	N/A
Nd	<10	N/A	<10	N/A	<10	N/A
Ni	<440	N/A	<430	N/A	<460	N/A
Pb	<350	N/A	<340	N/A	<370	N/A
Sn	<500	N/A	<500	N/A	<530	N/A
Th	<25	N/A	<25	N/A	<25	N/A
Ti	<5	N/A	<5	N/A	<5	N/A
U	<210	N/A	<210	N/A	<220	N/A
V	<5	N/A	<5	N/A	<5	N/A
W	<380	N/A	<380	N/A	<400	N/A
Zn	<10	N/A	<10	N/A	<10	N/A
Zr	<10	N/A	<10	N/A	<10	N/A
Uranium cannot be reported. Thorium cannot be reported. Recovery from spiked sample was low (30%) due to interaction with the column.						

3. PHASE DIAGRAM STUDY

3.1. Ternary Sample Preparation

The PCG is an MBRAUN, Ar glovebox whose atmosphere is maintained at less than 10ppm O_2 (typical operating range is 1–4ppm) and less than 0.5ppm H_2O (typical operating range is <0.1–0.2ppm). Oxygen and moisture content of the PCG atmosphere were monitored at the beginning of each session working in the box, as well as any time material was transferred into or out of the box, and when any other events occurred that could potentially cause a perturbation of the atmosphere to ensure the atmosphere stayed within an acceptable range while the salts were being utilized.

In total, seven Seaborg salt samples with compositions were made and are listed in Table 6. These UF_4 based salt ingots were fabricated to aid in the development of a phase diagram. The masses of salts used are provided Table 6. Melt temperature analysis was performed on all Seaborg 1-7 samples. All mass measurements were made on an Ohaus EX324 Explorer Analytical balance with a tolerance of +/-0.0009g whose calibration was checked daily by running an internal calibration and then confirming with 1g, 10g, and 200g standard calibration weights.

Table 6. Composition of Seaborg samples used for melting temperature analysis.

Sample Name	Composition (mol%)	UF_4 g	KF g	NaF g	Total g
Seaborg 1	$32.8UF_4$-22.2KF-45.0NaF	15.2835	1.9139	2.8036	20.0010
Seaborg 2	$28.5UF_4$-20.5KF-51.0NaF	14.5734	1.9393	3.4868	19.9995
Seaborg 3	$25.0UF_4$-25.0KF-50.0NaF	13.7638	2.5476	3.6827	19.9941
Seaborg 4	$22.5UF_4$-27.5KF-50.0NaF	13.1304	2.9688	3.9020	20.0012
Seaborg 5	$24.0UF_4$-25.5KF-50.5NaF	13.5325	2.6591	3.8073	19.9989
Seaborg 6	$26.8UF_4$-24.4KF-48.8NaF	14.1412	2.4098	3.4492	20.0002
Seaborg 7	$26.4UF_4$-24.7KF-48.9NaF	14.0773	2.4366	3.4865	20.0004

UF_4 was weighed out in the PCG and combined with the previously weighed NaF and KF components, mixed thoroughly, transferred to a nickel crucible (low form, 55mL capacity, Sigma Aldrich) or glassy carbon crucible, heated to 650–875°C, and held at temperature for approximately 120 minutes. Seaborg-1 to Seaborg-4 was prepared in a nickel crucible while Seaborg-5 to Seaborg-7 were prepared in a glassy carbon crucible. Each ingot was left in the furnace to cool overnight. Photographs of some Seaborg salt compositions are provided in Figure 5.

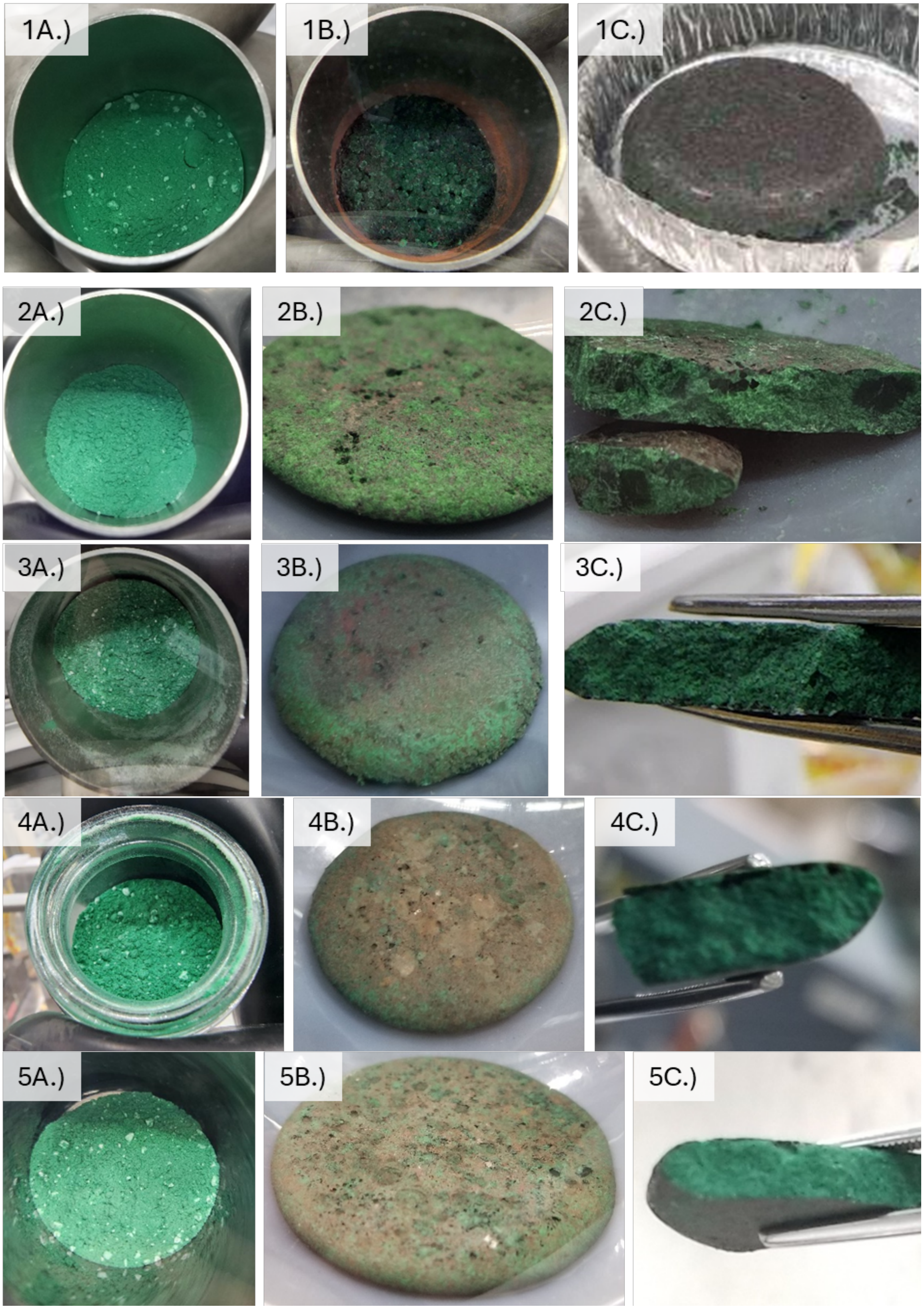

Figure 5. Seaborg composition 1 (1A–1C) thru composition 5 (5A–5C). (A) is the salt composition prior to heating, (B) mini-ingot after melting salt, and (C) inspection of mini-ingot prior to crushing.

After removal from the furnace, the Seaborg 1 sample released easily from the crucible. There appeared to have been some minor reaction with the crucible surface since there was a reddish-orange ring above the top of the ingot on the interior walls of the crucible (see Figure 5, 1B), but this did not appear to continue into the ingot itself. The top and interior of the ingot were a bright green color, while the bottom was darker brownish green. The Seaborg 2 sample released easily from the crucible after heating. There did not appear to be any reaction with the crucible surface, and the ingot had very little of the reddish-brown color seen earlier. The surfaces of the ingot appeared to have several visible phases, and when the ingot was broken open, there were large, distinct phases. The top and interior of the ingot were bright green, while the bottom was a brownish green.

The Seaborg 3 sample released from the crucible after heating as easily as the previous two ingots. There was no visible reaction with the crucible surface, although there were some reddish-brown areas on the top and bottom of the ingot as seen in the photographs 3B–3C in Figure 5. The ingot appeared much more homogeneous than the previous two samples, both on the external structure and the interior, which was highly uniform. The Seaborg 4 released well from the crucible after heating. There was a reddish-brown coating on most of the exterior and along the inside of the crucible where UF_4 had settled prior to being heated. The interior was very even with a uniform green coloring and apparently homogenous structure. When broken into pieces, the ingot had a bright green interior and was highly uniform.

The top of the Seaborg 5 ingot had a brownish-green top and bottom. The surfaces of the ingot were relatively uniform with small, shallow holes throughout. When broken into pieces for sampling and storage, the interior was a bright green color with highly uniform distribution. The ground sample had a bright green color. The interior of the Seaborg 6 ingot was a moderately dark green color. There was some reddish-orange residue on the walls of the glassy carbon crucible, as seen in previous runs, but it was minimal. The Seaborg 7 ingot had a slight brownish-orange color on top, while the bottom was bright green with some crystalline-appearing inclusions. When the ingot was broken into pieces, the internal structure had a very uniform appearance. A sample of each ingot and one of UF_4 were ground in an agate mortar and pestle, stored in its own glass vial, and transferred to the ARL for melt temperature analysis. Figure 6 shows a representative ground sample (Seaborg 1) that was used for melt temperature analysis. The remainder of each sample ingot was placed in a threaded glass jar and sealed in a metal paint can in the PCG to protect the integrity of the sample for future use.

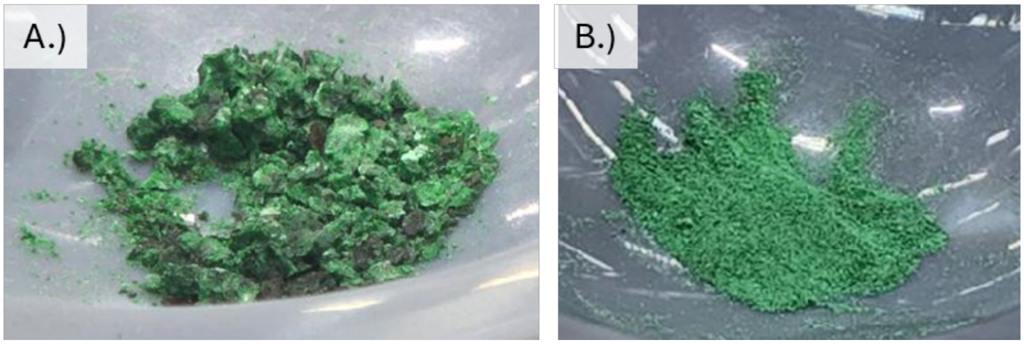

Figure 6. Representative (A) crushed and (B) powdered ingot sample (Seaborg 1), showing the bright green color of UF_4.

3.2. Analysis of Ternary Salts

Each sample was run on the STA to determine the stability and melting temperature. The STA can measure heat flow and mass change simultaneously. The STA was operated inside an Ar atmosphere glovebox using ultra-high-purity Ar protective gas and purge gas with a flow rate of 50 and 20 mL/min, respectively. Non-reactive, unsealed glassy carbon crucibles with glassy carbon lids containing a small hole were used for all calibration standards and samples. Since analysis of the samples spanned several months, several calibrations on the STA were made. They will not be summarized here, but the same procedure was followed as described in Section 4.2.1. Samples were run using a temperature and sensitivity calibration, accurate in the range of 20 to 950°C, generated using five high-purity calibration standards with heating rates of 20, 10, and 2°C/min.

A plot of the mass change as a function of temperature is provided for each of the seven Seaborg samples in Figure 7, and a summary of the mass changes is provided in Table 7. The mass change curves, in this case, should be viewed as semi-quantitative because a baseline run (i.e. two empty crucibles) was not preformed prior to running each sample. However, less than a 1% mass loss was seen for all samples.

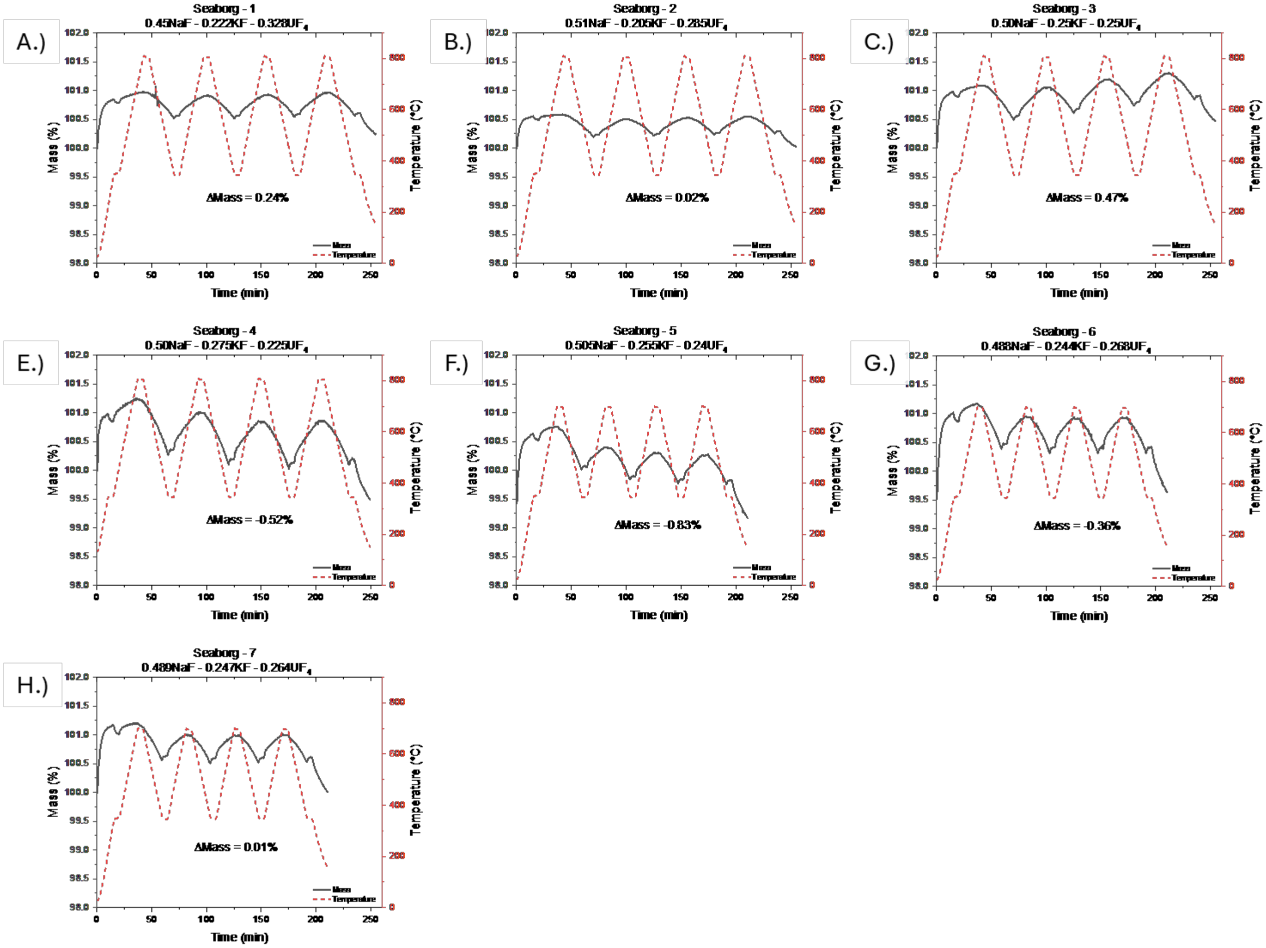

Figure 7. Mass change curves for all seven Seaborg samples, collected using a 20°C/min heating/cooling rate. Note: baselines were not run; therefore, the samples show some buoyance effects.

Table 7. Summary of mass change data determined using the plots from Figure 7.

Seaborg Sample	Starting Mass	Mass change, %	Mass Change, mg	Start T	End T	Temperature Range
	mg	%	mg	°C	°C	°C
1	64.5	0.2442	0.1575	25.2	149.9	340 – 810
2	84.5	0.0272	0.0230	28.6	154.1	340 – 810
3	50.4	0.4702	0.2370	26.3	151.1	340 – 810
4	30.9	-0.5113	-0.1580	136.1	149.7	340 – 810
5	38.9	-0.8278	-0.3220	24.6	146.3	345 – 700
6	47.1	-0.3626	-0.1708	26.9	156.7	345 – 700
7	60.3	0.0100	0.0060	27.8	156.2	345 – 700

Melting temperature analysis was performed by heating all Seaborg samples at three heating rates, 20, 10, and 2°C/min. Figure 8 is a summary of the Seaborg samples showing the heat flow curve for each at a heating rate of 2°C/min. The liquidus temperature (endset, end of final peak) for each sample is provided in Figure 8 along with labels of the peaks. Peaks were labeled to show similarities among samples. As an example, Seaborg 1, 2, 6, and 7 are labeled with a peak 1 (P1) which occurs at approximately 469 °C while Seaborg samples 3–5 do not show this transition occurring. P2 occurs in some samples at approximately 496°C while P3 occurs at 545°C. P5 is labeled as the liquidus peak for each sample, and the temperature of this peak varies. A summary of the peak temperatures for the data shown in Figure 8 is provided in Table 8.

Previous studies by Fache et al. [2] report two eutectic compositions, NaF-KF-UF_4 (55.6-18.7-25.7 mol%) and NaF-KF-UF_4 (50.4-23.2-26.4 mol%), at melting points of 536 and 537 ± 5°C. Seaborg 6, NaF-KF-UF_4 (48.8-24.4-26.8 mol%) and Seaborg 7, NaF-KF-UF_4 (48.9-24.7-26.4 mol%) are close in composition to the second eutectic reported by Fache et al. and have a melting temperature of 558 and 562 ± 5°C, respectively. The melting temperature of samples reported in this work are slightly higher than those reported in Fache et al.'s work possibly due to the slight composition difference, but it is most likely due to the Schacherl et al. [1] using the onset temperature of the liquidus peak rather than the peak or endset temperature, both of which are reported in this work. It should be noted that Schacherl et al. used the offset of the liquids if a shoulder was present, but for eutectics the onset temperature was used.

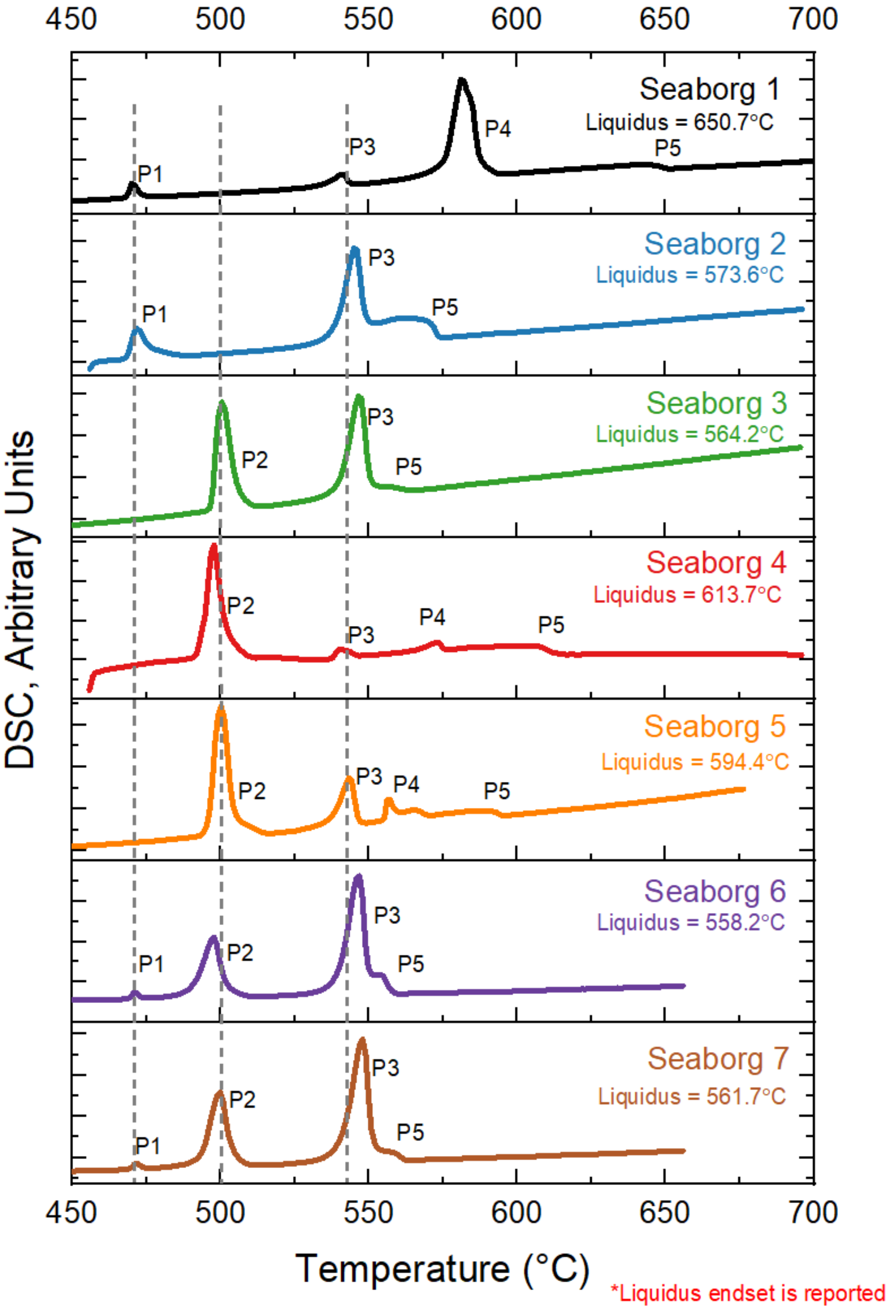

Figure 8. Summary of melting temperature curves for Seaborg samples determined using a heating rate of 2°C/min.

Table 8. Summary of data extracted from Figure 8 for Seaborg samples 1–7.

Seaborg 1

	Peak 1	Peak 2	Peak 3	Peak 4	Peak 5 (peak)	Peak 5 (endset)
Cycle 1	468.5	na	541.2	581.5	642.6	650.7
Cycle 2	468.5	na	540.4	581.6	642.2	650
Cycle 3	468.5	na	537	583.2	643.2	651.4
Average	468.5	-	539.5	582.1	642.7	650.7
Stdev	0.00	-	2.23	0.95	0.50	0.70
RSD, %	0.00	-	0.41	0.16	0.08	0.11

Seaborg 5

	Peak 1	Peak 2	Peak 3	Peak 4	Peak 5 (peak)	Peak 5 (endset)
Cycle 1	na	496	543.6	556.7	592.9	593.9
Cycle 2	na	495.9	543.6	556.6	593	594.7
Cycle 3	na	495.9	543.5	556.6	593.7	594.7
Average	-	495.9	543.6	556.6	593.2	594.4
Stdev	-	0.06	0.06	0.06	0.44	0.46
RSD, %	-	0.01	0.01	0.01	0.07	0.08

Seaborg 3

	Peak 1	Peak 2	Peak 3	Peak 4	Peak 5 (peak)	Peak 5 (endset)
Cycle 1	468.6	NA	545.4	NA	566.1	573.5
Cycle 2	ND	NA	545.8	NA	569.7	573.9
Cycle 3	ND	NA	545.7	NA	567.4	573.4
Average	468.6	-	545.6	-	567.7	573.6
Stdev	-	-	0.21	-	1.82	0.26
RSD, %	-	-	0.04	-	0.32	0.05

Seaborg 6

	Peak 1	Peak 2	Peak 3	Peak 4	Peak 5 (peak)	Peak 5 (endset)
Cycle 1	469.1	497.7	546.5	NA	553.4	557.9
Cycle 2	469.2	497.6	546.6	NA	553.9	558.5
Cycle 3	468.9	497.7	546.6	NA	554.2	558.3
Average	469.1	497.7	546.6	-	553.8	558.2
Stdev	0.15	0.06	0.06	-	0.40	0.31
RSD, %	0.03	0.01	0.01	-	0.07	0.05

Seaborg 3

	Peak 1	Peak 2	Peak 3	Peak 4	Peak 5 (peak)	Peak 5 (endset)
Cycle 1	NA	496.6	546.6	NA	ND	563.8
Cycle 2	NA	497	546.9	NA	ND	564
Cycle 3	NA	496.9	546.8	NA	ND	564.9
Average	-	496.8	546.8	-	-	564.2
Stdev	-	0.21	0.15	-	-	0.59
RSD, %	-	0.04	0.03	-	-	0.10

Seaborg 7

	Peak 1	Peak 2	Peak 3	Peak 4	Peak 5 (peak)	Peak 5 (endset)
Cycle 1	469.3	499.9	547.9	NA	558.9	561.7
Cycle 2	469.2	499.7	547.7	NA	558.9	562.3
Cycle 3	468.9	499.7	547.6	NA	558.9	561.2
Average	469.1	499.8	547.7	-	558.9	561.7
Stdev	0.21	0.12	0.15	-	0.00	0.55
RSD, %	0.04	0.02	0.03	-	0.00	0.10

Table 8. Continued.

Seaborg 4						
	Peak 1	Peak 2	Peak 3	Peak 4	Peak 5 (peak)	Peak 5 (endset)
Cycle 1	na	493.9	540.1	573.2	605.6	613.4
Cycle 2	na	493.1	540.1	753.5	603.7	613.6
Cycle 3	na	492.9	538.6	573.6	604.4	614
Average	-	493.3	539.6	633.4	604.6	613.7
Stdev	-	0.53	0.87	103.98	0.96	0.31
RSD, %	-	0.11	0.16	16.42	0.16	0.05

ND – Not Determined from data

NA – Not applicable from data

By plotting the liquidus temperature (endset) as a function of UF_4 concentration (mol%), the eutectic composition may be predicted to have 26.9 mol% UF_4; see Figure 9. However, this is only a prediction and has not been verified. Further literature data suggests the ternary eutectic composition contains lower amounts of UF_4. Additionally, Figure 9 does not consider the ratio of NaF to KF, again emphasizing that the predicted UF_4 concentration should only be viewed as an approximation.

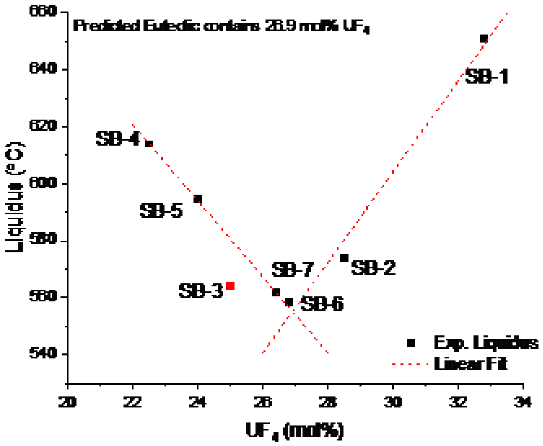

Figure 9. Proposed UF_4 concentration in ternary eutectic salt determined by the UF_4 concentration in the Seaborg samples and their melting temperatures.

While Seaborg 6 was determined to have a slightly lower melting temperature, the team of researchers at INL, under the guidance of Seaborg, moved forward determining the properties on salt having the same composition as Seaborg 7. In the subsequent section, the preparation of the bulk Seaborg 7 salt is discussed along with the methodology and results for each thermal and chemical property measured.

4. PROPERTY DETERMINATION – SEABORG 7

4.1. Preparation of Bulk Seaborg 7

Based on melting point analysis, Seaborg 7 was determined to be at or close to the ternary eutectic. Four 100g ingots were prepared in a glassy carbon crucible for further thermal property analysis. The mass of individual salts used to make each ingot is provided in Table 9. The interior walls of the crucible had a more significant coating of brownish-orange residue after Seaborg 7A was heated in the furnace than in earlier runs (see Figure 10B). The heating program for each Seaborg 7 ingot is provided in Table 10. The top of the ingot had a needle-like crystalline structure with a homogenous bottom, as seen in Figure 10C–D, respectively. The green color was even throughout the ingot.

Table 9. Summary of masses used to make the bulk Seaborg-7 samples that were combined and used for thermal property determination.

Component	Target Mass (g)	Seaborg 7A Actual Mass (g)	Seaborg 7B Actual Mass (g)	Seaborg 7C Actual Mass (g)	Seaborg 7D Actual Mass (g)
UF_4	70.3847	70.3852	70.3851	70.3845	70.3848
KF	12.1833	12.1836	12.1829	12.1831	12.1830
NaF	17.4320	17.4327	17.4321	17.4324	17.3425
Total (Initial)	100.0000	100.0015	100.0001	100.0000	100.0003
Total (After Heating)	100.0000	99.6002	99.5058	99.5530	ND

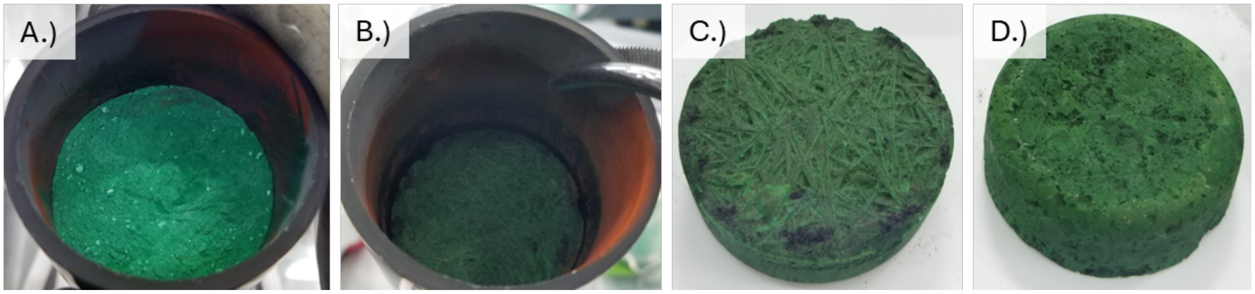

Figure 10. Seaborg 7A: (A) inside the crucible prior to heating; (B) inside the crucible after removal from the furnace; (C) top view after consolidation; (D) bottom view after consolidation.

Table 10. Heating profile for blending the three components (NaF, KF, UF_4) to make the bulk Seaborg-7 salt used for thermal property measurements.

Temp (°C)	Temp (°F)	SB-Comp 7A Hold Time (mins)	SB-Comp 7B Hold Time (mins)	SB-Comp 7C/D Hold Time (mins)
250	482	20	20	25
500	932	20	20	15
750	1382	20	70	15
875	1607	100	185	105

Seaborg samples 7B, 7C, and 7D were prepared using the same process given above. The appearance of all three ingots was similar to that of ingot A with its needle-like crystalline top and uniform color. However, there was a significantly smaller amount of orange residue on the crucible wall for these three runs. The Seaborg ingots (7A–7D) were crushed separately with an agate pestle in a steel jar and were all combined into a single container as shown in Figure 11. From the bulk Seaborg 7 material, subsamples were removed packaged into individual containers, placed in bags, and vacuum sealed into a secondary bag to prepare for transfer to respective facilities, for property measurements as summarized in Table 11.

Please note that the Seaborg-7 bulk salt samples were never sent for elemental analysis but have been reserved for analysis upon collaborator request.

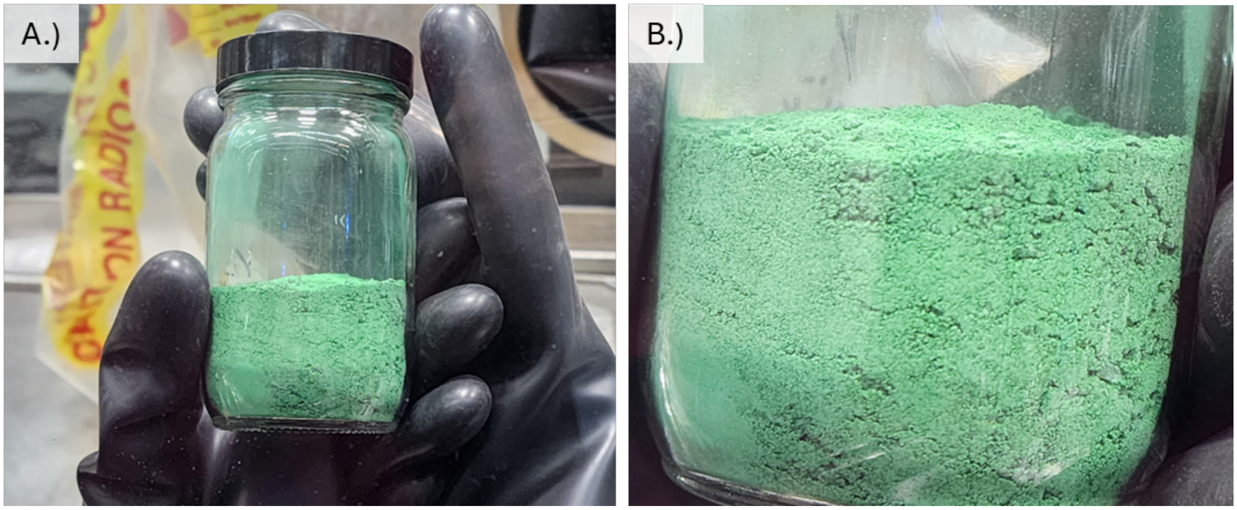

Figure 11. Photographs of the Seaborg-7 bulk salt used to thermal property measurements. Ingots from Seaborg 7A–7D were crushed and mixed together.

Table 11. List of samples needed for thermal property measurements.

Property	Mass (g)	Transfer Facility
Elemental Analysis	0.9857	Analytical Laboratory (AL)
	1.2959	
	0.9658	
Density (Liquid)	80.4609	Fuel Manufacturing Facility (FMF)
Melting Temperature, Enthalpy, and Specific Heat Capacity	2.1069	Analytical Laboratory–Fresh Fuels Glovebox (AL-FFGB)
Thermal Diffusivity	25.4104	Fuels & Applied Science Building (FASB)
Viscosity & Density (Solid)	218.74	Fuel Conditioning Facility (FCF)

4.2. Melting Temperature and Enthalpy of Fusion

4.2.1. Calibration and Methodology

A sample of the Seaborg-7 bulk material was transferred to the Fresh Fuels Glovebox (FFGB) at MFC for melting temperature analysis using the STA model STA449F1 containing a type-S, DSC-thermogravimetric (TG) sample carrier and rhodium furnace. The STA is capable of collecting thermal analysis DSC and TG data simultaneously for each sample calibrated. The STA was operated inside an Ar atmosphere glovebox using ultra-high-purity Ar protective gas and purge gas with a flow rate of 50 and 20 mL/min, respectively. Non-reactive, unsealed glassy carbon crucibles with glassy carbon lids containing a small hole were used for all calibration standards and samples. Samples were run using a temperature and sensitivity calibration, accurate in the range of 20 to 950°C, generated using five high-purity calibration (Table 12) standards with heating rates of 20, 10, and 2°C/min.

Table 12. Standards used to calibrate the STA.

	Standard	Transition Temperature, °C	Enthalpy, J/g
Std 1	In	156.6	28.6
Std 2	Bi	271.4	53.1
Std 3	Zinc (Zn)	419.5	107.5
Std 4	Aluminum (Al)	660.6	397
Std 5	Silver (Ag)	961.8	104.6

Table 13 is a summary of the temperature and heat flow calibration for the STA. The transition temperature and peak area (heat flow) of each standard were calculated by averaging the onset and peak area for three heating cycles. The average value was then used in the calibration file generated for each heating rate. The accuracy of the temperature and heat flow calibration curve was verified using Zn and Al standards (see Table 14). Verification of the calibration curves at each heating rate showed that the STA was calibrated to have deviation in the melting temperature from theoretical values of less than 1%, and the heat flow was calibrated to be less than 2% for Zn, providing confidence that the reported transition temperature and enthalpy for NaF-KF-UF_4 (Seaborg 7) samples were accurate within 1% on melting temperature and 2% for enthalpy (heating curves).

Table 13. Summary of transition temperatures and peak areas (heat flow) for the STA calibration standards.

In Standard						
	Temperature (°C)			Heat Flow (J/g)		
Heating Rate °C/min	20	10	2	20	10	2
Cycle 1	156.5	156.1	155.4	26.180	26.970	27.270
Cycle 2	156.2	156.0	155.4	26.000	26.990	27.340
Cycle 3	156.3	156.2	155.5	26.240	26.900	27.340
Avg	156.3	156.1	155.4	26.1	27.0	27.3
Stdev	0.15	0.10	0.06	0.12	0.05	0.04
RSD (%)	0.10	0.06	0.04	0.48	0.18	0.15
Bi Standard						
	Temperature (°C)			Heat Flow (J/g)		
Heating Rate °C/min	20	10	2	20	10	2
Cycle 1	273.0	271.4	269.7	41.720	41.890	42.380
Cycle 2	272.3	271.6	269.7	41.560	41.990	42.380
Cycle 3	272.7	271.6	269.7	41.480	42.010	42.610
Avg	272.7	271.5	269.7	41.6	42.0	42.5
Stdev	0.35	0.12	0.00	0.12	0.06	0.13
RSD (%)	0.13	0.04	0.00	0.29	0.15	0.31
Zn Standard						
	Temperature (°C)			Heat Flow (J/g)		
Heating Rate °C/min	20	10	2	20	10	2
Cycle 1	418.4	417.5	416.7	67.030	65.780	66.340
Cycle 2	418.3	417.6	416.7	66.710	66.190	66.800
Cycle 3	418.3	417.6	416.7	66.470	66.640	65.890
Avg	418.3	417.6	416.7	66.7	66.2	66.3
Stdev	0.06	0.06	0.00	0.28	0.43	0.46
RSD (%)	0.01	0.01	0.00	0.42	0.65	0.69
Al Standard						
	Temperature (°C)			Heat Flow (J/g)		
Heating Rate °C/min	20	10	2	20	10	2
Cycle 1	659.2	657.8	657.0	136.700	138.600	140.500
Cycle 2	659.4	657.9	657.0	137.000	138.900	140.800
Cycle 3	659.2	658.0	657.2	138.000	138.600	140.700
Avg	659.3	657.9	657.1	137.2	138.7	140.7
Stdev	0.12	0.10	0.12	0.68	0.17	0.15
RSD (%)	0.02	0.02	0.02	0.50	0.12	0.11

Table 13. Continued.

Ag Standard						
	Temperature (°C)			Heat Flow (J/g)		
Heating Rate °C/min	20	10	2	20	10	2
Cycle 1	957.9	957.7	957.2	25.150	25.760	25.770
Cycle 2	958.1	957.8	957.3	25.540	25.690	25.630
Cycle 3	958.2	957.8	957.4	25.550	25.620	25.470
Avg	958.1	957.8	957.3	25.4	25.7	25.6
Stdev	0.15	0.06	0.10	0.23	0.07	0.15
RSD (%)	0.02	0.01	0.01	0.90	0.27	0.59

Table 14. Results of calibration check.

Zn Heating						
	Temperature (°C)			Heat Flow (J/g)		
Heating Rate °C/min	20	10	2	20	10	2
Cycle 1	419.9	419.4	419.4	107	106.6	105.8
Cycle 2	419.8	419.4	419.4	105.8	106.3	106.8
Cycle 3	419.9	419.4	419.4	105.7	105	105.2
Avg	419.9	419.4	419.4	106.2	106.0	105.9
Stdev	0.058	0.000	0.000	0.723	0.850	0.808
RSD (%)	0.014	0.000	0.000	0.681	0.803	0.763
Deviation from Theoretical, %	**0.10**	**0.02**	**0.02**	**1.21**	**1.40**	**1.49**
Zn Cooling						
	Temperature (°C)			Heat Flow (J/g)		
Heating Rate °C/min	20	10	2	20	10	2
Cycle 1	414.0	416.1	418.4	-104.6	-104.7	-105.6
Cycle 2	413.8	416.2	418.4	-103.8	-104.4	-104.9
Cycle 3	413.8	416.3	418.4	-99.0	-103.3	-103.4
Avg	413.9	416.2	418.4	-102.5	-104.1	-104.6
Stdev	0.115	0.100	0.000	3.029	0.737	1.124
RSD (%)	0.028	0.024	0.000	-2.956	-0.708	-1.074
Deviation from Theoretical, %	**1.33**	**0.79**	**0.26**	**4.65**	**3.16**	**2.70**

During data collection and sample preparation, the glovebox atmosphere was maintained at less than 5 ppm O_2 and 0.1 ppm moisture. The reported polymorphic, eutectic, or melting-point temperatures were determined by averaging the onset temperature (first peak) and peak temperature (subsequent peaks) from three heating cycles. The averaged transition temperature for each sample was then plotted against the heat rate, and linear regression was used to remove the effects of thermal lag on the reported temperature value. Initially, a melting-point and stability analysis was performed on the Seaborg-7 sample to gain insight on purity.

4.2.2. Salt Stability

Prior to melting temperature and other TPP measurements, the stability of the salt at elevated temperatures was investigated by monitoring the mass change using the STA. Stability studies were performed by running a “correction” using two empty crucibles (i.e., sample and reference) under identical conditions to which the sample will be run. The goal of a baseline correction is to increase the measurement accuracy by subtracting the measurement without a sample from the measurement with a sample both carried out under identical measurement conditions. Once the correction file was generated, a sample was loaded into the same sample crucible used in the correction file.

Using a heating rate of 20°C/min the samples was heated to 900°C with a 5 minute isotherm (Figure 12) while the samples run with a heating rate of 10 and 2°C/min (Figure 12B–C) were subjected to lower temperatures. The TG curves in Figure 12A–C do not show any significant mass loss nor is there a “stairstep” of decreasing sample mass as a function of time. It can therefore be concluded that Seaborg 7 is stable up to 900°C. Each sample showed less than a 1% mass change confirming the sample was not volatile, there was no interaction between the sample and the glassy carbon crucible, and the purity of the atmosphere around the sample did not cause sample oxidation.

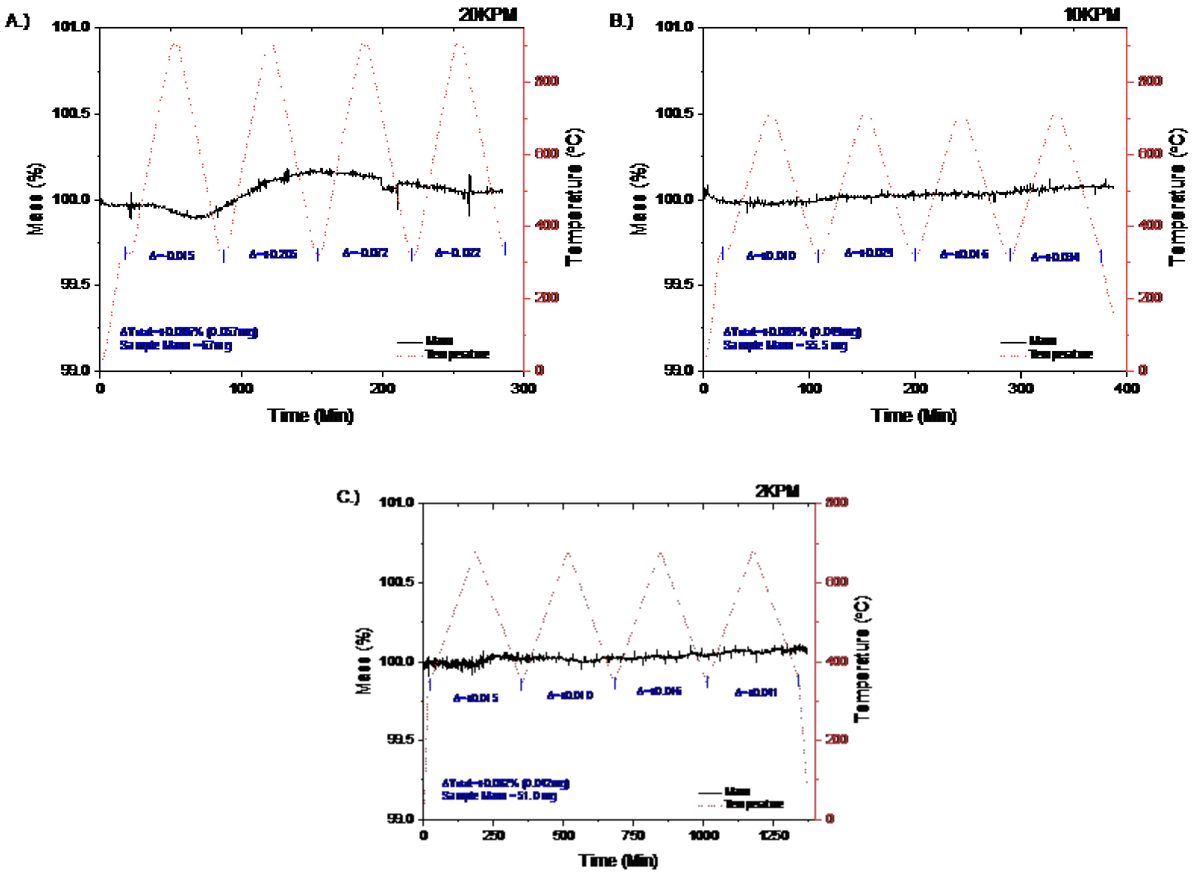

Figure 12. Mass changed curves as a function of time and temperature for the Seaborg 7: (A) 20°C/min, (B) 10°C/min, and (C) 2°C/min.

4.2.3. Melting Temperature

The melting point of the Seaborg-7 samples was investigated using three separate samples, each experiencing a different heating rate: 20, 10, and 2°C/min. Each sample was subjected to four heating and cooling cycles; the first was discarded, while inflections from the other three were averaged and used to report temperature-dependent transitions. The second heating thermogram for each heating rate is shown in Figure 13. As labeled in Figure 13, there were three distinct peaks: Peak 1 at 473°C, Peak 2 at approximately 505°C and Peak 3 at approximately 553°C. The peak occurring at 553°C with an endset temperature of 560°C represents the final transition of solid material into the liquid state. It was beyond the scope of work to identify the transitions occurring in the other peaks.

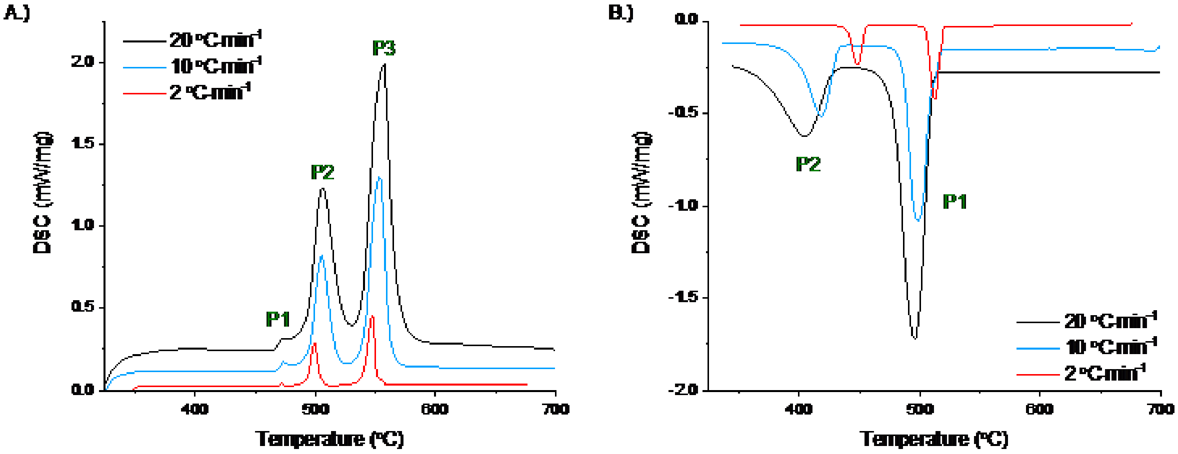

Figure 13. STA thermogram for three samples, each analyzed at a different heating rate.

A closer inspection of the sample response for each heating rate shows that decreasing the heating rate helps to resolve peaks and can aid in identifying overlapping peaks or peaks occurring close together, see Table 15 and Table 16. It can be seen from the 2°C/min heating curve in Figure 13 that a shoulder exists at the end of P3, indicating this sample is slightly off the eutectic composition. This is also supported by experiments run by others and indicated by Seaborg (collaborator) during discussions.

Table 15. Onset and area values determined from each heating cycle at 20 and 10°C/min rates with calculated averages and standard deviations.

20°C/min – Heating Data								
	Onset P1	Peak 1	P2 Onset	Peak 2	P3 Onset	Peak 3	Endset P3	Total Peak Area
	°C	°C	°C	°C	°C	°C	°C	J/g
1	466.3	473.8	492.8	506.7	536.8	556.3	566.7	165.4
2	466.4	473.9	492.6	516.3	537.1	556.6	567.0	164.1
3	466.5	473.8	492.6	506.3	536.8	556.9	567.6	165.9
Average	466.4	473.8	492.7	509.8	536.9	556.6	567.1	165.1
Stdev	0.100	0.058	0.115	5.662	0.173	0.300	0.458	0.929
RSD, %	0.021	0.012	0.023	1.111	0.032	0.054	0.081	0.563
20°C/min – Cooling Data								
	Onset P1	Peak 1	Onset P2	Peak 2	Peak 3	Total Peak Area	P1 Area	P2 Area
	°C	°C	°C	°C	°C	J/g	J/g	J/g
1	509.2	497.1	429.0	406.7	–	-136.9	-94.84	-44.84
2	509.8	496.0	426.7	404.6	–	-134.2	-94.68	-42.96
3	508.9	497.9	421.3	400.1	–	-130	-95.05	-39.86
Average	509.3	497.0	425.7	403.8	–	-133.7	-94.9	-42.6
Stdev	0.458	0.954	3.953	3.372	–	3.477	0.186	2.515
RSD, %	0.090	0.192	0.929	0.835	–	-2.601	-0.196	-5.910

Table 15. Continued.

10°C/min – Heating Data								
	Onset P1	Peak 1	P2 Onset	Peak 2	P3 Onset	Peak 3	Endset P3	Total Peak Area
	°C	°C	°C	°C	°C	°C	°C	J/g
1	468.5	473.5	494.5	505.0	538.3	553.6	561.3	170.4
2	468.6	473.5	494.5	505.4	538.3	553.8	561.3	170.7
3	468.4	473.4	494.2	505.2	537.9	554.2	560.9	170.4
Average	468.5	473.5	494.4	505.2	538.2	553.9	561.2	170.5
Stdev	0.100	0.058	0.173	0.200	0.231	0.306	0.231	0.173
RSD, %	0.021	0.012	0.035	0.040	0.043	0.055	0.041	0.102
10°C/min – Cooling Data								
	Onset P1	Peak 1	Onset P2	Peak 2	Peak 3	Total Peak Area	P1 Area	P2 Area
	°C	°C	°C	°C	°C	J/g	J/g	J/g
1	518.8	495.6	440.2	425.0	–	-151.3	-99.2	-54.7
2	517.2	498.1	431.8	418.4	–	-150.2	-99.2	-53.9
3	520.0	495.8	431.5	418.3	–	-147.7	-99.7	-52.0
Average	518.7	496.5	434.5	420.6	–	-149.7	-99.4	-53.5
Stdev	1.405	1.389	4.939	3.840	–	1.845	0.254	1.351
RSD, %	0.271	0.280	1.137	0.913	–	-1.232	-0.256	-2.523

Table 16. Onset and area values determined from each heating cycle at 2°C/min rates with calculated averages and standard deviations.

2°C/min – Heating Data											
	Onset P1	Peak 1	P2 Onset	Peak 2	P3 Onset	Peak 3	Endset P3	Total Peak Area	P1	P2	P3
	°C	°C	°C	°C	°C	°C	°C	J/g	J/g	J/g	J/g
1	469.5	472.1	493.1	499.5	539.9	547.1	558.5	166.2	2.1	59.1	101.9
2	469.5	471.9	493.0	499.3	539.8	547.5	558.0	167.1	1.5	61.0	101.8
3	469.5	472.1	493.1	499.3	540.1	547.4	557.6	167.4	2.1	60.1	102.2
Average	469.5	472.0	493.1	499.4	539.9	547.3	558.0	166.9	1.9	60.1	102.0
Stdev	0.000	0.115	0.058	0.115	0.153	0.208	0.451	0.624	0.331	0.935	0.208
RSD, %	0.000	0.024	0.012	0.023	0.028	0.038	0.081	0.374	17.336	1.556	0.204
2°C/min – Cooling Data											
	Onset P1	Peak 1	Onset P2	Peak 2	P3 Onset	Peak 3	Endset P3	Total Peak Area	P1 Area	P2 Area	P3
	°C	°C	°C	°C	°C	°C	°C	J/g	J/g	J/g	J/g
1	510.0	514.0	452.7	447.2	-	-	-	-160.9	-99.7	-59.4	-
2	519.7	512.4	454.8	446.9	-	-	-	-159.0	-99.6	-59.4	-
3	520.0	513.1	453.7	448.2	-	-	-	-160.4	-99.4	-59.5	-
Average	516.6	513.2	453.7	447.4	-	-	-	-160.1	-99.6	-59.4	-
Stdev	5.689	0.802	1.050	0.681	-	-	-	0.985	0.184	0.055	-
RSD, %	1.101	0.156	0.232	0.152	-	-	-	-0.615	-0.185	-0.093	-

The reported solidus and liquidus temperatures were ascertained using the average of the onset temperature or offset temperature for melting, derived from the heat flow curves of three separate heating and cooling cycles. The reported onset and melting temperatures were determined using linear regression to remove the effects of thermal lag from the samples [4]. All temperatures are reported with an accuracy of ± 3°C. Values extracted from the heating (Table 17) and cooling (Table 18) curves were to remove the thermal lag from solidus and liquid temperatures. Upon heating, the solidus for Seaborg 7 is reported to be 470°C while the liquidus is reported as 547°C (peak 3 max). Upon cooling, the liquidus was determined to be 519°C while the solidus was 450°C. It should be noted that salts have repeatedly shown to “super cool,” and therefore, the cooling data is only provided for completeness and is not recommended to be used as quantitative data.

Table 17. Summary of heat flow data from STA (Figure 13A) used to do linear regression to remove thermal lag from reported melt and transition temperatures.

Heating Rate, °C/min	Onset P1, °C	P1 Max, °C	Onset P2, °C	P2 Max, °C	Onset P3, °C	P3 Max, °C	Endset P3, °C
20	466.4	473.8	492.7	509.8	536.9	556.6	567.1
10	468.5	473.5	494.4	505.2	538.2	553.9	561.2
2	469.5	472.0	493.1	499.4	539.9	547.3	558.0
Regressed Value, °C	**469.7**	**472.1**	**493.7**	**498.7**	**540.1**	**547.2**	**556.7**
R^2	0.9811	0.8528	0.0911	0.9821	0.9749	0.9146	0.9874

Table 18. Summary of heat flow data from STA (Figure 13B) used to do linear regression to remove thermal lag from reported melt and transition temperatures.

Cooling Rate, °C/min	Onset P1, °C	Peak 1, °C	Onset P2, °C	Peak 2, °C
20	509.3	497.0	425.7	403.8
10	518.7	496.5	434.5	420.6
2	516.6	513.2	453.7	447.4
Regressed Value, °C	**519.4**	**511.4**	**454.3**	**449.5**
R^2	0.6097	0.668	0.9264	0.9617

4.2.4. Enthalpy

The enthalpy of fusion, and enthalpy of crystallization were determined by integrating the area under the peaks for heating and cooling, respectively. As previously mentioned, a Zn standard was run as a sample to verify the heat flow calibration. Heat flow (enthalpy) for the Zn sample was shown to agree with theoretical values to within less than 2% for heating and less than 5% for cooling. Calculated peak areas for the Seaborg-7 sample are provided in Table 19. The was determined to be 167.5 ± 2.7 J/g while was -147.8 ± 13.3 J/g. Using the 2°C/min heating and cooling curves, the enthalpies of the individual peaks were determined as shown in Table 19.

Table 19. Summary of enthalpy data for both heating and cooling.

	Heating						Cooling			
Heat Rate	Total Peak Area	P1	P2	P3	P1+P2+P3	Cool Rate	Total Peak Area	P1 Area	P2 Area	P1+P2

C/min	J/g	J/g	J/g	J/g	J/g	C/min	J/g	J/g	J/g	J/g
20	165.1	ND	ND	ND	0	20	-133.7	-94.9	-42.6	-137.4
10	170.5	ND	ND	ND	0	10	-149.7	-99.4	-53.5	-152.9
2	166.9	1.9	60.1	102	164	2	-160.1	-99.6	-59.4	-159
ND – Not determined due to overlapping peaks.										

4.3. Specific Heat Capacity

4.3.1. Calibration and Methodology

Specific heat capacity measurements were conducted using a Netzsch 404 F1 DSC with a type-S sample carrier and rhodium furnace. Prior to heat capacity measurements, the DSC was calibrated for temperature and heat flow as described previously for the STA. The standards used to calibrate the DSC are listed in Table 20. For the calibration standards, the onset of the transition temperature of the standards was calculated by averaging the onset of the melting peak for three heating cycles. The heat flow calibration was generated using a sapphire standard and was calibrated prior to running each sample. In total, four heating/cooling cycles were generated; however, data from the initial cycle were not considered in the analysis. The accuracy of the temperature and sensitivity calibration was verified using one or more standards and performed according to ASTM E967-18. A heating rate of 10°C/min was used for all calibration standards and during specific heat capacity measurements.

Table 21 is a summary of the temperature data generated from each standard and used to make the calibration file for DSC. The melting temperature of each standard was calculated by averaging the onset melting temperatures for three successive heating cycles. The average value was then used in the calibration file generated. Sapphire heat flow calibration is shown with each sample because it was verified immediately before heat capacity determination. The accuracy of the temperature calibration curve was verified using a Zn standard. The verification of the calibration curves at each heating rate showed that the DSC was calibrated to have deviation in experimental melting temperature from theoretical values of less than 1°C, while the heat flow calibration from the sapphire was ≤5% of theoretical values; otherwise, the instrument was recalibrated.

Table 20. Standards used to calibrate the DSC and theoretical temperature and enthalpy values.

	Standard	Transition Temperature, °C
Std 1	In	156.6
Std 2	Bi	271.4
Std 3	Zn	419.5
Std 4	Al	660.6
Std 5	Ag	961.8

Table 21. Summary of temperature and heat flow calibrations on the DSC. Performed prior to heat capacity measurements.

Temperature Calibration						
	In	Bi	Zn	Al	Ag	
Cycle 1	155.8	270.9	417.8	658.0	958.4	
Cycle 2	155.1	270.7	418.2	659.5	958.4	
Cycle 3	155.1	271.0	417.9	658.0	958.3	
Avg	155.3	270.9	418.0	658.5	958.4	
Stdev	0.40	0.15	0.21	0.87	0.06	

RSD (%)	0.26	0.06	0.05	0.13	0.01	

Heat capacity was determined using the Cp ratio method where the measurement consisted of several experimental runs including baseline (empty crucible, no sample), standard-and-baseline (sapphire with same crucibles as baseline), and sample-and-baseline (same crucible as baseline and standard). When determining heat capacity, a new sensitivity calibration file may be generated from the sapphire standard; however, the sensitivity calibration generated using the high-purity standards may also be used, depending on which one provides the most accurate heat capacity for sapphire within the temperature range of interest. Specific heat is a function of temperature at constant pressure and was calculated following Equation 1. It requires three measurements to be taken at the same heating rate.

(1)

Previous experience at INL showed that crucible mass, reproducible crucible location and orientation, sample mass, and instrument calibration all have a significant influence on heat capacity measurements. Therefore, it is important to use sample and reference crucibles with a mass difference of approximately less than 1%, when possible, match the sample mass to the sapphire mass when possible, and mark the crucibles for orientation. Glassy carbon crucibles are difficult to reproducibly place in the same location but seem to be inert to fluorides salts for short durations and were used for all heat capacity measurements. Measurement of heat capacity involved 10 separate measurements using the same sample and reference crucible. Three baseline correction measurements were performed; the first was always discarded while the second and third baseline corrections were used to verify reproducibility. Next, four measurements were run using the sapphire standard using either baseline correction two or three. The first sapphire run was discarded, the second sapphire run was used to generate a sapphire heat flow calibration, and the third and fourth sapphire runs were used to verify that the measured specific heat capacity of sapphire matched the theoretical sapphire heat capacity values. Finally, the NaF-KF-UF_4 (Seaborg 7) sample was loaded into the crucible and run three times using the same baseline as the sapphire sample. The average heat capacity of the three sample measurements is reported as the heat capacity for that sample.

4.3.2. Solid State

Solid-state heat-capacity measurements were made as described above with an added step of melting and fusing the sample prior to heat taking capacity measurements. This was done to allow the sample to be in good contact with the bottom of the crucible for optimal heat transfer. Three samples were used for measuring heat capacity in the solid phase, and the temperature profile/steps are outlined in Table 22.

Table 22. Temperature profile for solid heat capacity samples.

Description	Temperature, °C	Heating Rate, °C/min	Time, min
Initial	~25	–	–
Dynamic (heating)	30	2	2
Isothermal	30	–	5
Dynamic (heating)	600	10	57
Isotherm	600	–	15
Dynamic (cooling)	30	20	36

Prior to the triplicate solid-state heat-capacity measurements, a calibration of the DSC and experimental setup was performed using a sapphire calibration standard. The sapphire calibration verification and solid-state heat-capacity measurements are shown for the three Seaborg-7 samples in Figure 14–Figure 16. In each heat capacity measurement, the same sample was analyzed three times, and the average of these three runs was used to report the heat capacity of that sample between 50 to 450°C. Figure 17 (left) shows the averaged heat capacity and standards deviation for the three solid-state samples. All samples show a slight upward trend, and the average heat capacity of all the samples is shown as a function of temperature in Figure 17 (right).

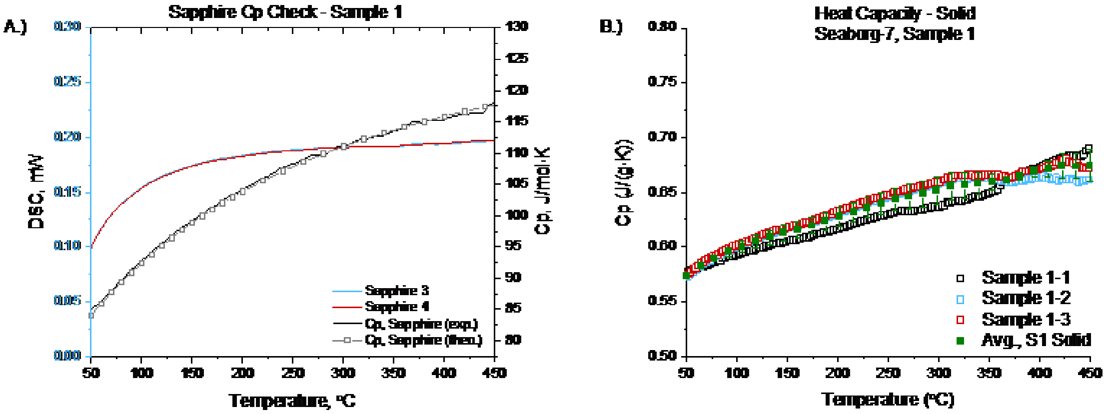

Figure 14. Seaborg-7 (NaF-KF-UF_4) solid sample 1. Sapphire calibration check (left) and specific heat capacity of sample (right).

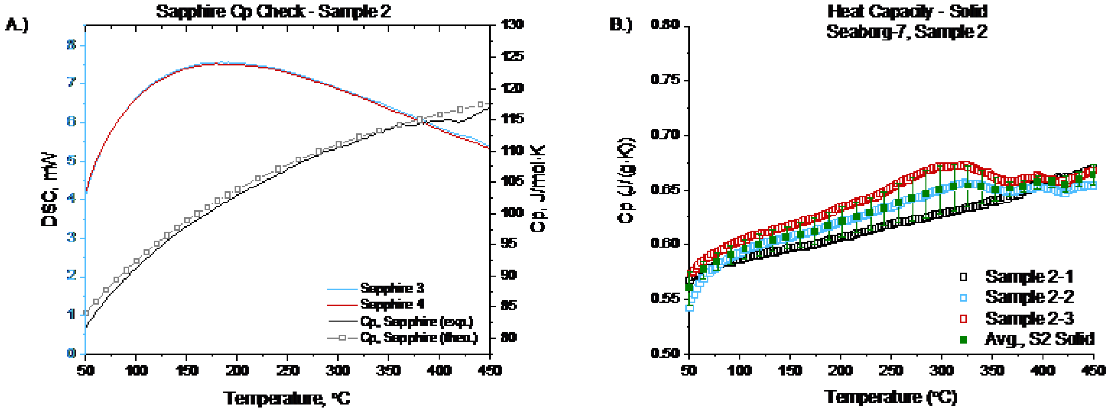

Figure 15. Seaborg-7 (NaF-KF-UF$_4$) solid sample 2. Sapphire calibration check (left) and specific heat capacity of sample (right).

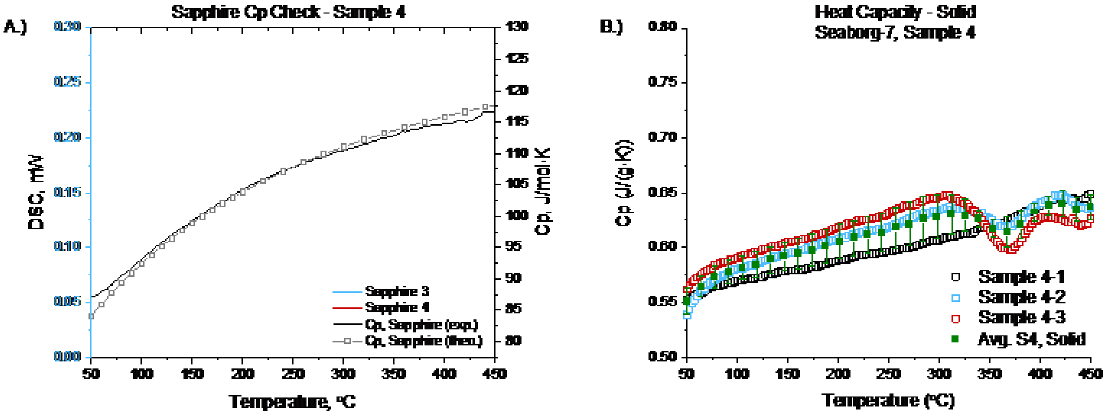

Figure 16. Seaborg-7 (NaF-KF-UF$_4$) solid sample 4. Sapphire calibration check (left) and specific heat capacity of sample (right).

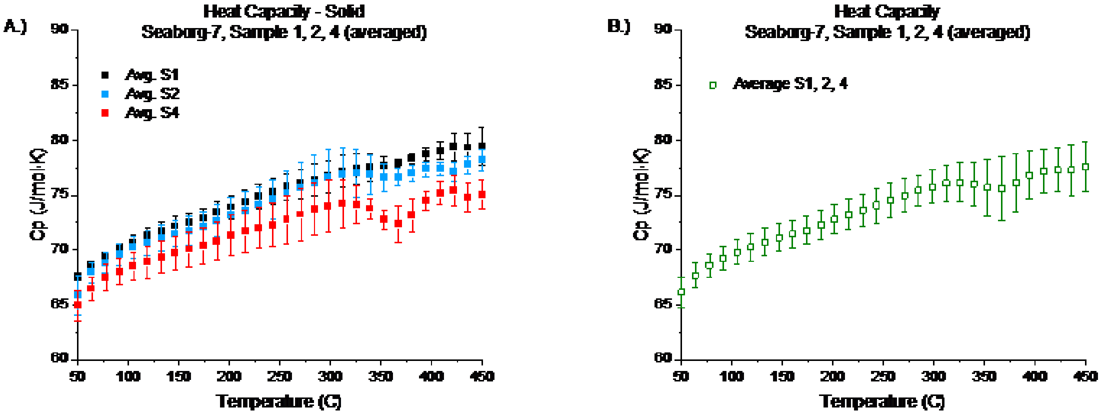

Figure 17. Averaged solid heat capacity results for each Seaborg-7 sample: black = sample 1, blue = sample 2, red = sample 4 (left). Reported heat capacity and associated error of NaF-KF-UF$_4$ material, derived from the averaged results of samples 1, 2, 4 (right).

4.3.3. Liquid State

The temperature profile for the liquid samples is shown in Table 23 and was followed for every measurement associated with liquid heat capacity determination.

Table 23. Temperature profile for liquid heat capacity samples.

Description	Temperature, °C	Heating Rate, °C/min	Time, min
Initial	25	–	–
Dynamic (Heating)	30	5	3
Isothermal	30	–	5
Dynamic (Heating)	600	10	57
Isotherm	600	–	8
Dynamic (Heating)	805	10	21
Isotherm	805	–	8
Dynamic (Cooling)	25	20	39

Three individual liquid-state heat-capacity measurements were performed using a new sample for each group of heat capacity measurements. In total, three samples were analyzed. Before heat capacity measurements were run, the calibration on the instrument and experimental system was verified using the sapphire calibration standard. The sapphire calibration verification (left) and heat capacity measurements (right) are shown in Figure 18–Figure 20. The reported heat capacity for each sample was determined by taking the average of the three runs for each sample from 600 to 800°C and is shown in Figure 21 (left) for each sample along with the standard deviation at each point.

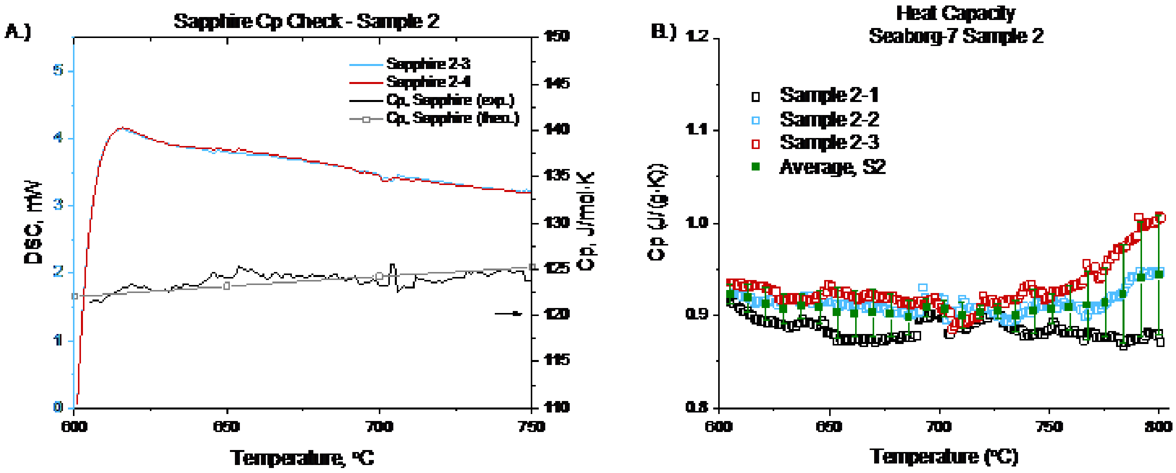

Figure 18. NaF-KF-UF$_4$ (Seaborg-7) liquid sample 2. Sapphire calibration check (left) and specific heat capacity of sample (right).

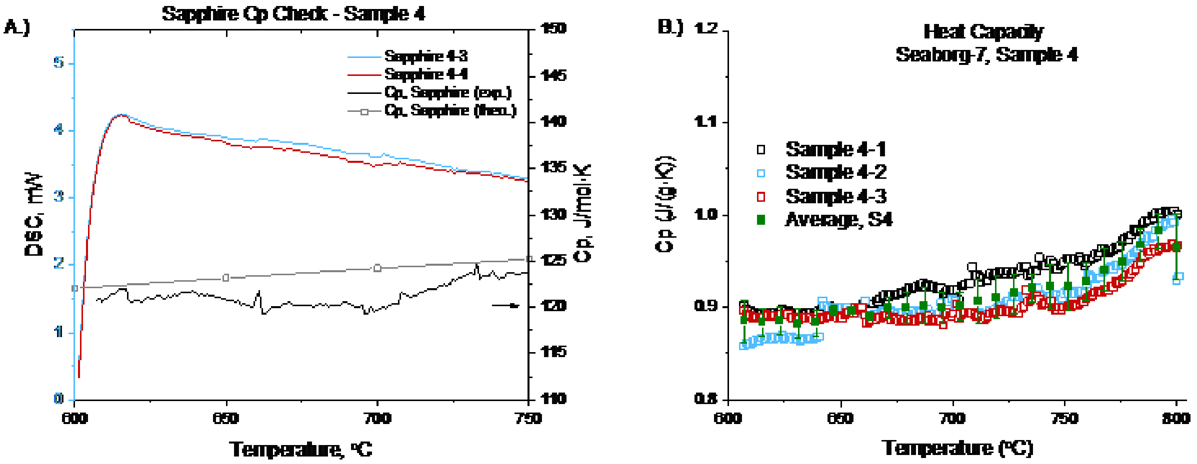

Figure 19. NaF-KF-UF$_4$ (Seaborg-7) liquid sample 4. Sapphire calibration check (left) and specific heat capacity of sample (right).

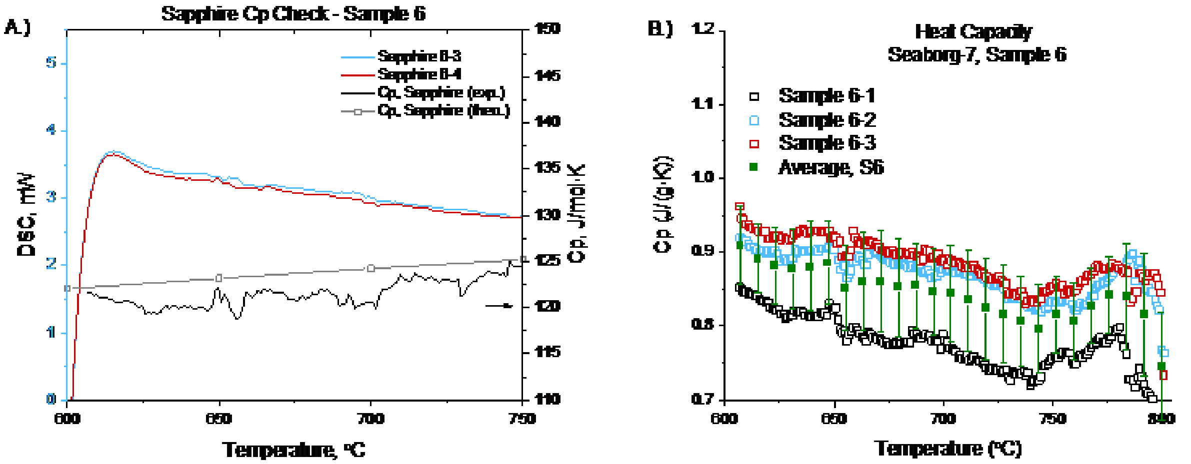

Figure 20. NaF-KF-UF$_4$ (Seaborg-7) liquid sample 6. Sapphire calibration check (left) and specific heat capacity of sample (right).

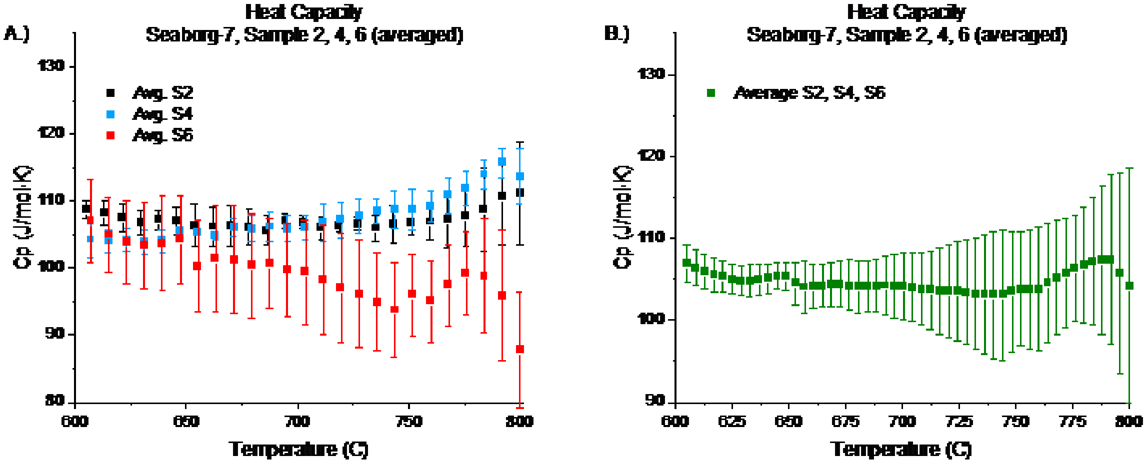

Figure 21. Averaged liquid heat capacity results for each sample: black = sample 2, blue = sample 4, red = sample 6 (left). Reported heat capacity and associated error of NaF-KF-UF_4 (Seaborg-7) liquid sample, derived from the averaged results of samples 2, 4, and 6 (right).

4.3.4. Summary

All heat capacity data on the Seaborg-7 material are summarized in Figure 22A–C. This material shows a slight increasing trend in heat capacity as a function of temperature in the solid state and a slightly increasing to flat heat capacity as a function of temperature in the liquid state. The values used to construct Figure 22 are provided in Table 24. Two plots summarizing the heat capacity are shown. Figure 22A does not eliminate any sample runs when reporting the average values for each sample; however, Figure 22B provides the average values for each sample where run 1 of sample 6 was omitted. This is because run 1 for sample 6 (liquid) is far below other measurements, and the authors of this report believe this value to be unreasonably low. Because the authors do not want to omit data, two plots for the average Cp both with and without run 1 from sample 6 have been included. The reported Cp values from this study, shown in Figure 22C and Table 24, do not include run 1 from sample 6.

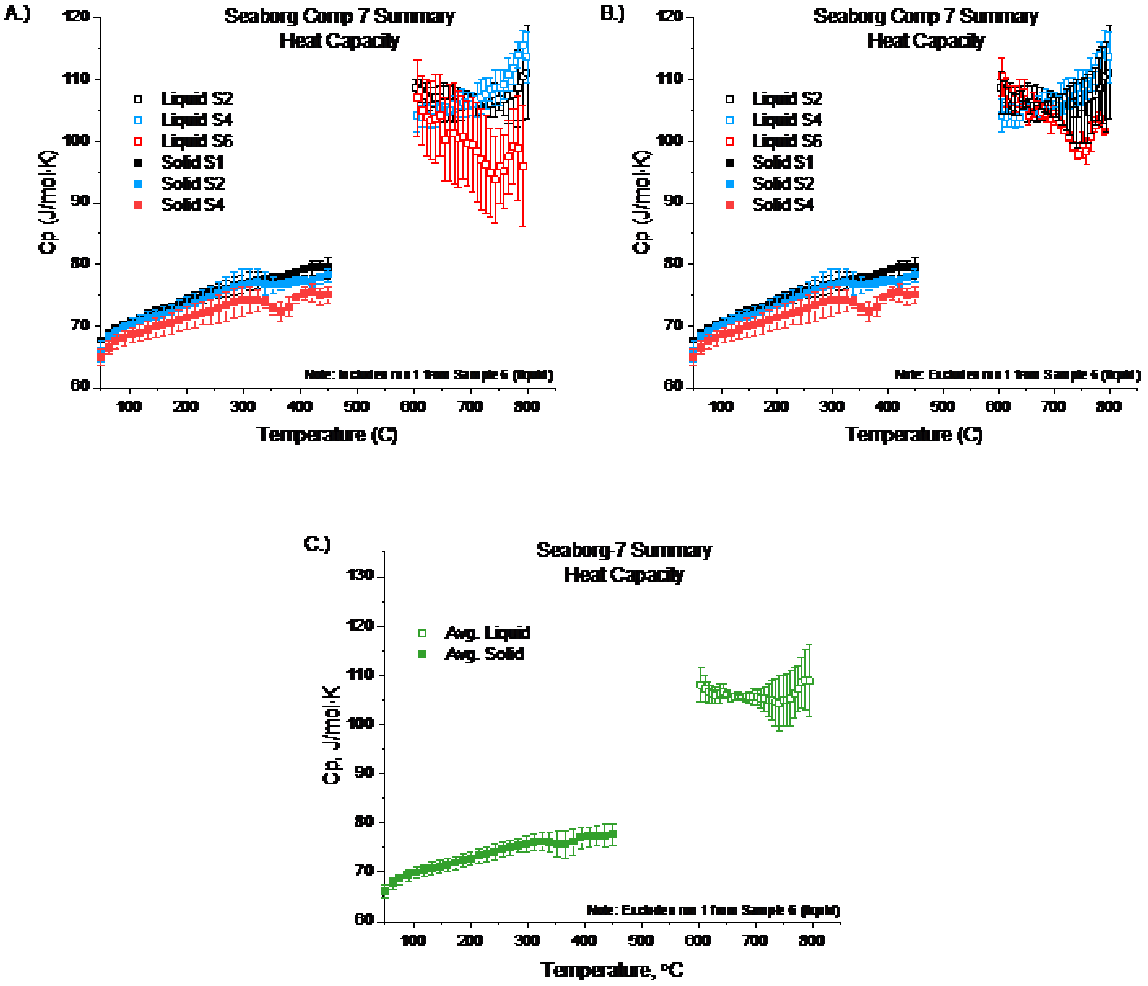

Figure 22. Summary of experimentally determined, averaged, heat capacity for the Seaborg-6 material, 26.4UF_4-24.7KF-48.9NaF.

Table 24. Averaged temperature and heat capacity data used to construct Figure 22C.

Average Solid Cp				Average Liquid Cp		
Avg. Temperature	Avg. Cp	Standard Deviation		Avg. Temperature	Avg. Cp	Standard Deviation
°C	J/mol·K	J/mol·K		°C	J/mol·K	J/mol·K
50.0	66.1	1.36		605.0	108.0	3.44
63.8	67.7	1.12		611.6	107.2	2.66
77.6	68.6	1.02		618.1	106.5	2.11
91.4	69.2	1.10		624.7	106.2	1.76
105.2	69.8	1.16		631.2	105.9	1.72
119.0	70.2	1.25		637.8	106.3	1.96
132.8	70.7	1.23		644.3	106.7	1.48
146.6	71.1	1.25		650.9	106.1	0.56
160.3	71.4	1.26		657.4	105.4	0.84
174.1	71.8	1.30		664.0	105.7	0.63
187.9	72.3	1.33		670.5	106.0	0.20
201.7	72.8	1.33		677.1	105.7	0.50
215.5	73.2	1.39		683.6	105.5	0.73
229.3	73.6	1.47		690.2	105.5	1.14
243.1	74.1	1.59		696.7	105.5	1.67
256.9	74.6	1.58		703.3	105.6	1.54
270.7	75.0	1.53		709.8	105.3	1.85
284.5	75.4	1.45		716.4	105.2	2.59
298.3	75.7	1.51		722.9	105.1	3.30
312.1	76.1	1.60		729.5	104.9	3.98
325.9	76.1	1.78		736.0	104.5	4.89
339.7	76.0	2.01		742.6	104.4	5.64
353.4	75.7	2.59		749.1	104.8	5.20
367.2	75.6	2.92		755.7	104.9	5.30
381.0	76.1	2.68		762.2	105.3	5.50
394.8	76.8	2.16		768.8	106.4	5.04
408.6	77.2	1.95		775.3	107.3	4.60
422.4	77.3	2.01		781.9	108.4	4.99
436.2	77.3	2.31		788.4	109.1	6.25
450.0	77.6	2.26		795.0	108.9	7.28

4.4. Density

4.4.1. Solid Density

4.4.1.1. Methodology

The gas expansion Micromeritics pycnometer is designed to accurately measure the volume of samples that are irregularly shaped (e.g., porous monolithic, powdered, and granular) based on the Boyle-Mariotte law, which can then be used to calculate the sample's density. The gas pycnometer consists of two chambers, as seen in Figure 23; the first chamber holds the sample, and the second chamber has a fixed internal reference volume (Figure 23, No. 2 and No. 3). There are three internal gas line valves, A, B, and C. Valve A allows gas to fill the first chamber to a specified pressure (Figure 23, No. 4) and closes once the chamber is at the desired pressure P1. Valve B opens to allow gas to flow into the second chamber of known volume to achieve P2. Valve C is used to vent the chambers.

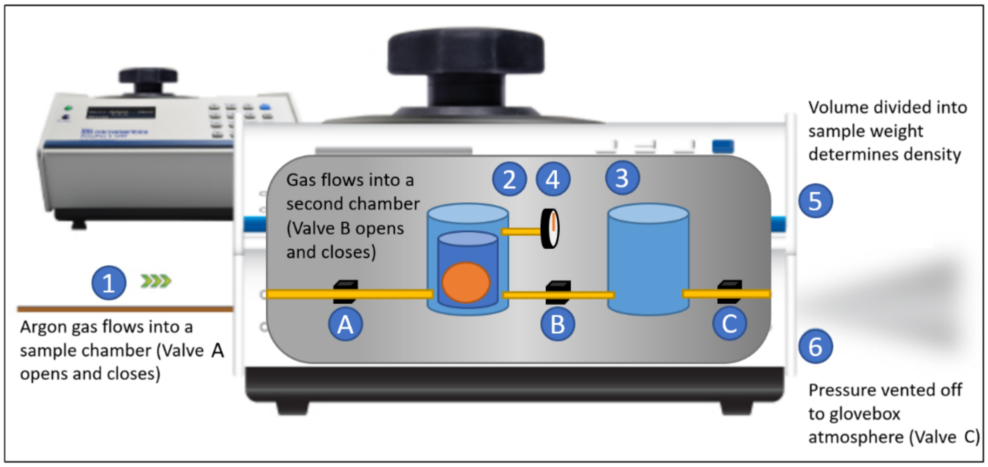

Figure 23. Schematic of gas expansion pycnometer internals.

The volume of a sample was calculated using Equation 7, where is the volume of the sample, is the volume of the empty first chamber, is the reference volume of the second chamber, is the initial specified pressure, and is the pressure after Valve B has opened, and the gas pressure has equilibrated in both chambers.

(7)

Using a calibrated balance to measure the mass of the sample, Equation 8 was used to solve for the sample's density, where is the density of the sample, is the mass of the sample, and is the volume of the sample. The pycnometer instrument was calibrated using a W sphere standard with a known volume and weight.

(8)

4.4.1.2. Experimental Setup

The pycnometer and analytical balance were installed in an inert Ar atmosphere glovebox in the fuel cycle glovebox (FCG) located in FCF for the solid-state density analysis. The oxygen and moisture concentrations in the FCG were monitored and remained below 10 ppm O_2 and 1 ppm H_2O during experimentation.

All mass measurements were made on an Ohaus EX324 Explorer Analytical balance with a tolerance of +/-0.0008 g whose calibration was checked daily via internal calibration. The pycnometer was equipped with an internal heater and was capable of measuring density from room temperature (RT) to 200°C. The effect of temperature on density was measured at 30, 50, 100, 150, and 200°C.

Prior to experimentation, the pycnometer was leak tested to ensure proper sealing and isolation of the Ar during the measurements and calibrated. The calibration standard is a NIST-certified standard with a mean diameter of 0.437503 ± 0.000006 inches and a volume of 0.718527 cm^3. A table of experimentally obtained standard volume values, collected during instrument calibration, is provided in Table 25. The calibration standard was used to calibrate the pycnometer and then separately measured, as a sample, to ensure the instrument's uncertainty was as expected.

Table 25. Theoretical and experimentally determined calibration standard volumes.

Temperature °C	Theoretical Volume cm^3	Experimental Volume cm^3	Difference
30	0.7187	0.7184	0.0003
60	0.7192	0.7195	-0.0003
100	0.7198	0.7196	0.0002
150	0.7205	0.7204	0.0001
200	0.7212	0.7210	0.0002

A 1 cm^3 aluminum (Al) cup was used to hold the samples. Through optimization testing, it was determined that there is an upper and lower limit to the volume of sample that should be loaded into the pycnometer cup (i.e., roughly ½–¾ cm^3 of the 1 cm^3 cup). Figure 24 shows the UF_4 salt loaded into the Al cup, the cup with salt on the balance, and the sample loaded into the pycnometer prior to measurements. Care was taken to record accurate sample masses prior to each experiment as density is a function of mass, measured using a balance and volume displacement, using the pycnometer. Pictures of the pycnometer sample are shown in Figure 24.

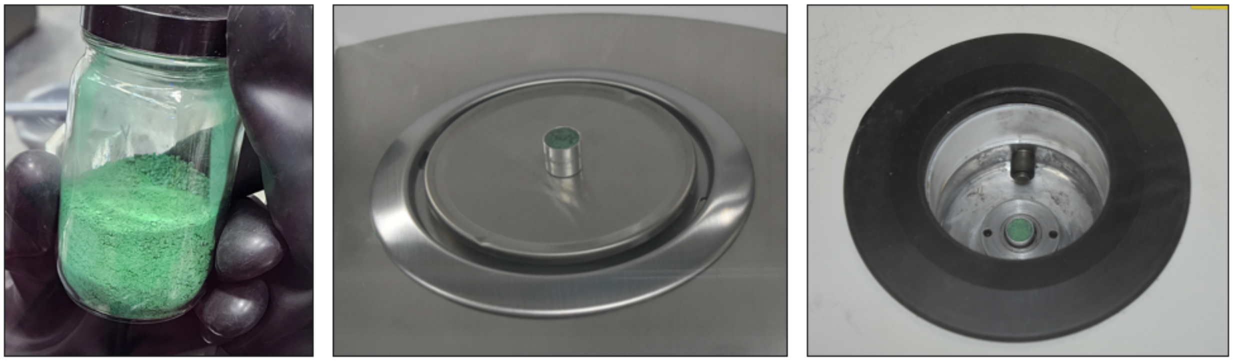

Figure 24. The bulk Seaborg-7 salt sample (left); sample loaded in pycnometer density cup, loaded sample cup on the balance (middle), and the loaded sample cup placed in the pycnometer chamber (right).

4.4.1.3. Results

A set of experiments was conducted to determine the solid-state density of UF_4 Seaborg-7 salt up to 200°C. Density measurements were taken in triplicate at each temperature: ambient temperature (~32°C), 100, 150, and 200°C while a single data point was taken at 60°C. The individual density measurements are shown in Figure 25A while the averaged values are shown in Figure 25B. The solid-state density date is provided in Table 26. For each sample, 10 density measurements were taken, and the average of the 10 density values is reported in Table 26. A linear fit of the averaged density values along with the equation to determine density as a function of temperature (solid-state only) is shown in Figure 25B.

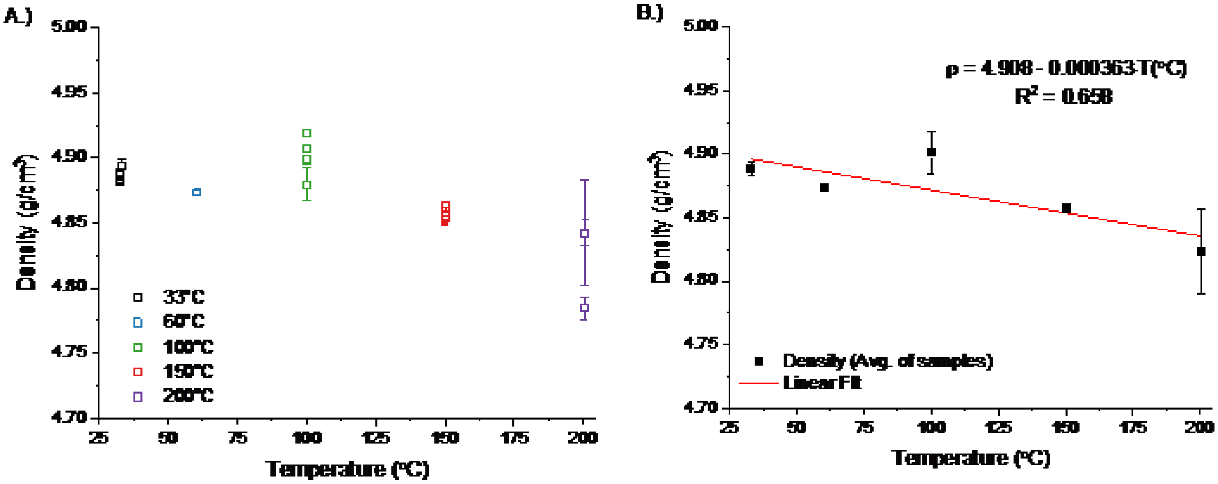

Figure 25. Measured, averaged, and linear fit for UF_4 composition 7 solid-state density as a function of temperature.

Table 26. Average density measurements with temperature,

Temperature	Density	Stdev
°C	g/cm^3	g/cm^3
32.7	4.8880	0.0016
32.9	4.8885	0.0034
33.2	4.8945	0.0041
32.8	4.8820	0.0017
60.4	4.8734	0.0023
100.2	4.8797	0.0126
100.3	4.8987	0.0035
100.1	4.9189	0.0028
100.1	4.9073	0.0024
150.2	4.8535	0.0043
150.4	4.8570	0.0015
150.4	4.8625	0.0035
150.4	4.8559	0.0060
200.7	4.8422	0.0099
200.7	4.8424	0.0406
200.5	4.7845	0.0088

Numerous sample measurements were performed at ambient temperature. However, only four the last four (Sample 8–Sample 11, Table 27) were reported in Figure 25 and Table 26. A summary of all solid-state density data collected on the Seaborg-7 composition is provided in Table 27–Table 31.

Table 27. Summary of density values collected on Seaborg-7 samples at ambient temperature.

Sample 1		**Sample 2**		**Sample 3**		**Sample 4**	
Temperature (°C)	Density (g/cm^3)	Temperature (°C)	Density (g/cm^3)	Temperature (°C)	Density (g/cm^3)	Temperature (°C)	Density (g/cm^3)
28.60	4.8970	28.72	4.8899	28.77	4.8494	31.75	4.8733
28.58	4.8894	28.68	4.8867	28.79	4.8977	31.73	4.8686
28.60	4.8936	28.73	4.8881	28.78	4.8922	31.74	4.8740
28.67	4.8965	28.73	4.8884	28.83	4.8801	31.77	4.8687
28.60	4.8918	28.73	4.8646	28.85	4.8862	31.73	4.8746
28.61	4.8784	28.76	4.8907	28.82	4.8806	31.79	4.8711
28.63	4.8979	28.72	4.8866	28.80	4.8680	31.73	4.8703
28.61	4.8719	28.74	4.8807	28.82	4.8898	31.75	4.8682
28.59	4.8924	28.72	4.8829	28.83	4.8796	31.71	4.8698
28.65	4.8988			28.86	4.8875	31.80	4.8702

Sample 5		**Sample 6**		**Sample 7**		**Sample 8**	
Temperature (°C)	Density (g/cm^3)	Temperature (°C)	Density (g/cm^3)	Temperature (°C)	Density (g/cm^3)	Temperature (°C)	Density (g/cm^3)
31.84	4.8940	31.92	4.8606	32.73	4.8838	32.71	4.8872
31.84	4.8941	31.92	4.8624	32.76	4.8763	32.76	4.8881
31.85	4.8955	31.95	4.8610	32.78	4.8770	32.72	4.8859
31.85	4.8964	31.93	4.8647	32.70	4.8857	32.73	4.8868
31.86	4.8962	31.95	4.8619	32.80	4.8740	32.73	4.8901
31.84	4.8974	31.95	4.8614	32.79	4.8833	32.75	4.889
31.85	4.8946	31.91	4.8595	32.74	4.8710	32.68	4.8889
31.83	4.8981	31.90	4.8630	32.74	4.8783	32.74	4.8878
31.87	4.8940	31.89	4.8622	32.73	4.8835	32.71	4.8852
31.85	4.8965	31.95	4.8608	32.74	4.8742	32.72	4.8909

Sample 9		**Sample 10**		**Sample 11**	
Temperature (°C)	Density (g/cm^3)	Temperature (°C)	Density (g/cm^3)	Temperature (°C)	Density (g/cm^3)
32.82	4.886	33.14	4.8935	32.86	4.8793
32.86	4.8842	33.14	4.8918	32.8	4.8793
32.88	4.8904	33.22	4.8903	32.79	4.8819
32.9	4.8927	33.15	4.8921	32.82	4.8835
32.86	4.888	33.2	4.894	32.85	4.8821
32.87	4.8858	33.19	4.898	32.84	4.884
32.92	4.8938	33.2	4.8992	32.82	4.8812
32.86	4.8923	33.14	4.8952	32.85	4.8828
32.85	4.8889	33.19	4.8855	32.84	4.8824
32.91	4.8827	33.17	4.9053	32.85	4.883

Table 28. Summary of density values collected on Seaborg-7 samples at 60°C.

Sample 1

Temperature (°C)	Density (g/cm³)
60.38	4.8714
60.41	4.8723
60.4	4.8723
60.4	4.875
60.36	4.8734
60.35	4.8754
60.4	4.8731
60.39	4.8693
60.39	4.877
60.35	4.875

Table 29. Summary of density values collected on Seaborg-7 samples at 100°C.

Sample 1		**Sample 2**		**Sample 3**		**Sample 4**	
Temperature (°C)	Density (g/cm³)	Temperature (°C)	Density (g/cm³)	Temperature (°C)	Density (g/cm³)	Temperature (°C)	Density (g/cm³)
100.3	4.8829	100.3	4.895	100.21	4.9221	100.11	4.9093
100.25	4.8867	100.31	4.897	100.1	4.9235	100.12	4.9044
100.3	4.8476	100.34	4.902	100.15	4.9183	100.13	4.9088
100.24	4.8874	100.32	4.905	100.15	4.9175	100.12	4.9094
100.21	4.8812	100.24	4.894	100.18	4.9215	100.1	4.9033
100.29	4.8846	100.32	4.897	100.13	4.9178	100.19	4.9088
100.28	4.8797	100.3	4.898	100.12	4.919	100.1	4.9045
100.22	4.87	100.28	4.902	100.18	4.9187	100.16	4.9093
100.2	4.8911	100.26	4.9	100.14	4.9168	100.13	4.9062
100.19	4.8853	100.27	4.897	100.13	4.914	100.15	4.9089

Table 30. Summary of density values collected on Seaborg-7 samples at 150°C.

Sample 1		**Sample 2**		**Sample 3**		**Sample 4**	
Temperature (°C)	Density (g/cm³)	Temperature (°C)	Density (g/cm³)	Temperature (°C)	Density (g/cm³)	Temperature (°C)	Density (g/cm³)
150.13	4.8441	150.4	4.851	150.39	4.8666	150.36	4.8609
150.18	4.8502	150.4	4.857	150.38	4.8588	150.38	4.858
150.13	4.8518	150.38	4.858	150.42	4.8656	150.34	4.8505
150.18	4.8473	150.4	4.858	150.4	4.8594	150.41	4.8661
150.19	4.8513	150.43	4.856	150.41	4.8647	150.37	4.8511
150.2	4.8539	150.38	4.854	150.43	4.869	150.39	4.8551
150.18	4.8546	150.38	4.858	150.45	4.8602	150.39	4.857
150.2	4.8525	150.36	4.857	150.4	4.8592	150.36	4.8553
150.23	4.8618	150.41	4.856	150.38	4.8643	150.45	4.8473

Table 31. Summary of density values collected on Seaborg-7 samples at 200°C.

Sample 1		**Sample 2**		**Sample 3**	
Temperature	Density	Temperature	Density	Temperature	Density

(°C)	(g/cm^3)	(°C)	(g/cm^3)	(°C)	(g/cm^3)
200.7	4.8427	200.66	4.7817	200.49	4.7828
200.68	4.8177	200.65	4.7851	200.49	4.7831
200.73	4.8415	200.79	4.8594	200.51	4.7737
200.69	4.8518	200.71	4.8963	200.43	4.7984
200.7	4.8431	200.73	4.8729	200.49	4.7845
200.67	4.849	200.69	4.8238	200.46	4.7724
200.66	4.8469	200.62	4.8536	200.52	4.7947
200.69	4.8467	200.6	4.8766	200.49	4.788
200.65	4.8408	200.71	4.8352	200.49	4.787
200.61	4.8423	200.65	4.7786	200.55	4.7789

4.4.2. Liquid Density

The Archimedean densitometer was designed to measure the density of samples based on the Archimedes principle of a mass suspended in a fluid. With this technique, the bobber was calibrated at RT with water and ethanol, whose densities are well known, to determine the true mass and volume of the bobber. The apparent mass of the bobber immersed in the fluid of interest was then measured. From these measurements, the density of the fluid () was calculated using Equation 2.

(2)

where is the mass of the bobber measured in atmosphere, is the apparent mass of the bobber submerged in salt, and is the true volume of the bobber. Due to the large temperature differential between the bobber volume calibration temperature (~20°C) and the measurement temperature for most molten salt systems (~500°C or greater), the volume term in Equation 2 is modified through Equation 3.

(3)

where is the calibrated volume at RT, is the linear coefficient of thermal expansion for the bobber material, and is the difference in temperature between the calibration temperature and the measurement temperature. The mass of the wire used to suspend the bobber from the balance was incorporated into the measurements of and but is canceled out, as the density equation is a differential measurement. The small wire diameter of ~0.1mm minimizes the effects of surface tension and wire volume on the submerged mass measurement. The effect of surface tension of the molten salts pulling downward on the wire is considered negligible. In practice, all measurements were performed in triplicate to increase precision. By making a series of measurements over a range of temperatures, the equation for the density of the fluid as a function of temperature was determined.

The density calculations were performed using the direct Archimedean method based on measurement of buoyancy force exerted on a bobber submerged in molten salts. The density of the liquid salts can be calculated using Equation 4 where is the measured mass of the bobber and wire suspended in argon, is the measured mass of the bobber and wire suspended in the salts, D is the diameter of the wire, is the surface tension of the salts, is the acceleration due to gravity, α is the linear thermal coefficient of expansion of nickel, and is the reference temperature for , the reference volume of the nickel bobber. The surface tension of each mixture was estimated by the mean of the surface tension of the pure components, weighted by mole fractions [5, 6]. The linear thermal coefficient of expansion of nickel was calculated based on a polynomial fit of reference data [7] while the linear thermal coefficient of expansion of tantalum was assumed to be 6.6 x 10^{-6} m m^{-1} °C^{-1} [8].

(4)

The experimental uncertainty of the density was calculated by the propagation of individual uncertainties. Equation 5 shows the fundamental form of the uncertainty propagation of Equation 4. Equation 6 shows the simplified experimental uncertainty function, and Table 32 lists the individual uncertainties and their explanations.

(5)

(6)

Table 32. Definition of terms used to calculate the error associated with liquid density measurements.

Symbol	Explanation
	Standard deviation of the five weight measurements in Ar
	Standard deviation of the five weight measurements in salt
	Standard deviation of the two calculated volumes from water and ethanol benchtop trial
	Assigned as 1% of value of
	OMEGA assigned 0.05% * T + 0.3°C

4.4.2.1. Methodology

The approximately 80 grams of the Seaborg-7 made in FASB was transferred to the Advanced Fuel Cycle Initiative (AFCI) glovebox in the Fuel Manufacturing Facility (FMF) where all liquid-state density experiments were performed. For experiments, approximately 60 g of the prepared salt was removed from the transfer container and ground up to large chunk form as seen in Figure 26. The salt was then added to a glassy carbon crucible previously cleaned with deionized water and isopropyl alcohol and baked in a furnace within an Ar atmosphere at 800°C for 2 hours.

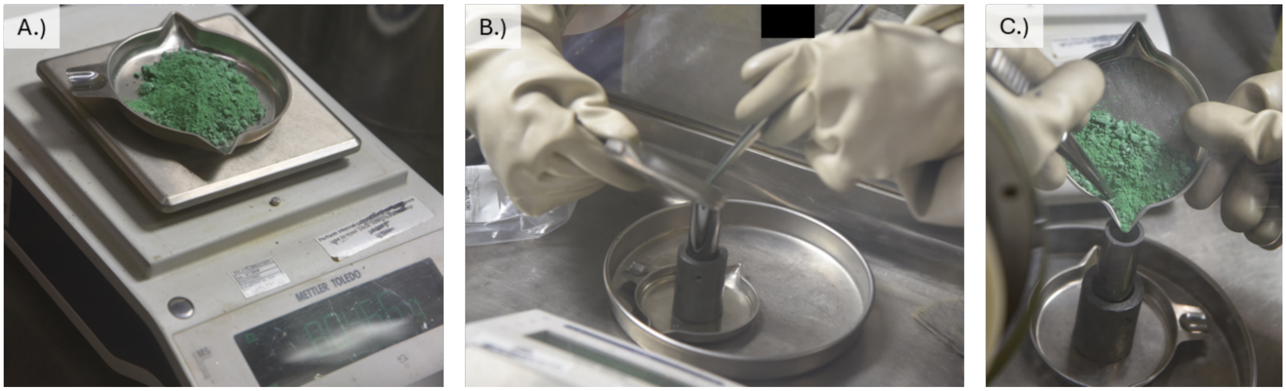
[redacted]

Figure 26. Seaborg-7 sample used for molten density experiments. (A) material on balance; (B) and (C) material being loaded into glassy carbon crucible.

The crucible with salt was then placed in a Ventura Electromelt furnace modified for density experiments. Figure 27 shows the setup within the AFCI glovebox including the furnace, stand, and balance. On the benchtop, the bobbers were secured to a 0.1 mm diameter tungsten wire and their volumes at 20°C were calculated using measurements of their masses from a hang down balance (Mettler Toledo WXSS204, tolerance 0.8 mg) in 10 mL of both deionized water and ethanol, which have well defined densities at the calibration temperature. The averages of the calculated volumes in water and ethanol provide reference values of the bobbers at 20°C for their calculated volumes at high temperatures.

In the glovebox, prior to each experimental trial, the mass of the bobber and wire was measured in Ar using the hang-down balance. A unique bobber was used for each trial of measurements. The crucible with salts, quartz lid, and bobber with wire were added to the setup and the salts melted. Mass readings were performed after 5 minutes of thermal stability at each temperature as measured by an Inconel-sheated K-type thermocouple (Omega) inserted directly into the salts. This equilibration was on average 60 minutes after each temperature change of approximately 50°C. An internal adjustment of the balance was performed before each set of mass measurements at a unique temperature and the balance tared before each measurement. A summary of the equipment used in the densitometer setup is provided in Table 33.

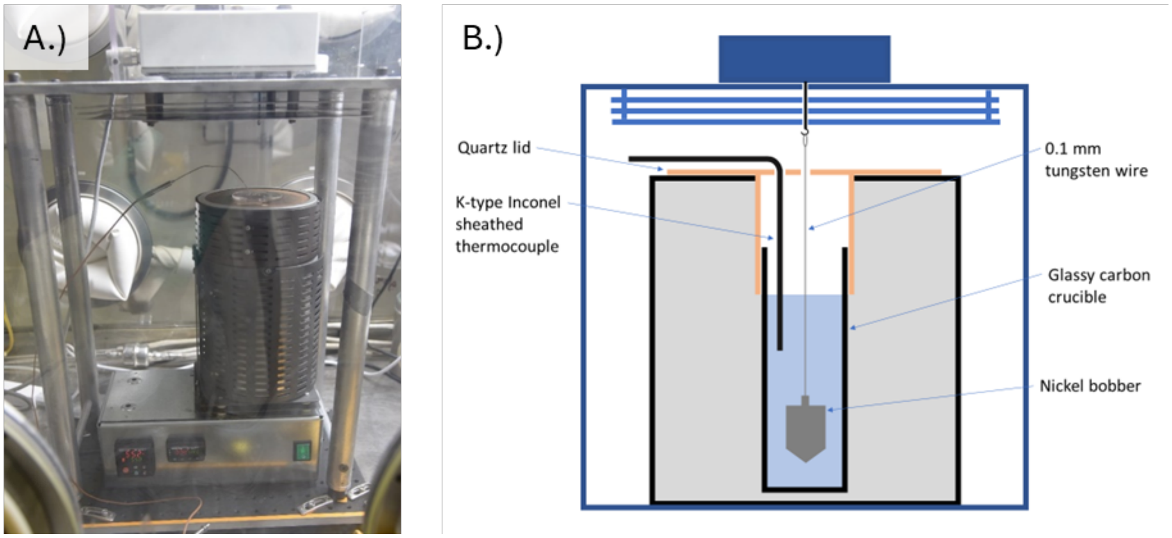

Figure 27. Liquid-state density setup. (A) Picture and (B) diagram of the experimental density setup showing a bottom-loading balance on the stand above a furnace with quartz lid and thermocouple inserted within the AFCI glovebox.

Table 33. Summary of experimental materials.

Furnace	Ventura Electromelt with graphite crucible
Bobber	Ni or Ta,, ESPI Metals 99.9%, approx. 1 cm^3 volume
Wire	0.1 mm W, Alfa Aesar, 99.95% metals basis, Batch #10404 Lot #X28G043
Crucible	GAZA2, 25 mL Sigradur cylindrical crucible, HTW Germany
Balance, Bottom-loading	Mettler Toledo WXSS204, INL ID#525063 tolerance 0.8 mg
Thermocouple	Omega TJ36-CAIN-116U-8-SMPW-M, Inconel sheathed K-type ungrounded
Thermocouple Reader	Omega HH502, s/n 21000159, uncertainty 0.05% of reading + 0.3°C

4.4.2.2. Results

The final set of four trials studied SB-7 (26.4UF_4–24.7KF–48.9NaF) using Ni bobbers at increasing and decreasing temperatures, as shown in Figure 28. The measurements from the first day, denoted by the black symbols in Figure 28A, were taken while heating the salt and have a slightly different slope than the Day 2–4 data. It is unknown if the Day 1 data is different due to human error or due to heating (instead of cooling) the salt. It is the opinion of these authors that Day 1 data was influenced by human performance since it was the first time the operators had performed density measurements for an extended period of time. Additionally, all other salts that this team has analyzed have shown no temperature program dependance during density measurements.

A linear fit using all density data is provided in shown in Figure 28B (black symbols) yields a density equation of ρ(T (°C)) = 4.8082 – 0.0012·T(°C). While the red symbols and linear fit line were determined by omitting Day 1 data, these measurements provide a density equation of ρ(T (°C)) = 4.7509 – 0.00113·T(°C). The density data is provided in Table 34.

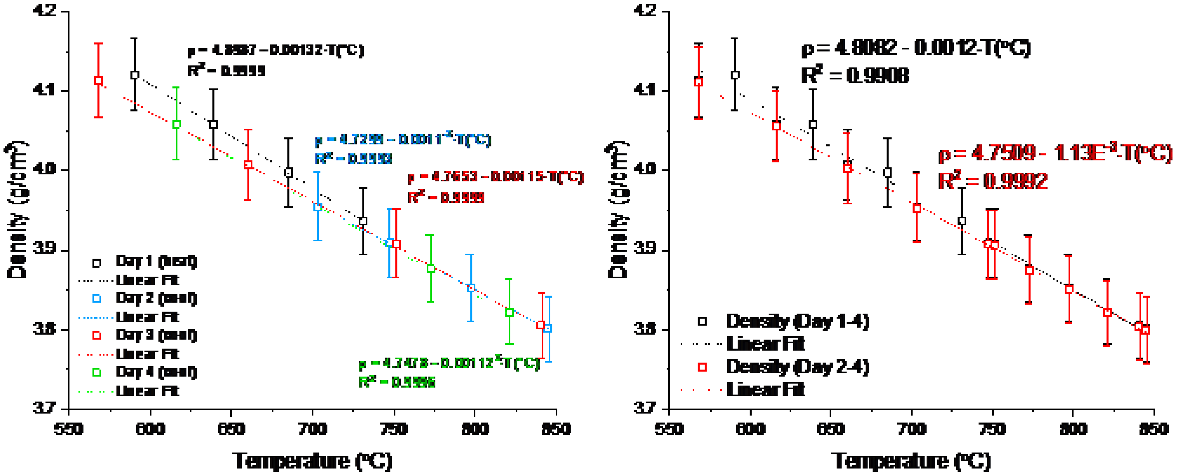

Figure 28. Experimental density values determined on the Seaborg-7 salt from four trials with different temperature schedules.

Table 34. Experimental density data for the Seaborg-7 sample used to construct Figure 28.

	Temperature	Temperature	Density	Density Error	Temp. Error
	°C	K	g/cm^3	g/cm^3	°C
Day 1, Heat	590	863	4.1215	0.0461	2.7706
	639	912	4.0591	0.0451	2.9167
	685	958	3.9976	0.0441	3.0547
	731	1004	3.9366	0.0432	3.1930
Day 2, Cool	845	1118	3.8002	0.0414	3.5356
	797	1070	3.8525	0.0421	3.3910
	748	1021	3.9098	0.0431	3.2428
	703	976	3.9553	0.0436	3.1096
Day 3, Cool	841	1114	3.8047	0.0415	3.5227
	751	1024	3.9087	0.0428	3.2539
	660	933	4.0069	0.0442	2.9803
	568	841	4.1144	0.0459	2.7046
Day 4, Cool	821	1094	3.8220	0.0417	3.4630
	772	1045	3.8765	0.0424	3.3172
	616	889	4.0593	0.0450	2.8474

4.4.2.3. Density of Binary KF-UF$_4$ Salts

The first trial studied the density of Seaborg Binary-1 (67 mol% UF$_4$ – 33 mol% KF). A Ni bobber with hanging mass 9.1450 ± 0.0003 g and calculated volume at 20°C of 1.0219 ± 0.0025 cm^3 was used. Measurements of the hanging weight in the salts were recorded at increasing temperatures of 806.1, 815, 824.2, 834.6, and 844.4°C. However, the stability of the balance readings and trend of the calculated density values, as seen in Figure 29A, indicated an issue with the experimental design.

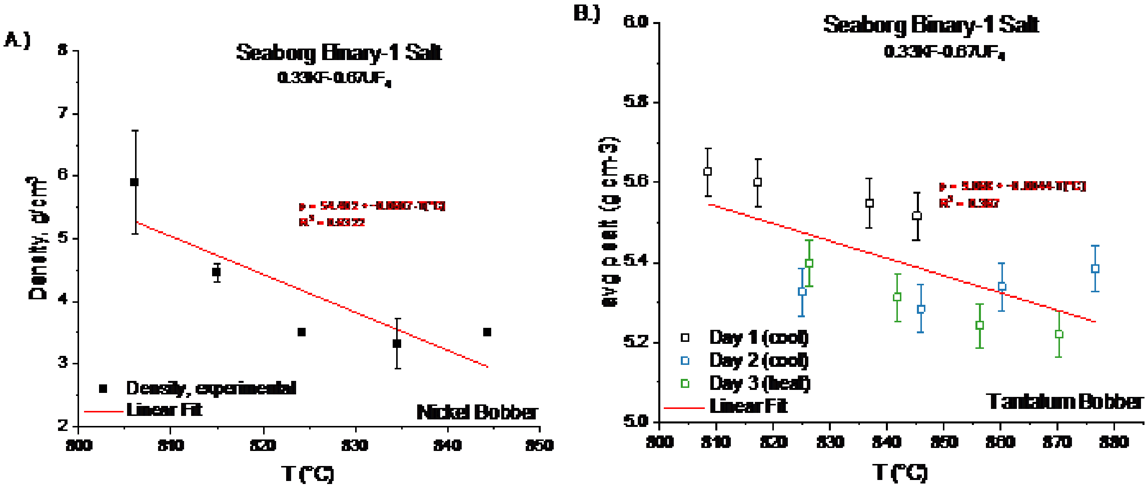

Figure 29. Experimental density values of the 67 mol% UF$_4$-KF system. (A) Nickel bobber and (B) Tantalum bobbers.

It was determined that the density of the salts at these temperatures, later determined to be 5.20–5.65 g/cm^3 in the experimental temperature range, was too similar to the density of the bobber, approximately 8.6 g/cm^3, causing the bobber to experience excessive motion within the salts due to thermal convection. Additionally, this was the highest density salt the INL team has measured to date, and because of this, the team also questioned if the volume (depth) of salt in the crucible was enough for the bobber to be completely submerged. Therefore, more salt was added to the crucible, and the tantalum (Ta) bobbers with tungsten (W) wires were then used for density measurements of this salt in following three trials, as shown in Figure 29B. The data are more scattered than other density tests; however, the team at INL agrees the data accurately represents the salt being investigated.

The next set of density experiments was performed on Seaborg Binary-2 salt, containing 15 mol% UF_4 in KF. Because the density of this salt was lower than the previous sample, Ni bobbers were used. The density of the 15mol%UF_4 salt is shown in Figure 30. The density can be predicted using the linear equation calculated from the density values in Figure 30, $\rho(T\ (°C)) = 3.547 - 0.000807 \cdot T(°C)$.

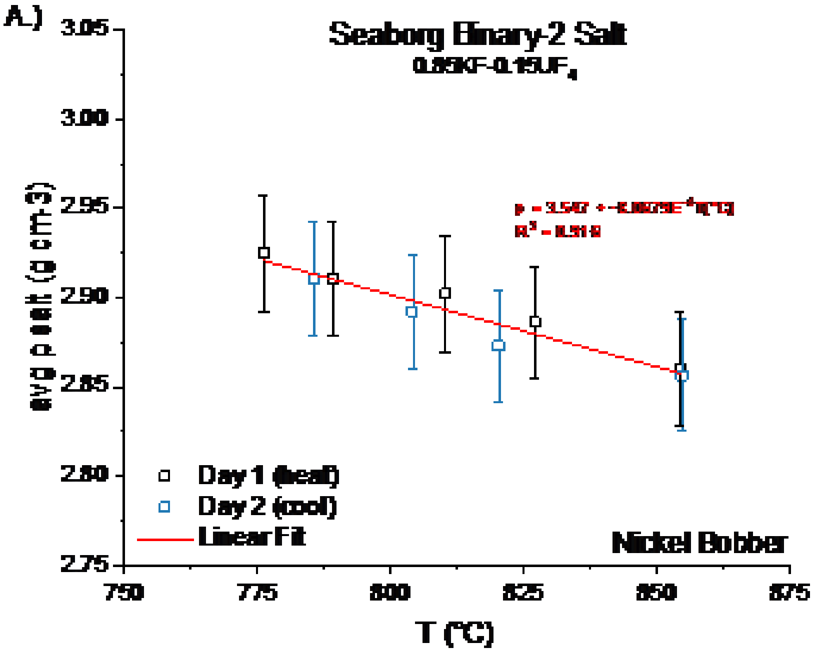

Figure 30. Experimental density values of the 15 mol% UF_4-KF system.

Table 35. Experimental density data for the Seaborg Binary-1 and -2 samples used to construct Figure 29 and Figure 30.

	Temperature	Temperature	Density	Density Error
	°C	K	g/cm^3	g/cm^3
Seaborg Binary-1, Ni Bobber, Trial 1	806.1	1079.1	5.90572	0.822298
	815	1088	4.456282	0.139845
	824.2	1097.2	3.498806	0.051413
	834.6	1107.6	3.312748	0.402179
	844.4	1117.4	3.508313	0.052231
Seaborg Binary-1, Ta Bobber, Trial 1	860.3	1133.3	5.64134	0.062009
	845.2	1118.2	5.516507	0.060954
	836.8	1109.8	5.54909	0.060484
	817.3	1090.3	5.60023	0.061045
	808.5	1081.5	5.626906	0.061358
Seaborg Binary-1, Ta Bobber, Trial 2	876.6	1149.6	5.384744	0.059717
	860.1	1133.1	5.338139	0.059157
	845.9	1118.9	5.284475	0.058589
	824.9	1097.9	5.325794	0.059249
Seaborg Binary-1, Ta Bobber, Trial 3	826.3	1099.3	5.397331	0.058992
	841.8	1114.8	5.311529	0.057885
	856.3	1129.3	5.241053	0.057133
	870.1	1143.1	5.219104	0.056871
Seaborg Binary-2, Ni Bobber, Trial 1	776.3	1049.3	2.927299	0.032425
	789.2	1062.2	2.912641	0.032229
	810.3	1083.3	2.903907	0.032133
	827.1	1100.1	2.887484	0.031884
	854.3	1127.3	2.861261	0.031572
Seaborg Binary-2, Ni Bobber, Trial 2	854.7	1127.7	2.870103	0.031535
	820.3	1093.3	2.887353	0.031775
	804.2	1077.2	2.907225	0.032032
	785.5	1058.5	2.926	0.032278

4.4.3. Summary

The density of the Seaborg-7 salt, 26.4UF_4-24.7KF-48.9NaF, was determined for the solid and molten phases. The density data is summarized in Figure 31. The linear fit of the data (black, dashed line) was extrapolated to near the first transition temperature of this salt composition as indicated on the heat flow curve (red) in Figure 31. Similarly, a linear fit of the liquid density data (blue, dashed line) was extrapolated to the liquidus temperature and beyond measuring temperatures for the density setup. The density changes between approximately 450 to 550°C are unknown.

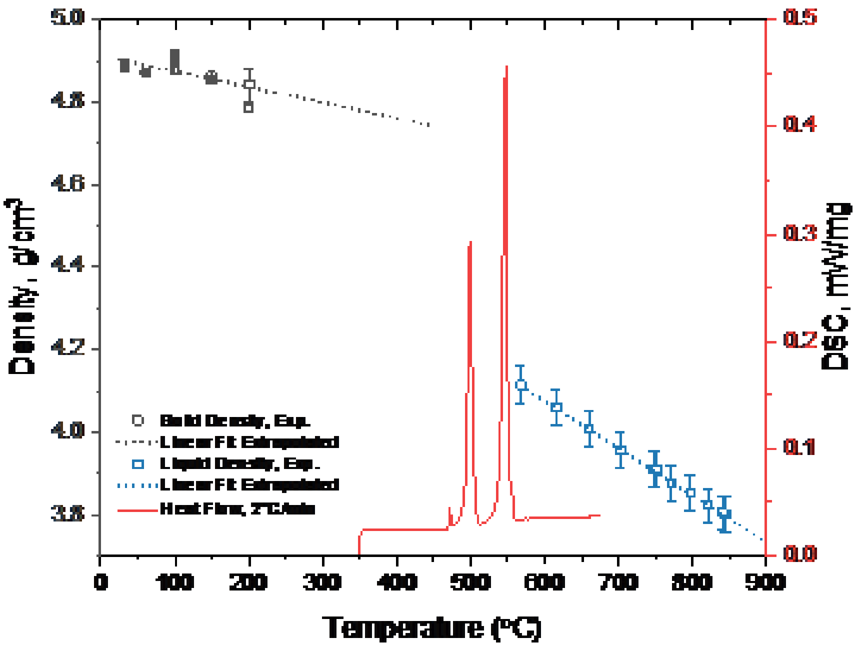

Figure 31. Experimental solid and liquid density data along with the extrapolated linear fit of the data. Density data is overlayed on the heat flow curve used to determine the Seaborg-7 melting temperature.

4.5. Thermal Diffusivity

Thermal diffusivity values were measured as a function of temperature using an LFA, NETZSCH LFA427, instrument located within an inert Ar glovebox in the Analytical Research Laboratory (ARL). The layout of the laser flash system and the LFA located in ARL are shown in Figure 32. Thermal diffusivity measurements on the Seaborg-7 salt were performed in ARL because the LFA was located within a glovebox, which eliminated concerns of oxygen/moisture contamination during measurement.

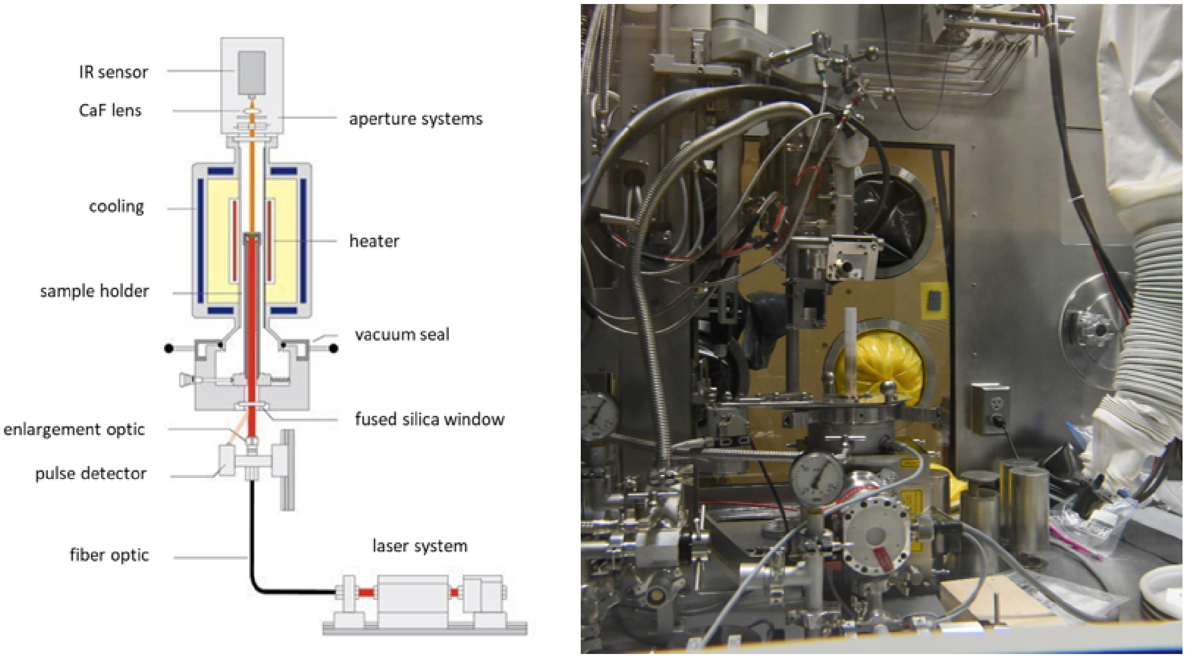

Figure 32. Layout of the NETZSCH LFA system (left). Picture of the NETZSCH LFA system in the Irradiated Materials Characterization Laboratory (IMCL, right).

4.5.1. Experimental Setup

The Seaborg-7 salt samples were contained in a stainless steel 316 custom designed and fabricated crucible, depicted in Figure 33. The crucible design was established to ensure minimal convection and avoid an erroneous conduction response across the steel base and walls. The sample and crucible dimensions were verified using a combination of vernier calipers and a micrometer. Prior to performing the sample measurement, the empty crucible was cleaned and sonicated in deionized water, conditioned by heating to 850°C, externally coated with a graphite coating, and conditioned again to 500°C to remove any organics from the graphite coating. See Figure 33 for picture of LFA crucible and lids.

Several methods were attempted to obtain a flat salt surface with a well-adhered crucible lid. Development of a sample preparation method was necessary, since the crucible lids sat at an angle on top of the salts in the first couple of runs, which inhibits the ability to obtain an accurate LFA measurement. In these samples, the crucible lid was easily separated from the crucible, which also impeded the necessary conductivity. The selected sample perpetration method involved adding salt to the LFA crucibles, placing these smaller crucibles in a glassy carbon secondary crucible, and heating them to temperature without lids and heating the salt to 800°C. Once the samples cooled, the LFA lids were added, and a 2-inch diameter steel weight was placed on top to maintain a level surface before the samples were again heated to temperature using the same heating profile. After the samples cooled, they were evaluated for LFA suitability, based on the flat angle of the lid and adherence of the lid to the salt in the crucible. These samples were then sent to ARL for analysis. All sample preparation steps except for the initial sonication (cleaning) were performed in an inert atmosphere glovebox.

Figure 33. LFA crucible for determining thermal diffusivity of high-temperature liquids. (A) Clean, as manufactured crucibles and (B) LFA crucibles after initial heat treatment and cleaning.

Each crucible containing the Seaborg-7 salt sample was placed in an alumina holder, which was subsequently placed inside the LFA furnace. The sample was then heated to predetermined temperatures in a high-purity Ar atmosphere under a pressure of 1.1 bar; see Table 36 for the measurement parameter guide. After reaching equilibrium, the front (bottom) surface of the specimen was subjected to a short laser pulse (0.6 milliseconds [ms] to 1.2 ms).

Table 36. Temperature range and LFA shot temperatures were used for determining thermal diffusivity on each Seaborg-7 sample.

Temperature Range (°C)	Guide	Temp. for Shot (°C)	Heating Rate (°C/min)	# of Shots at Each Temp.
Ambient to 400	100°C	200, 300, 400	10	5
450 to 850	Every 50°C increment	450, 500, 550, 600, 650, 700, 750, 800, 850	3	5
850 to 600 (cooling)	Every 100°C increment	800, 700, 600	10	5

The top surface, x_o, temperature response was recorded via an infrared detector as a function of time. This transient temperature response was also calculated using a three-layer heat transfer model (see Figure 34). The light-red top component in Figure 34 represents the crucible lid while the green bottom is the crucible base, both of which were made of stainless-steel 316 (SS 316). The salt was contained between the base and the lid (x_0 = top crucible surface boundary condition, x_1 = SS 316/salt interface, x_2 = salt/SS 316 interface, and x_3 = bottom crucible surface boundary condition). Thermal diffusivity was evaluated by minimizing the least square difference between the measured and calculated transients. A Pyroceram 9606 standard was measured as an equipment calibration check prior to testing the salt samples to ensure that the measured diffusivity values were within less than 5% (typically within less 2.5%) of the standard reference values. The one-dimensional (1-D) approximation can be improved by developing a 2-D finite element analysis model and examining the importance of heat transfer phenomena in 2-D such as radial conduction, but that step has not been done for this work.

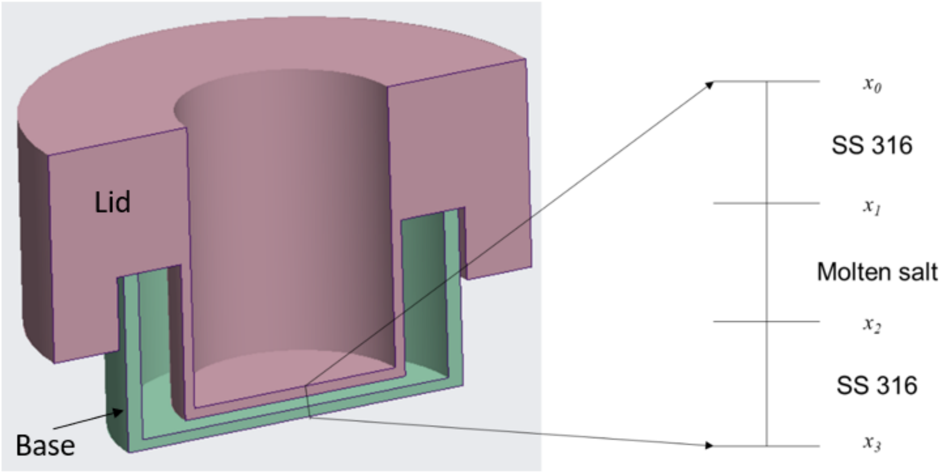

Figure 34. Schematic representation of a cross section of the 3-D crucible geometry (left) and 1-D approximation (right).

The initial validation of this novel method was performed on molten NaCl and LiCl-KCl samples and was shown to correlate well with literature data. The INL method has been designed to mitigate potential erroneous effects encountered in other studies, such as natural convection and conduction across the crucible.

4.5.2. Results

Experimentally determined thermal diffusivity data for the three Seaborg-7 samples are shown in Figure 35A–C. Each Seaborg-7 sample was heated/cooled three times to ensure reproducibility within each sample run and run in triplicate. Experimental data for each sample is represented as an open box, where the black boxes are the first heating, blue is the second heating, and red is the third heating cycle. The linear fit for each heating cycle is shown as a dashed line. Figure 35D provides a summary for all thermal diffusivity data, while the linear fit of all data is shown in Figure 35E. From the linear fit line of each sample, it can be assumed that there was good reproducibility between each sample run on the LFA.

It was assumed that the sample was is the solid phase when T = <550°C, while the sample was in the liquid phase when T = ≥550°C. Data for solid phase, thermal diffusivity measurements are also provided in Figure 36; however, the sample preparation and measuring technique is not recommended for the solid phase measurements, and the data may not accurately reflect the actual thermal diffusivity of the solid phase. It is interesting to note that the data collected in the solid phase is reproducible during each sample run and between samples. The intent in providing the solid phase data is to provide all data measurements performed at INL; using the solid-state thermal diffusivity data is at the discretion of Seaborg Technologies.

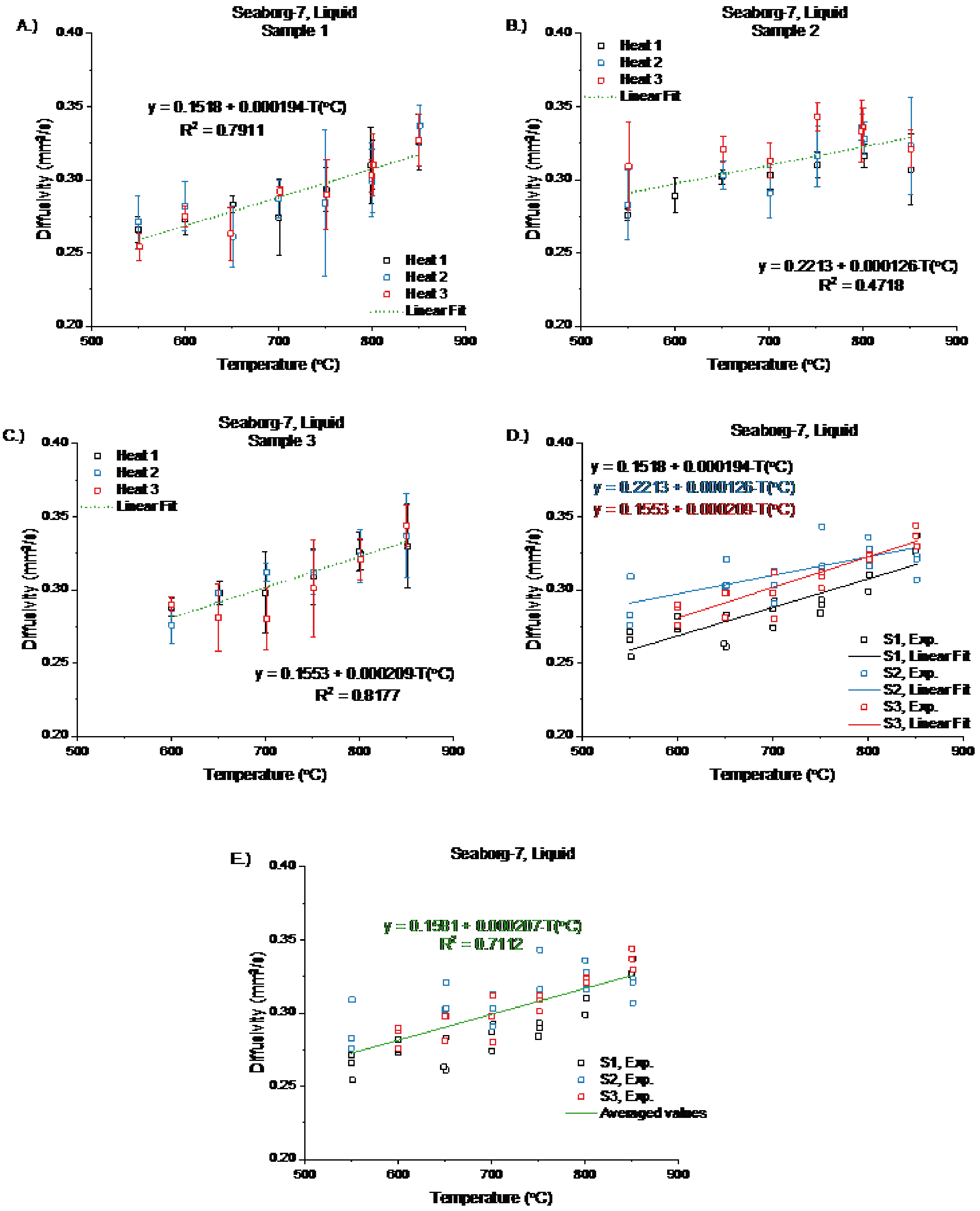

Figure 35. Thermal diffusivity results for Seaborg-7 molten salt. (A) Sample 1 with linear fit, (B) Sample 2 with linear fit, (C) Sample 3 with linear fit, (D) summary of thermal diffusivity data for Seaborg samples, and (E) all experimental thermal diffusivity data in the liquid phase with linear fit.

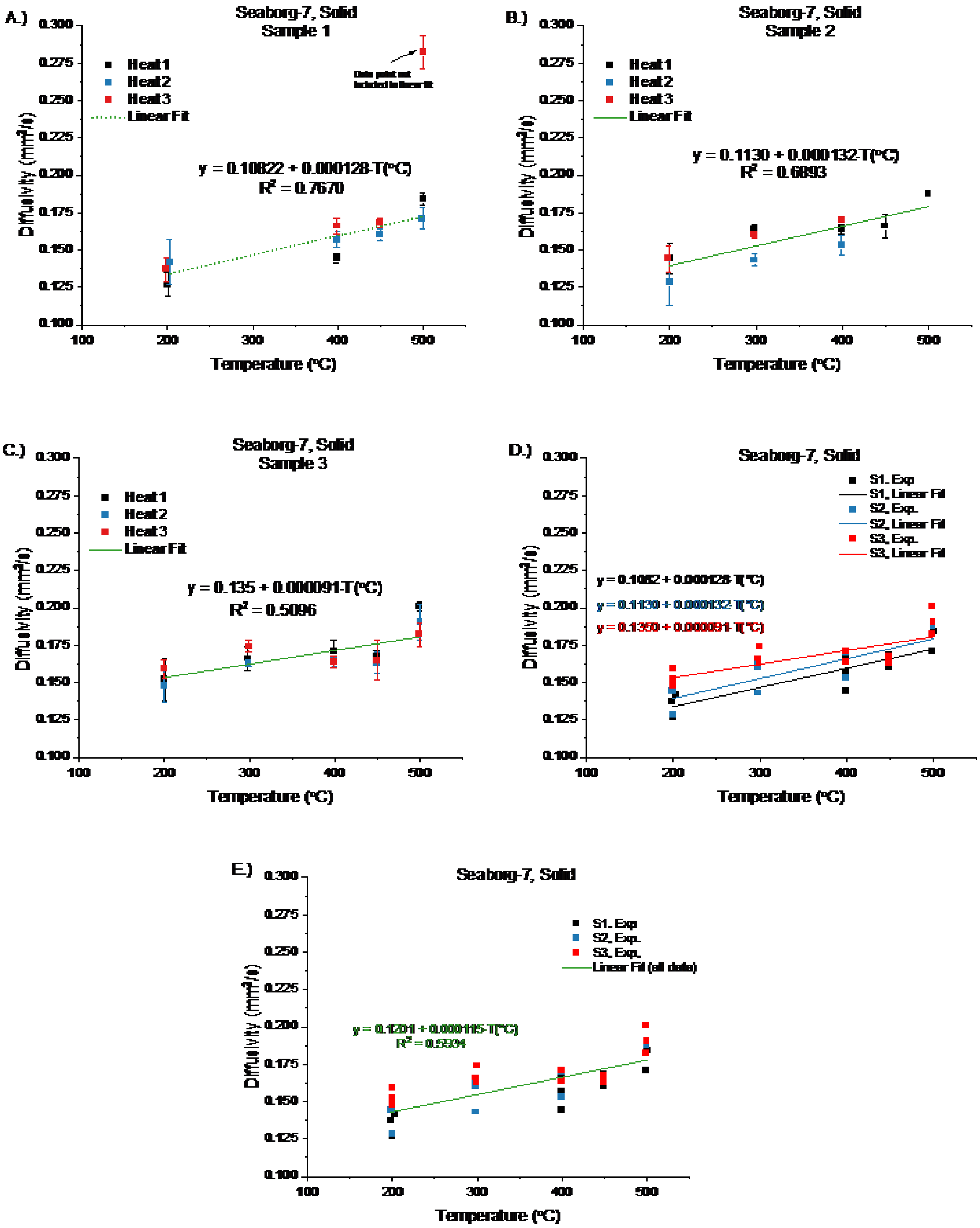

Figure 36. Thermal diffusivity results for Seaborg-7 solid salt. (A) Sample 1 with linear fit, (B) Sample 2 with linear fit, (C) Sample 3 with linear fit, (D) summary of thermal diffusivity data for Seaborg samples, and (E) all experimental thermal diffusivity data in the solid phase with linear fit.

Information for each Seaborg-7 sample is provided in Table 37, where the calculated salt thickness is the molten salt layer referenced between x_1 and x_2 in Figure 34. All experimentally determined thermal diffusivity data used to construct the plots in Figure 35 and Figure 36 are provided in Table 38.

Table 37. Masses of the Seaborg-7 salt in the LFA sample holder and measure thickness of the salt layer.

Sample Name	Salt Thickness (mm)	UF_4-NaF-KF Mass (g)
SB-7 S1	0.4792	1.8473
SB-7 S2	0.4934	1.8487
SB 7 S3	0.4792	1.8479

Table 38. Experimentally determined thermal diffusivity data collected using the LFA for Seaborg-7 salt.

Sample 1-1				**Sample 1-2**				**Sample 1-3**			
Temp.	Diffusivity	Dif. Error		Temp.	Diffusivity	Dif. Error		Temp.	Diffusivity	Dif. Error	
°C	mm²/s	mm²/s		°C	mm²/s	mm²/s		°C	mm²/s	mm²/s	
200.4	0.127	0.008		202.5	0.142	0.015		198.4	0.137	0.008	
398.8	0.144	0.003		399.2	0.157	0.005		398.9	0.166	0.005	
				449.7	0.16	0.004		449.7	0.168	0.003	
500.2	0.184	0.004		499.9	0.171	0.007		500.2	0.282	0.011	
549.8	0.266	0.009		550	0.271	0.018		550.6	0.254	0.009	
600.3	0.273	0.011		600.1	0.282	0.017		600.3	0.275	0.007	
650.9	0.283	0.006		651.1	0.261	0.021		649.1	0.263	0.018	
700.6	0.274	0.026		700.4	0.287	0.013		701.9	0.292	0.003	
751.1	0.293	0.015		749.9	0.284	0.05		751.5	0.29	0.024	
801.1	0.31	0.017		800.2	0.299	0.022		801.1	0.31	0.021	
850.3	0.326	0.019		850.8	0.337	0.014		850.5	0.327	0.018	
798.9	0.31	0.026		799.3	0.3	0.025		799.4	0.303	0.011	
699.8	0.309	0.006		699.3	0.277	0.03		699.8	0.272	0.021	
599.8	0.29	0.006		599.8	0.279	0.008		599.6	0.282	0.002	
Sample 2-1				**Sample 2-2**				**Sample 2-3**			
Temp.	Diffusivity	Dif. Error		Temp.	Diffusivity	Dif. Error		Temp.	Diffusivity	Dif. Error	
°C	mm²/s	mm²/s		°C	mm²/s	mm²/s		°C	mm²/s	mm²/s	
200.1	0.144	0.01		199.6	0.128	0.015		199.1	0.144	0.009	
298.5	0.164	0.003		298.8	0.143	0.004		298.5	0.16	0.002	
399	0.164	0.003		399.2	0.153	0.007		399.4	0.17	0.001	
449.8	0.166	0.008		549.8	0.283	0.024		550.5	0.309	0.03	
500	0.188	0.002		651.4	0.303	0.01		651.3	0.321	0.009	
549.4	0.276	0.004		700.8	0.291	0.017		700.8	0.313	0.012	
600.3	0.289	0.012		751.9	0.316	0.021		751.9	0.343	0.01	
650.2	0.302	0.005		801.4	0.328	0.011		800.5	0.336	0.013	
701.6	0.303	0.01		851.2	0.323	0.033		851.1	0.321	0.013	

Table 38. Continued.

Sample 2-1				**Sample 2-2**				**Sample 2-3**			
Temp.	Diffusivity	Dif. Error		Temp.	Diffusivity	Dif. Error		Temp.	Diffusivity	Dif. Error	
°C	mm^2/s	mm^2/s		°C	mm^2/s	mm^2/s		°C	mm^2/s	mm^2/s	
751.9	0.31	0.009		799.2	0.336	0.009		799.2	0.333	0.021	
801.4	0.316	0.008		699.8	0.286	0.062		699.6	0.328	0.01	
851.3	0.307	0.024		599.8	0.296	0.009		599.7	0.3	0.005	
798.8	0.307	0.013									
699.8	0.297	0.015									
599.7	0.281	0.017									
Sample 3-1				**Sample 3-2**				**Sample 3-3**			
Temp.	Diffusivity	Dif. Error		Temp.	Diffusivity	Dif. Error		Temp.	Diffusivity	Dif. Error	
°C	mm^2/s	mm^2/s		°C	mm^2/s	mm^2/s		°C	mm^2/s	mm^2/s	
200.4	0.152	0.014		199.9	0.148	0.011		199.8	0.159	0.006	
298.2	0.166	0.008		299	0.163	0.002		299.1	0.174	0.004	
399	0.171	0.007		399.2	0.164	0.003		399.2	0.164	0.004	
449.1	0.167	0.004		449.7	0.163	0.007		449.7	0.165	0.013	
499.7	0.201	0.003		500	0.19	0.012		499.9	0.182	0.008	
600.3	0.288	0.006		600.4	0.276	0.013		600.2	0.29	0.005	
651.5	0.298	0.008		649.9	0.298	0.006		650.3	0.281	0.023	
700	0.298	0.028		701.3	0.312	0.006		701	0.28	0.021	
750.9	0.309	0.019		751.4	0.312	0.015		751	0.301	0.033	
801.4	0.324	0.01		801.1	0.323	0.018		801.1	0.321	0.014	
851.3	0.33	0.029		850.6	0.337	0.029		850.7	0.344	0.014	
799.3	0.326	0.013		799.3	0.307	0.049		799.4	0.322	0.016	
699.9	0.31	0.014		699.9	0.301	0.011		699.2	0.297	0.027	
599.1	0.291	0.016		599.9	0.292	0.009		599.9	0.282	0.016	

4.6. Viscosity

The viscosity of a fluid is its ability to resist deformation or flow. Accurate viscosity measurements are important when planning for equipment design, which, with faulty data, can be either under- or over-designed, resulting in poor operation or unexpected capital costs and project delays. For Seaborg, a concentric cone geometry was used for viscosity measurements, where the sample is sheared in the gap between two cylinders. The outer cylinder (i.e., the sample cup) remains stationary, while the inner cylinder, also called the spindle or bob, rotates at a set angular velocity. The torque needed to overcome the viscous forces of the fluid to reach the chosen angular velocity was measured and could, for a known measuring geometry, be used to calculate viscosity by Equation 7, where η is dynamic viscosity, k is the flow zone coefficient, M is torque, and Ω is the angular velocity.

(7)

The flow zone coefficient can be calculated based on the measurement geometry or determined by calibration with standards of the known viscosity. For an ideal system where the flow in the system is steady, laminar, isothermal, and with no cylinder end effects, the flow zone coefficient can be calculated according to Equation 8, where L is the length of the spindle submerged in the sample, and R_a and R_i are the inner radius of the sample cup and the outer radius of the spindle, respectively.

(8)

Most practical measurement systems do not fulfill the criteria for the ideal system. Eccentric or off-centered spindle positions, flow effects at the end faces of the spindle, and other secondary flow instabilities result in a measured torque response that is greater than the torque from the flow in the measurement gap alone. To compensate for some of these discrepancies from an ideal system, samples with known viscosity can be measured, and the flow zone coefficient can be determined by Equation 9, where η (known) is the viscosity of a known standard.

(9)

However, the probability of inflated torque responses is not only dependent on the measurement geometry but also on fluid properties, such as viscosity and density. When interpreting rheological data, the Reynolds number (Re) and the Taylors number (Ta) can help understand the probability of secondary flows. Re and Ta are defined by Equations 10 and 11, respectively, where ρ is the density of the liquid measured.

(10)

(11)

As can be seen in Equations 10 and 11, for a set measurement geometry, fluids with higher density and lower viscosity give elevated Re and Ta numbers. Higher Re and Ta indicate the likelihood of secondary flows, which would result in inflated torque responses.

4.6.1. Experimental Setup and Calibrations

For viscosity measurements, a DVNext viscometer from Brookfield Amatek and a Kerr Maxi-Melts furnace were used. The head of the DVNext was mounted (see Figure 37) on a base plate equipped with leveling legs and metal brackets to lock the furnace in place. The brackets prevented movement of the furnace during or between measurements that would result in off-centered spindle positions relative to the sample cup. An outer metal crucible was fabricated for the furnace as a safety measure to protect the furnace from potential salt leakage. Both the spindle and the sample cup were stainless steel with an elongated shaft to distance the viscometer head from the hot zone of the furnace. A metal ring placed in the bottom of the furnace ensured that the sample cup was stationary and centered in the furnace.

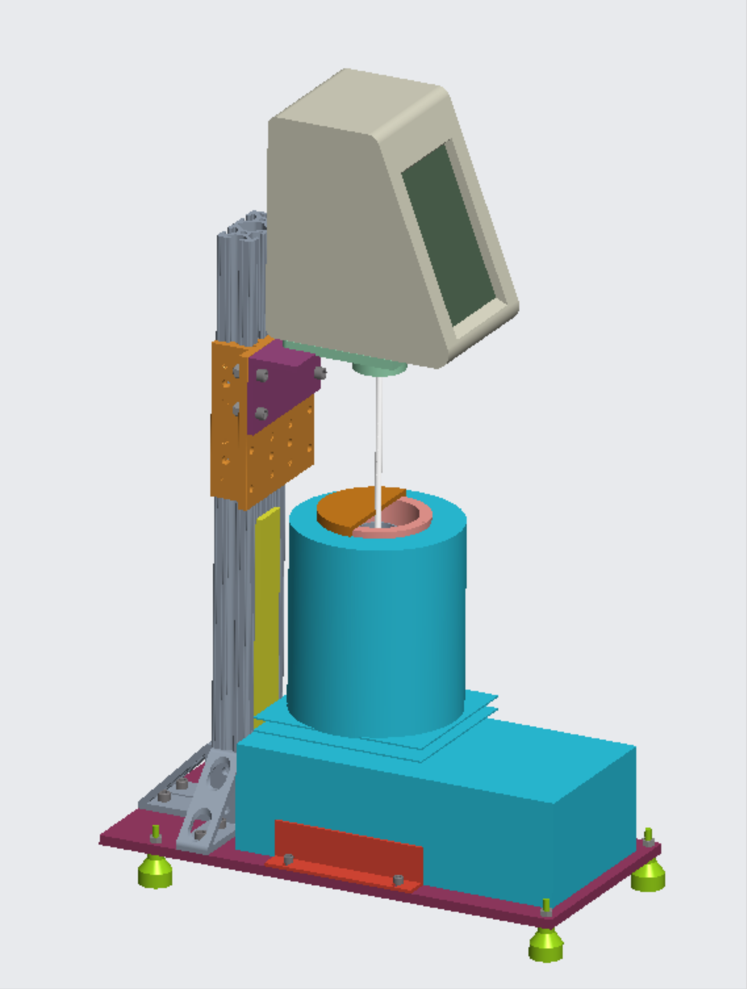

Figure 37. Schematic of the viscometer setup.

4.6.2. Results

4.6.2.1. Spindle and Cup Iteration 1

4.6.2.1.1. Standards

The viscometer experimental setup was tested by measuring viscosities of S3, S6, N10 viscosity calibrations standards (Canon Instruments). Table 39 provides the values for density and dynamic viscosity as a function of temperature for each standard. The torque response of each sample was measured at rotational velocities somewhere between 10 to 55 rotations per minute (RPM). The exact RPM interval for each sample was chosen dependent on torque response for each sample. Five measurements were taken at each rotational velocity. The raw data of the measurements are presented in Table 40.

Table 39. Density and viscosity of standards used to determine flow zone coefficient for the viscometer measurement geometry. Values for standards S3, S6, and N10 from bottle labels.

	S3		S6		N1.0	
Temperature	ρ	η	ρ	η	ρ	η
°C	g/cm^3	mPa·s	g/cm^3	mPa·s	g/cm^3	mPa·s
20	0.868	3.99	0.878	9.66	0.864	18.710
25	0.864	3.54	0.874	7.78	0.861	15.050
37.78	0.855	2.65	0.866	5.2	0.853	9.224
40	0.854	2.48	0.864	4.92	0.851	8.552
50	0.847	2.03	0.858	3.78	0.844	6.256
60	-	-	-	-	-	-
80	0.826	1.24	0.837	2.01	0.825	3.007
98.89	0.812	0.974	0.824	1.48	0.812	2.113
100	0.811	0.973	0.823	1.48	0.812	2.074

Table 40. Viscometer torque response (raw data) as a function of rotation speed for viscosity standards. Torque is measured in % of maximum. Maximum torque, given by the fabricator of the viscometer, is 0.0673 mN·m.

Speed	Speed, Ω	Torque 1	Torque 2	Torque 3	Torque 4	Torque 5	Torque Avg.	Torque,M	Temp.	Theo Visc.	M/Ω
RPM	rad/s	%	%	%	%	%	%	mN·m	°C	mPa·s	mN·s/rad·m
30	3.1	9.4	9.4	9.3	9.5	9.3	9.4	0.0063	24.1	3.5	0.002009
35	3.7	12.1	10	11.8	10.3	11.6	12.1	0.0075	24.1	3.5	0.002049
40	4.2	12.9	13.1	12.8	13.6	13.4	12.9	0.0089	24.1	3.5	0.002114
45	4.7	14.9	14.7	14.7	14.6	15.1	14.9	0.0100	24.4	3.5	0.002114
50	5.2	15.7	16	16.1	15.9	15.8	15.7	0.0107	24.4	3.5	0.002044
55	5.8	18.3	18.3	17.6	18.4	18	18.3	0.0122	24.4	3.5	0.002117
30	3.1	10.3	10.1	9.5	9.7	8.6	9.64	0.0065	25.3	3.4	0.002065
35	3.7	11.4	11.3	11.4	11.4	11.2	11.34	0.0076	25.3	3.4	0.002082
40	4.2	12.7	12.7	12.7	12.7	12.5	12.66	0.0085	25.3	3.4	0.002034
45	4.7	14.4	14	14.2	13.7	14	14.06	0.0095	25.3	3.4	0.002008
50	5.2	15.9	15.7	15.6	15.7	15.8	15.74	0.0106	25.3	3.4	0.002023
55	5.8	17	17.7	17	18	17.1	17.36	0.0117	25.3	3.4	0.002028

Speed	Speed, Ω	Torque 1	Torque 2	Torque 3	Torque 4	Torque 5	Torque Avg.	Torque,M	Temp.	Theo Visc.	M/Ω
RPM	rad/s	%	%	%	%	%	%	mN·m	°C	mPa·s	mN·s/rad·m
35	3.7	25.0	26.0	25.2	25.9	25.7	25.6	0.0172	29	7.1	0.004693
30	3.1	21.6	22.0	21.5	21.9	21.9	21.8	0.0147	29	7.1	0.004666
25	2.6	18.8	17.8	19.2	17.7	19.5	18.6	0.0125	29	7.1	0.004781
20	2.1	15.5	15.9	15.7	15.1	15.3	15.5	0.0104	27.7	7.4	0.004981
15	1.6	9.4	10.6	8.9	11.1	9.6	9.9	0.0067	27.7	7.4	0.004250
40	4.2	30.5	30.8	30.7	30.7	30.8	30.7	0.0207	27.7	7.4	0.004932
35	3.7	27.7	25.9	28.2	26.0	28.1	27.2	0.0183	27.5	7.4	0.004991
30	3.1	23.2	23.4	23.5	23.6	23.3	23.4	0.0157	27.5	7.4	0.005013
25	2.6	20.2	18.0	20.2	18.1	20.8	19.5	0.0131	27.4	7.5	0.005003
20	2.1	14.0	14.2	13.3	13.7	13.4	13.7	0.0092	27.4	7.5	0.004409
15	1.6	10.2	13.4	10.2	12.5	9.7	11.2	0.0075	27.4	7.5	0.004799
40	4.2	31.8	31.6	31.8	32.8	31.6	31.9	0.0215	27.4	7.5	0.005128

Speed	Speed, Ω	Torque 1	Torque 2	Torque 3	Torque 4	Torque 5	Torque Avg.	Torque,M	Temp.	Theo Visc.	M/Ω
RPM	rad/s	%	%	%	%	%	%	mN·m	°C	mPa·s	mN·s/rad·m
20	2.1	33.7	34.1	33.8	33.6	33.9	33.82	0.0228	24.4	15.4	0.010867
15	1.6	22.4	26.2	22.3	27.3	22.1	24.06	0.0162	24.4	15.4	0.010308
10	1.0	17.6	18.1	17.9	17.5	17.9	17.8	0.0120	24.6	15.3	0.011439
17	1.8	28.3	26.4	28.1	26.5	28	27.46	0.0185	24.1	15.6	0.010381
20	2.1	32.8	32.7	33.4	33.3	32.5	32.94	0.0222	24.4	15.4	0.010585
15	1.6	27	22.9	26.9	23.1	27.8	25.54	0.0172	24.4	15.4	0.010942
10	1.0	17	16.7	17.3	16.8	16.7	16.9	0.0114	24.3	15.5	0.010861
17	1.8	29.9	27.2	29.4	27	30	28.7	0.0193	23.6	16.0	0.010850

The viscosity of a Newtonian fluid is independent of the rotational speed. As shown by Equation 7, for a Newtonian fluid, the torque response is directly proportional to the rotational speed, meaning that, at low rotational speeds, the measured torque response is low, which results in large measurement errors due to measurement noise. The manufacturer of the DVNext recommends not to measure torques <10% of the maximum torque. The rotational speed of each sample was chosen so that these torque response criteria were met whenever possible. However, as can be seen in Equations 10 and 11, increased rotational speeds increase the likelihood of secondary flows. A balance must be struck between having a rotational speed high enough for an adequate torque response to minimize measurement error, while being low enough to reduce the probability of secondary flows. As shown in Figure 38, a linear relationship between rotational speed and torque was observed for all standards, as it should be for a Newtonian fluid. This leads to the conclusion that the measurements were conducted within an appropriate range of rotational speeds. The slope of the curved corresponds to M/Ω in Equation 7 and will later be used to calculate viscosity when k is determined.

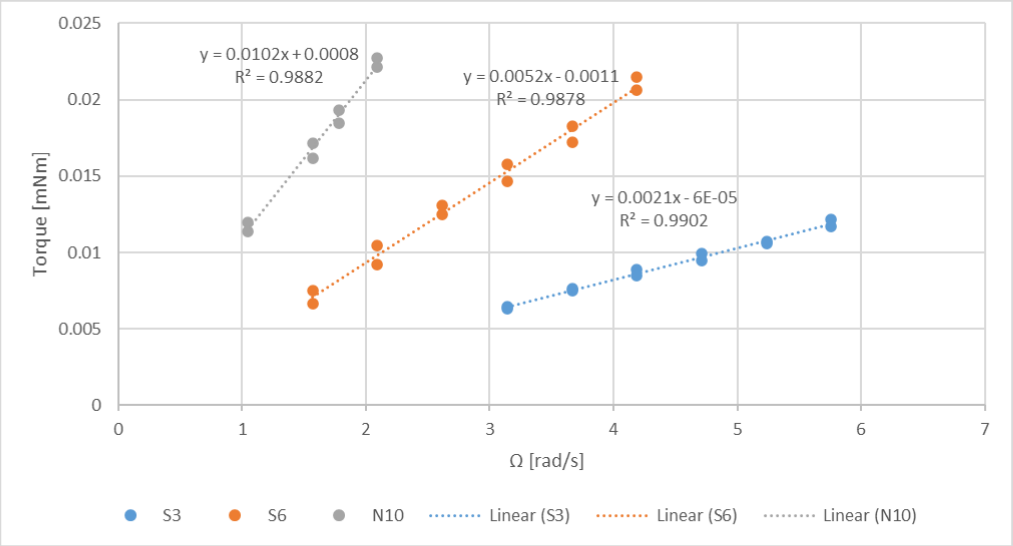

Figure 38. Torque response as a function of rotational speed for standard samples.

For the ideal case, the flow zone coefficient, k, was calculated using Equation 8 to be 1617.6 m^{-3}. This represents an ideal system with laminar flow and no end effects. Corresponding viscosity values for the standards can be found in Table 41. As can be seen, these viscosity values are significantly higher than the expected viscosity values of the standards. That is because, when using Equation 8, the system was assumed to be ideal, and the torque response was fully attributed to the viscosity of the sample. Instead, by using Equation 9 to determine the flow zone coefficient, the discrepancies from an ideal system can be captured. The flow zone coefficient was determined for each measurement point, resulting in an average flow zone coefficient equal to 1487.3 m^{-3}, and the resulting viscosities for the standards can be found in Table 41. The resulting viscosities were about 10% lower than the ideal case, which is in the expected range if end effects are taken into consideration.

Table 41. Tabulated and measured viscosity of standard samples. M/Ω is given by the slope of curves in Figure 38. Viscosities are calculated by Equation 7.

	η Theoretical	η (ideal) (k = 1617.6)	η (non-ideal) (k = 1487.3)
	mPa·s	mPa·s	mPa·s
S3	3.4	3.4	3.1 ± 0.2
S6	7.3	7.9	7.7 ± 0.5
N10	15.5	17.3	15.2 ± 0.9

4.6.2.1.2. Seaborg-7 (48.9NaF - 24.7KF - 26.4UF_4)

For the viscosity measurements, 130.95g salt was loaded into the sample cup, which was loaded into the furnace (see Figure 39) and heated to at least 30°C above the melting temperature of the salt. The spindle was lowered into the molten salt, and the salt was heated to the measuring temperature. When the measurement temperature was reached, the system was left to equilibrate for at least 30 minutes before measurements were initiated. To ensure correct temperature, a thermocouple calibrated to the temperature of the sample was kept inside the oven for the duration of the experiment.

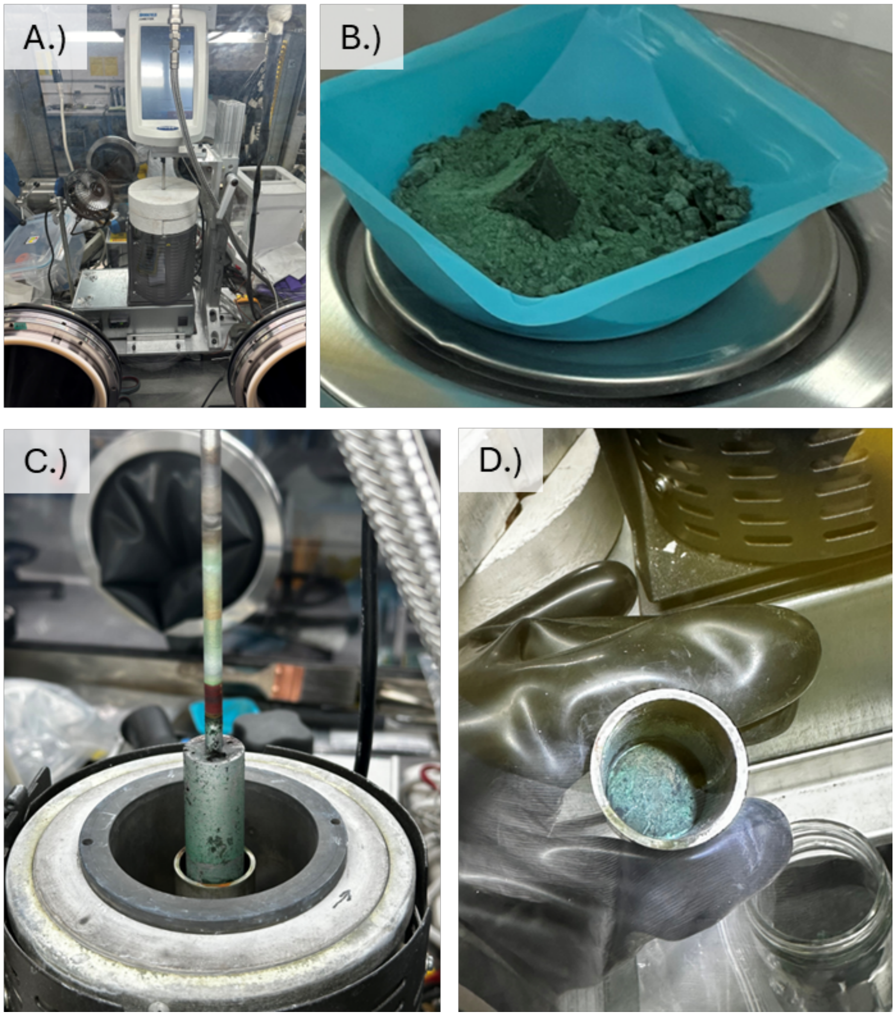

Figure 39. (A) Setup for viscometer measurements in FCG, (B) fluoride salt prior to viscosity measurements, (C) measurement spindle after measurement, and (D) fluoride salt frozen in measurement cup after measurement.

Five measurements were taken at 35, 40 and 45 RPM, respectively. The raw data from these measurements can be found Table 42. Like the standards, the sample's torque response should exhibit a linear relationship as a function of rotational speed. In Figure 40, the torque response appears to be constant with respect to RPM. Upon observation, a linear response was noted; however, the data presents two distinct issues:

1. The torque response does not vary with rotational speed, suggesting the sample behaves like a non-Newtonian, shear-thickening fluid.
2. The torque response remains constant across a temperature range of 650 to 750°C, indicating that the sample's viscosity does not change with temperature variations.

It is improbable for the salt to exhibit these characteristics. A more plausible explanation is that the measuring spindle was being displaced upward due to buoyancy forces. As a point of reference, LiCl-KCl, which is a less dense salt, was successfully measured and data for LiCl-KCl-eutectic is shown in Figure 40. Utilizing a heavier spindle of the same dimensions could potentially mitigate the influence of buoyancy forces on the measurement. Unfortunately, the viscometer has a limitation on spindle weight, precluding the use of a heavier spindle.

Table 42. Viscometer torque response (raw data) as a function of rotation speed for Seaborg-7 salt. Torque is measured in % of maximum. Maximum torque, given by the fabricator of the viscometer, is 0.0673 mN·m.

Temp.	Speed	Speed, Ω	Torque 1	Torque 2	Torque 3	Torque 4	Torque 5	Torque Avg.	Torque,M	M/Ω
°C	RPM	rad/s	%	%	%	%	%	%	mNm	mN·s/rad·m
659	35	3.7	42.8	41	42.4	41.1	41.1	41.68	0.02805	0.00765
657	40	4.2	41.5	41.2	41	41.1	41.1	41.18	0.02771	0.00662
659	45	4.7	40.6	39.6	40.5	40.5	39.3	40.1	0.02699	0.00573
706	45	4.7	40	39.5	39.6	39.7	40.4	39.84	0.02681	0.00569
707	40	4.2	39.9	39.9	40	41.8	39.5	40.22	0.02707	0.00646
706	35	3.7	40.2	38.9	39.8	39.2	39.7	39.56	0.02662	0.00726
751	35	3.7	39.6	39.1	39.6	39	39.8	39.42	0.02653	0.00724
747	40	4.2	39.5	39.5	39.7	39.8	40.6	39.82	0.02680	0.00640
748	45	4.7	39.8	39.4	40.3	39.7	39.9	39.82	0.02680	0.00569

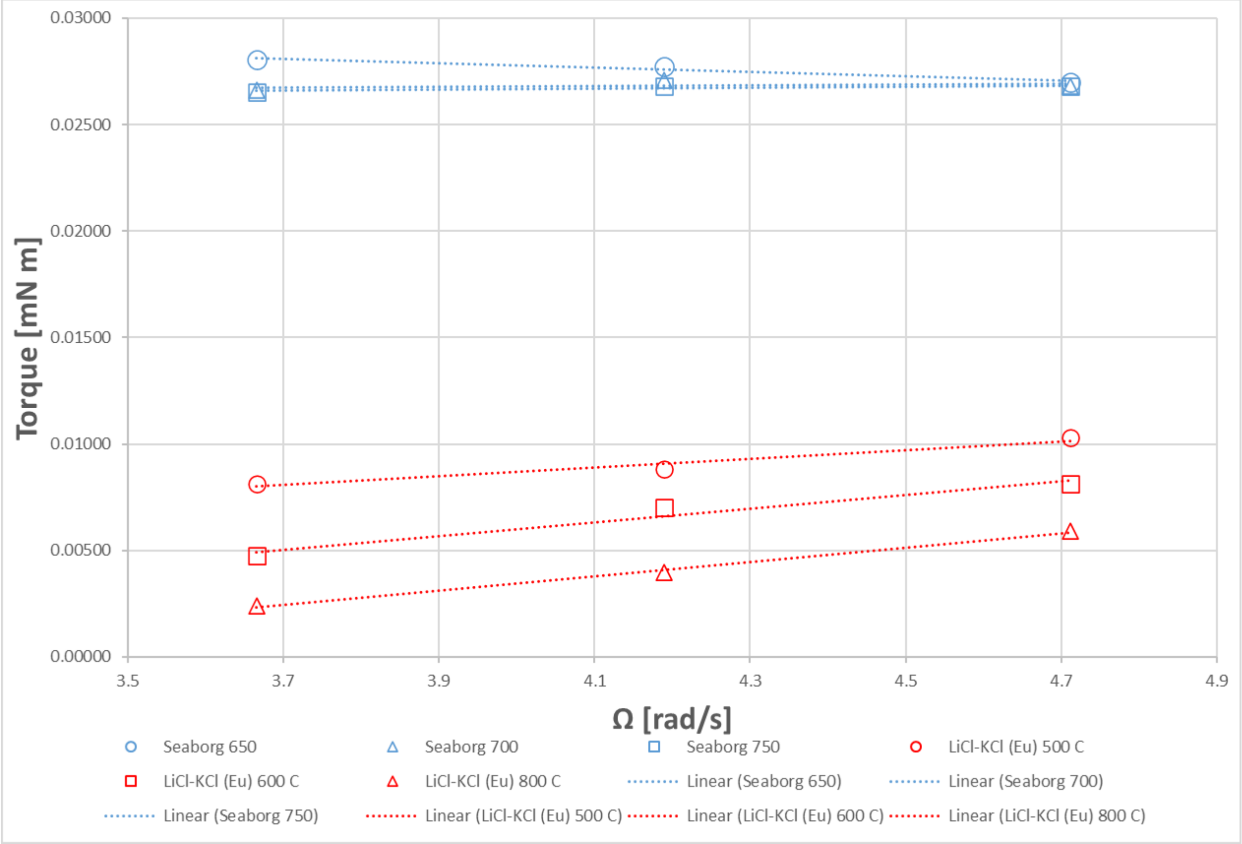

Figure 40. The torque response of the Seaborg-7 salt as a function of rotational speed. LiCl-KCl eutectic salt, as a less dense salt, is included as a point of reference.

4.6.2.2. Spindle and Cup Iteration 2

The data set collected with the initially used spindle and cup was determined to be highly physically improbable. It was hypothesized that the relatively high density of the salt resulted in buoyant forces which, in turn, affected the torque response of the equipment. The buoyant force, F_b, on an object submerged in a fluid, is dependent on fluid density, ρ, and volume of the object, V, as follows

(12)

where g is acceleration due to gravity. To keep an object submerged in a fluid, the gravitational force, which is directly proportional to the mass of the object, must be equal to or exceed the buoyant force. Thus, by reducing the volume of the spindle while keeping the spindle's weight constant, the likelihood of measurement error due to buoyant forces would be reduced. Based on this reasoning, a new measurement geometry, that is a spindle and sample cup, was designed and fabricated. A schematic of the iteration 1 and iteration 2 measurement geometries can be seen in Figure 41.

As before, the iteration 2 geometry was tested, and the flow zone coefficient was determined by measuring the viscosities of viscosity Newtonian calibration standards. However, this time, only standards S6 and N10 were used due to (1) limit the amounts of organic liquid in the rad glove box and (2) the prediction that the torque response of standard S3 would be too small. The raw data from the measurements are presented in Table 43. As shown in Figure 42, a linear relationship between rotational speed and torque was observed for both standards, as expected for a Newtonian fluid. The resulting flow zone coefficient was determined to be 2383.5 m^{-3} by the same method as previously used. Corresponding viscosity values for the standards can be found in Table 44. It is worth noting that the measured viscosity for standard S6 differs somewhat from the theoretical tabulated value. This discrepancy is unfortunate but unavoidable as the measurements are in the lower range of what the equipment can accurately measure.

For the viscosity measurements of the salt, the same procedure as outlined in the previous section was performed, with the following exceptions: (1) due to the smaller measuring geometry, 93.68g of salt was loaded into the sample cup, compared to the previous 130.95g; (2) measurements were taken at 10, 15, 20, 25, 30, and 35 RPM, respectively. The raw data from these measurements can be found Table 45, and the torque response as a function of rotation speed is shown in Figure 43. The slope of each curve in Figure 43 corresponds to M/Ω in Equation 7. By multiplying the slope by $k = 2383.5\ m^{-3}$, which was determined by measuring the organic standards, the viscosity of the salt at each temperature is obtained. The measured viscosities are listed in Table 46, and the viscosity as a function of temperature is plotted in Figure 44. An exponential fit of the experimentally determined viscosity data yielded the equation, η (mPa·s) = 736.58, relating the viscosity of the Seaborg-7 to temperature.

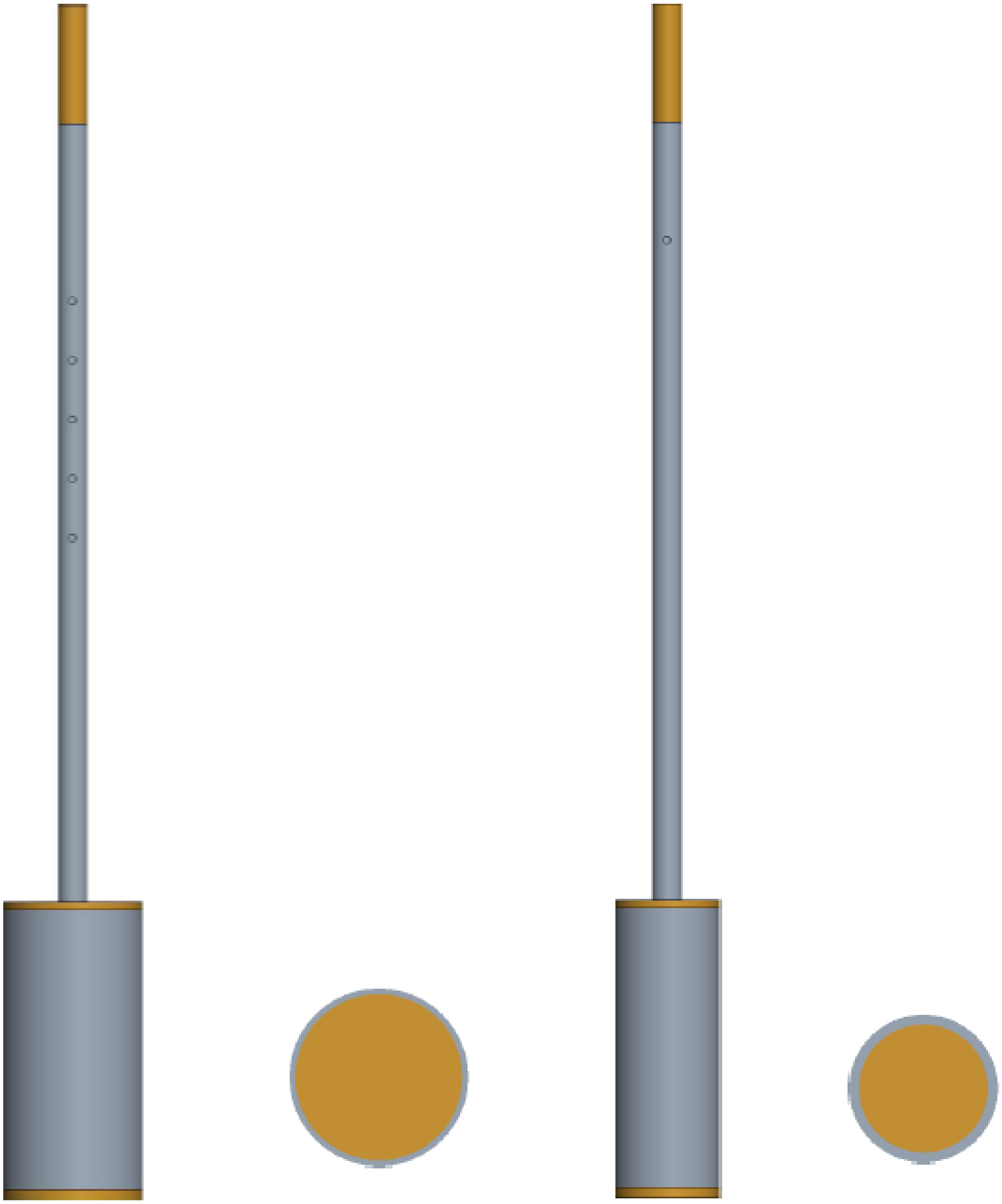

Figure 41. Iteration 1 (left) and 2 (right) of the spindle and cup, respectively. Shown in scale 1:1.

Table 43. Viscometer torque response (raw data) as a function of rotation speed for viscosity standards. Torque is measured in % of maximum. Maximum torque, given by the fabricator of the viscometer, is 0.0673 mNm.

Speed	Speed, Ω	Torque 1	Torque 2	Torque 3	Torque 4	Torque 5	Torque Avg.	Torque, M	Temp.	Theo Visc.	M/Ω
RPM	rad/s	%	%	%	%	%	%	mNm	°C	mPa·s	mN·s/rad ·m
30	3.1	13.8	13.8	13.8	13.8	13.8	13.8	0.0093	32.4	6.3	0.0030
35	3.7	16.7	16.7	16.7	16.7	16.6	16.68	0.0112	32.8	6.2	0.0031
40	4.2	19.9	19.9	19.9	19.9	19.9	19.9	0.0134	32.8	6.2	0.0032
45	4.7	21.1	21.1	21.2	21.5	21.4	21.26	0.0143	32.4	6.3	0.0030

Speed	Speed, Ω	Torque 1	Torque 2	Torque 3	Torque 4	Torque 5	Torque Avg.	Torque, M	Temp.	Theo Visc.	M/Ω
RPM	rad/s	%	%	%	%	%	%	mNm	°C	mPa·s	mN·s/rad ·m
25	2.6	13.9	19.3	14	14.1	14.2	15.1	0.0102	32.8	11.0	0.0039
30	3.1	19.3	19.3	19.2	19.2	19.3	19.26	0.0130	32.8	11.0	0.0041
35	3.7	24.1	24	23.8	23.4	23.3	23.72	0.0160	32.8	11.0	0.0044
40	4.2	26.8	26.8	26.8	26.8	26.8	26.8	0.0180	32.8	11.0	0.0043

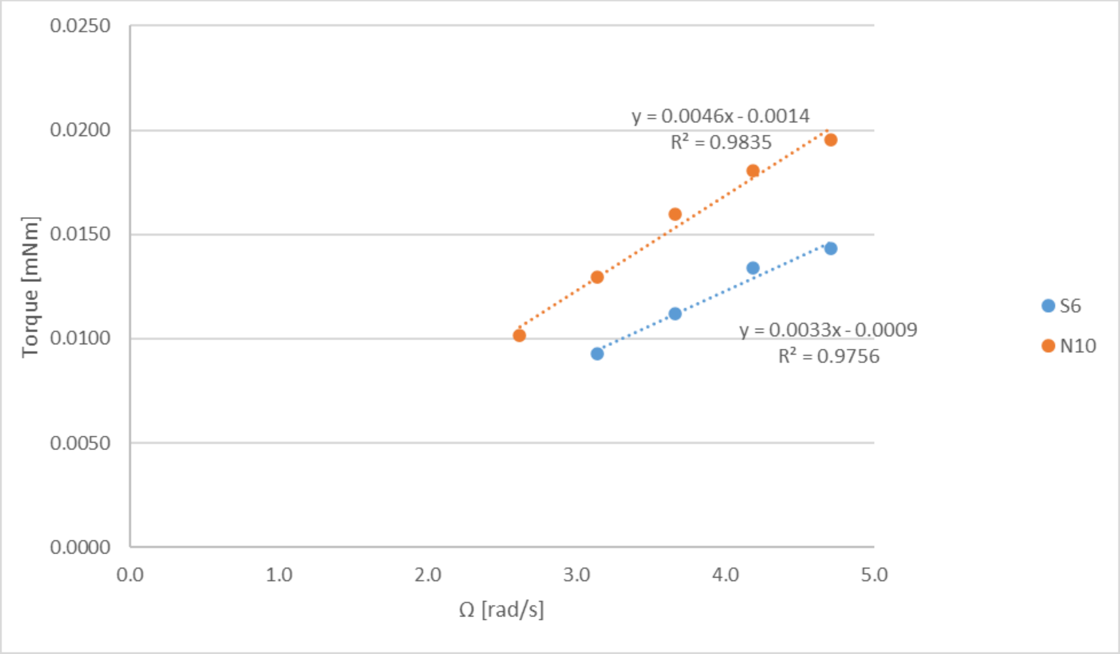

Figure 42. The torque responses of viscosity standards as a function of rotational speed. Data taken from Table 43.

Table 44. Tabulated and measured viscosity of standard samples. Viscosities are calculated by Equation 7 from slopes given in Figure 42 and k = 2383.5 m^{-3}.

	η Theoretical	η (experimental) (k = 2383.5)
	mPa·s	mPa·s
S6	6.3	7.8 ± 1.1
N10	11.0	10.9 ± 1.5

Table 45. Viscometer torque response (raw data) as a function of rotation speed for Seaborg-7 salt. Torque is measured in percent of maximum torque. Maximum torque, given by the fabricator of the viscometer, is 0.0673 mN·m. Each temperature setpoint is separated by a thicker line.

Temp.	Speed	Speed, Ω	Torque 1	Torque 2	Torque 3	Torque 4	Torque 5	Torque Avg.	Torque,M
°C	RPM	rad/s	%	%	%	%	%	%	mNm
599.1	35	3.7	47	47.7	47.5	47.1	47.1	47.3	0.0318
599.1	30	3.1	39.7	39.6	39.8	40.1	40.6	40.0	0.0269
598.1	25	2.6	33.1	33.8	33.6	34.4	34.3	33.8	0.0228
595.1	20	2.1	28.4	27.5	29.2	27.4	28.2	28.1	0.0189
591.1	15	1.6	21.2	25.2	21.5	25.1	21.5	22.9	0.0154
588.1	10	1.0	16.7	16	16.9	16.8	14.7	16.2	0.0109
614.1	35	3.7	39.5	39.8	39.5	39.4	38.9	39.4	0.0265
618.1	30	3.1	34.7	34.9	34.4	34.5	33.3	34.4	0.0231
623.1	25	2.6	30.2	29.9	30.5	29.5	30.4	30.1	0.0203
624.1	20	2.1	25.3	25	25.3	25.4	25.1	25.2	0.0170
623.1	15	1.6	21.1	19.3	21.4	18.9	21.6	20.5	0.0138
620.1	10	1.0	16	17.4	16.5	17.4	16.3	16.7	0.0113
648.1	10	1.0	13.4	13.2	11.7	11.8	11.8	12.4	0.0083
649.1	15	1.6	17	18.7	17.9	17.2	17.3	17.6	0.0119
648.1	20	2.1	20.8	20.3	20.5	21.8	20.6	20.8	0.0140
646.1	25	2.6	25	25.2	25	24.7	25.4	25.1	0.0169
643.1	30	3.1	29.9	27	29.4	29.2	29.9	29.1	0.0196
641.1	35	3.7	34.4	33.9	33.9	33.2	33.6	33.9	0.0228
680.1	10	1.0	13.2	13.5	14.5	13.5	13.2	13.6	0.0091
675.1	10	1.0	15.5	18.3	16.1	17.5	15.7	16.6	0.0112
671.1	15	1.6	20.6	19.3	20.9	20.2	20.9	20.4	0.0137
667.1	20	2.1	24.1	23.4	23.8	23.5	24	23.8	0.0160
671.1	25	2.6	27.1	27.3	27.2	27.4	28	27.4	0.0184
663.1	30	3.1	29.1	29.8	30.3	30	29.4	29.7	0.0200
680.1	35	3.7	13.2	13.5	14.5	13.5	13.2	13.6	0.0091
700.1	10	1.0	12	11	10.6	11.6	11.1	11.3	0.0076
698.1	15	1.6	14.7	12.7	16.5	12.9	15.4	14.4	0.0097
692.1	20	2.1	17.3	18	17.8	17.3	17.3	17.5	0.0118
694.1	25	2.6	20.5	18.9	20.3	20.2	20.6	20.1	0.0135
693.1	30	3.1	22.9	24.2	24	24.6	23.5	23.8	0.0160
696.1	35	3.7	26.2	26.3	26.5	26.4	26.2	26.3	0.0177
719.1	10	1.0	13	13.1	11.5	12.7	12.2	12.5	0.0084
717.1	15	1.6	12.9	16.4	13.1	16.7	14	14.6	0.0098
720.1	20	2.1	16.8	16.2	16	16.7	16.6	16.5	0.0111
720.1	25	2.6	18.6	17.7	18.7	19.2	19.1	18.7	0.0126
722.1	30	3.1	23	21.9	21.5	22.6	22.1	22.2	0.0150

Table 45. Continued.

Temp.	Speed	Speed, Ω	Torque 1	Torque 2	Torque 3	Torque 4	Torque 5	Torque Avg.	Torque,M
°C	RPM	rad/s	%	%	%	%	%	%	mNm
723.1	35	3.7	25.1	24.3	24.5	24.1	23.7	24.3	0.0164
745.1	10	1.0	7.8	8.9	8.3	6.4	8.5	8.0	0.0054
748.1	15	1.6	11.5	13.2	12.1	12.7	11.4	12.2	0.0082
749.1	20	2.1	15	14.5	14.8	14.3	15.2	14.8	0.0099
747.1	25	2.6	18.4	18.5	17.5	17.9	18	18.1	0.0122
748.1	30	3.1	20	20.3	20.4	20.4	22	20.6	0.0139
748.1	35	3.7	22.7	22.6	22	23.4	22.8	22.7	0.0153
775.1	10	1.0	11.9	10.3	11.5	10.2	11.1	11.0	0.0074
774.1	15	1.6	12.7	11.2	14	11.4	12	12.3	0.0083
775.1	20	2.1	15.3	14.2	13.7	14.3	13.9	14.3	0.0096
774.1	25	2.6	15.9	15.7	17.9	16.8	16.5	16.6	0.0111
773.1	30	3.1	18.5	18.7	18.8	20.2	18.1	18.9	0.0127
771.1	35	3.7	19.7	19.3	19.9	19.4	20.1	19.7	0.0132
800.1	10	1.0	11.5	10.2	10.5	9.9	11.6	10.7	0.0072
796.1	15	1.6	12.9	15.6	12.7	15.8	13	14.0	0.0094
797.1	20	2.1	15.2	15.8	15.4	14.6	13.5	14.9	0.0100
797.1	25	2.6	15.3	15.5	15.6	16	16.3	15.7	0.0106
798.1	30	3.1	16.9	15.6	16.8	16.4	17.3	16.6	0.0112
796.1	35	3.7	19.5	18.7	18.7	18.4	18.9	18.8	0.0127

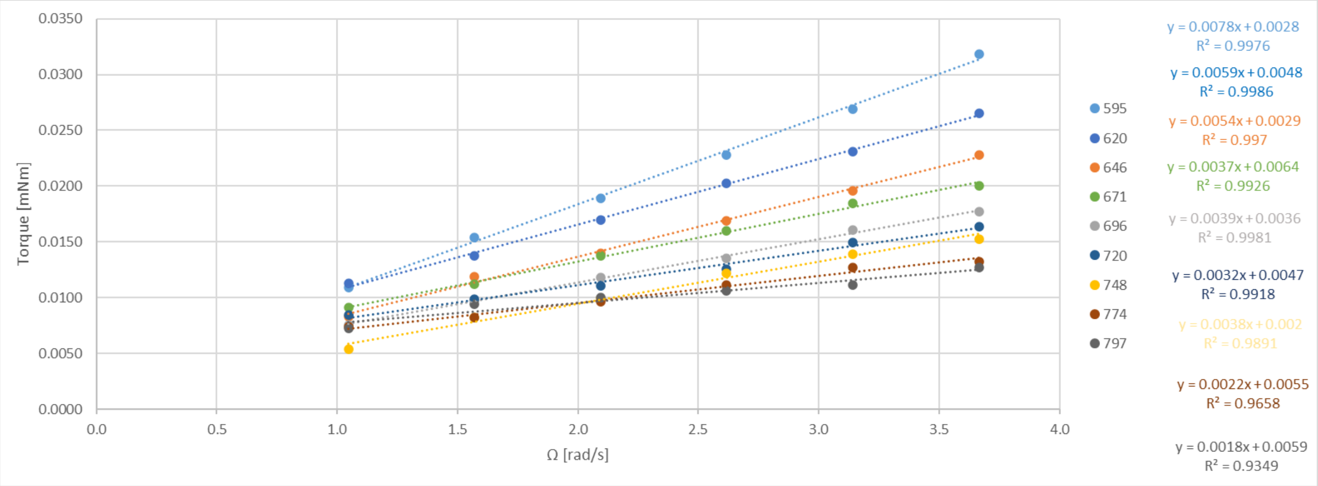

Figure 43. The torque response of Seaborg-7 salt as a function of rotational speed with data taken from Table 45. Temperatures are given as averages over the temperature variation at each setpoint.

Table 46. Measured viscosity of the Seaborg-7 salt (48.9NaF - 24.7KF - 26.4UF_4). Viscosities are calculated by Equation 7 from slopes given in Figure 43 and k = 2383.5 m^{-3}.

Temperature	η (experimental) (k = 2383.5)
°C	mPa·s
595 ± 5	18.6 ± 2.6
620 ± 5	14.0 ± 1.9
646 ± 5	12.8 ± 1.8
671 ± 6	10.2 ± 1.4
696 ± 5	9.3 ± 1.3
720 ± 5	7.4 ± 1.0
748 ± 5	8.9 ± 1.2
774 ± 5	5.7 ± 0.8
797 ± 5	4.3 ± 1.0

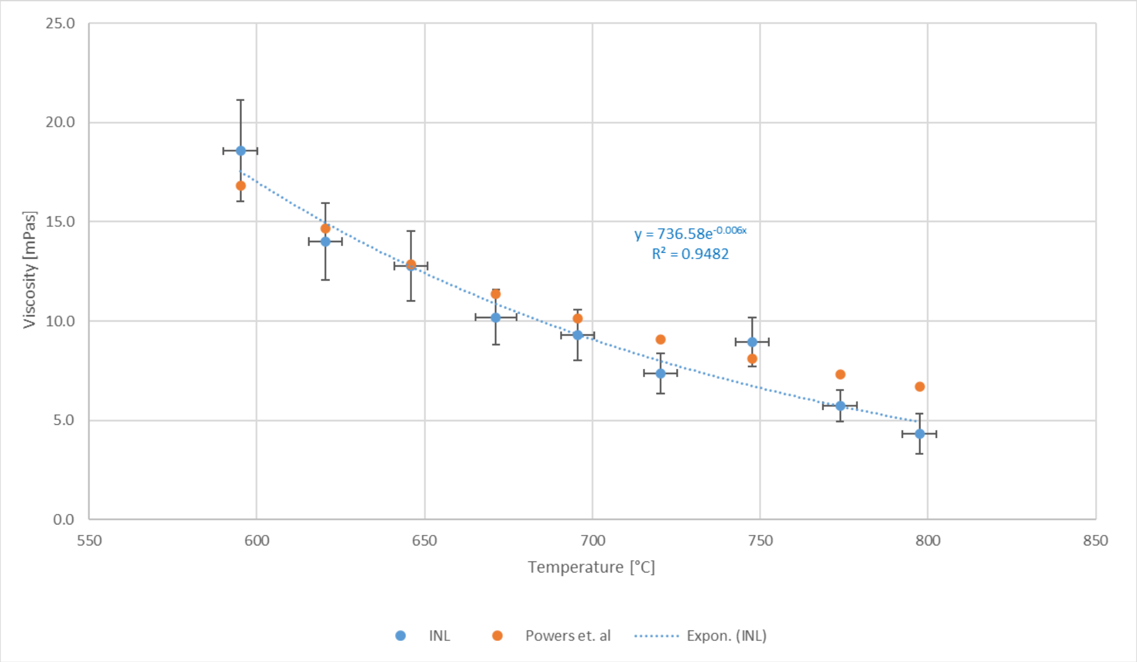

Figure 44. Viscosity of Seaborg-7 salt (48.9NaF - 24.7KF - 26.4UF_4) as a function of temperature. Data from Powers et al. [9] are included as reference.

Molten salt viscosity determinations present a significant challenge due to their inherently low viscosity coupled with high density. These properties often lead to a diminished signal-to-noise ratio when assessed at low-shear rates, thereby increasing the potential for experimental inaccuracies. Aware of this, INL developed a measurement geometry intended to enhance the signal, thus improving measurement precision. However, during the design phase, the impact of buoyancy forces on the measuring spindle was overlooked. While buoyancy forces are typically negligible, the unfortunate combination of the measuring device's limitations, the specific geometry designed for measurement, and the high density of the UF_4-salt rendered viscosity assessments with the existing apparatus unfeasible.

By reducing the overall volume of the spindle, the effect of buoyancy was eliminated, and measurements were successfully performed. It should be noted, as can be seen in Equations 7 and 8, that when reducing the spindle size, the measured torque signal is also reduced, potentially increasing measurement errors. However, even with a reduced spindle size, satisfactory data was collected. A mathematical fit of the experimental viscosity data collected shows that the viscosity varies with temperature, resulting in the following relationship η (mPa·s) = 736.58, with coefficient of determination (R^2) of 0.9482.

5. DISCUSSION AND CONCLUSIONS

The melting temperatures of seven different Seaborg salt samples were determined in this work. The composition of the Seaborg-7 salt sample was determined to be near a ternary eutectic point and had the following composition, 26.4UF_4-48.9NaF-24.7KF. Four ingots, approximately 100g in mass each, were made and combined. This combined Seaborg-7 bulk salt was then used to determine thermal properties such as salt stability, melting temperature, enthalpy of fusion/crystallization, heat capacity, density (solid/liquid), thermal diffusivity, and viscosity. The UF_4 used in this work was of high purity. Additionally, the NaF and KF salt was purified (with respect to moisture) by vacuum drying. The NaF, KF, and UF_4 salts were examined on the XRD as well as the STA for purity. Elemental analysis was only performed on samples of the UF_4 salt. However, the INL team recommends that samples of the Seaborg-7 bulk sample be sent to the ARL for elemental analysis to confirm composition.

The stability of the salt was investigated by using a heating rate of 20°C/min and heating the salt to 900°C, holding for 5 minutes, cooling, and repeating this cycle four times. No mass change was observed at each 900°C isotherm. Additionally, lower heating rates were used to heat the sample to lower temperatures; again, no observable mass change was seen as a function of temperature below 700°C. The peak melting temperature of the Seaborg-7 salt was determined to be 547 ± 3°C. This reported melting temperature is slightly higher than that reported in literature because in literature the onset of the liquidus peak is used to report the melting temperature. The INL team does not necessarily agree with this approach as the peaks observed in the Seaborg-7 sample did not sufficiently return to a baseline for accurate calculation of an onset temperature. The enthalpy of fusion, , ranged from 171 to 165 J/g with an average for all three heating rates of 167.5 ± 2.7 J/g. The enthalpy of crystallization, , ranged from -134 to -160 J/g with an average for all three heating rates of -147.8 ± 13.3 J/g.

Specific heat capacity measurements showed a slightly increasing trend with respect to temperature in the solid phase while the liquid-specific heat capacity showed a nearly flat trend ranging from 104–109 J/mol·K, with an average heat capacity of 106.1 ± 1.24 J/mol·K between 600 to 800°C. Because it is complicated to show heat capacity data from every sample, the calculated average values from each sample in the solid and liquid phase are shown in Figure 45 along with a linear fit for each phase. While the solid phase may warrant a different fit than linear, Seaborg Technologies can manipulate the data as they best see fit.

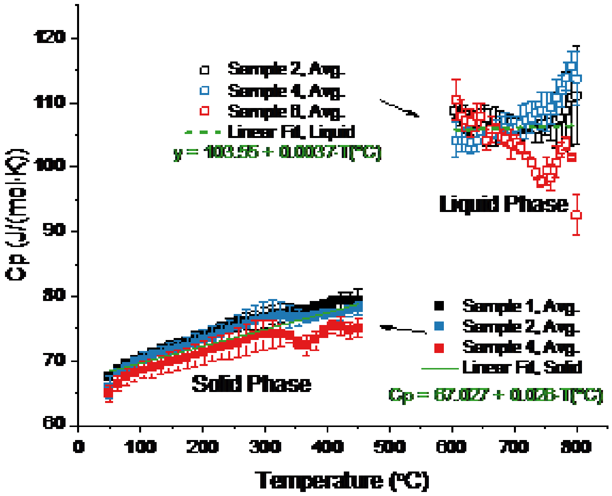

Figure 45. Summary of the averaged heat capacity values determined for the solid and liquid phase for Seaborg-7 salt.

Solid-state density was determined by several independent trials using fused Seaborg-7 salt material, where the density was found to be represented by the equation: $\rho(T) = 4.908 - 0.000363 \cdot T(°C)$, validated between 30 to 200°C. Liquid-state density was determined by three independent trials, where the density was found to be represented by the equation: $\rho(T) = 4.808 - 0.00113 \cdot T(°C)$, validated between ~575 to 850°C.

Thermal diffusivity was determined for the liquid state and is represented by the linear equation $y = 0.1581 + 0.000207 \cdot T(°C)$ between 550 to 850°C. Thermal diffusivity of the solid phase was also experimentally determined to be $y = 0.1201 + 0.000115 \cdot T(°C)$; however, this experimental setup and sample preparation technique have not been validated by the INL team and should therefore be noted but not used. Because we have determined the heat capacity, density, and thermal diffusivity, it is possible to calculate the thermal conductivity of the Seaborg-7 salt; calculations performed by Seaborg Technologies concluded that the average thermal conductivity is approximately 1 W/m·K.

Viscosity measurements of molten salts are challenging due to their relatively low viscosity and high density. This combination of properties results in an increased probability of secondary flows, which gives inflated viscosity values. In most cases, these secondary flows are not considered in published data, resulting in ambiguity between different authors.

Molten salt viscosity determinations present a significant challenge due to their inherently low viscosity coupled with high density. These properties often lead to a diminished signal-to-noise ratio when assessed at low-shear rates, thereby increasing the potential for experimental inaccuracies. Aware of this, INL developed a measurement geometry intended to enhance the signal, thus improving measurement precision. However, during the design phase, the impact of buoyancy forces on the measuring spindle was overlooked. While buoyancy forces are typically negligible, the unfortunate combination of the measuring device's limitations, the specific geometry designed for measurement, and the high density of the UF_4-salt rendered viscosity assessments with the existing apparatus unfeasible. By reducing the overall volume of the spindle, the effect of buoyancy was eliminated, and measurements were successfully performed. A mathematical fit of the experimental viscosity data collected shows that the viscosity varies with temperature, resulting in the relationship η (mPa·s) = 736.58 with coefficient of determination (R^2) of 0.9482.

6. REFERENCES

1. Schacherl, B., et al., *Thermodynamic Assessment of the NaF-KF-UF4 System.* Thermo, 2021. **1**(2): p. 232-250.
2. Fache, M., et al., *Thermophysical Properties of FUNaK (NaF-KF-UF4) Eutectics.* Materials, 2024. **17**(11): p. 2776.
3. Park, J., A. Leong, and J. Zhang, *Density Measurements of Molten Salts.* Journal of Chemical & Engineering Data, 2023. **68**(8): p. 1892-1898.
4. *Standard Test Method for Thermal Lag of Thermal Analysis Apparatus*. 2018, ASTM International, E3142-18a: West Conshohocken, PA.
5. Goodisman, J., *Surface tensions of molten salt mixtures.* Journal of Colloid and Interface Science, 1980. **73**(1): p. 115-123.
6. Janz, G.J., et al., *Molten Salts: Volume 4, Part 1, Fluorides and Mixtures Electrical Conductance, Density, Viscosity, and Surface Tension Data.* Journal of Physical and Chemical Reference Data, 1974. **3**(1): p. 1-115.
7. Hidnert, P., *Thermal Expansion of Some Nickel Alloys.* Journal of Research of the National Bureau of Standards, 1957. **58**(2): p. 89 - 92.
8. Hidnert, P., *THERMAL EXPANSION OF TANTALUM.* Bureau of Standards Journal of Research, 1929: p. 887-896.
9. Powers, W.D., S.I. Cohen, and N.D. Greene, *Physical Properties of Molten Reactor Fuels and Coolants.* Nuclear Science and Engineering, 1963. **17**(2): p. 200-211.